Behaviour and Elastic Buckling Analysis for Design of Thin-Walled Channel Sections with Narrow Flanges in Shear

Xuyang Chen

THE UNIVERSITY OF SYDNEY

Supervisor:

Associate Professor Cao Hung Pham

A thesis submitted in fulfilment of
the requirement for the degree of
Master of Philosophy

School of Civil Engineering

Faculty of Engineering

The University of Sydney

Australia

May 2023

ABSTRACT

This thesis presents a comprehensive numerical study on elastic shear buckling of thin-walled channel sections with narrow flanges under predominantly shear. The primary aim is to investigate the elastic shear buckling behaviour by different numerical methods and to develop a new proposed explicit approach to determine the shear buckling coefficient (k_v) of such sections.

The research involves developing numerical modelling to perform shear buckling analysis using the finite element method (FEM), semi-analytical finite strip method (SAFSM) and resemi-analytical finite strip method (reSAFSM). SAFSM assumes that the ends of the half-wavelength are free to distort, and the buckle is part of a very long length without end restraints. reSAFSM assumes no cross-sectional distortion at both section ends, and hence all edges of the channels can be treated as simply supported. The method uses multiple series terms to allow for producing multiple buckle half-waves as the sections become longer. The FE models are developed using the commercial ABAQUS software package. The results are benchmarked against those from the reSAFSM models developed using the computer program **bfinst8R.cpp**. reSAFSM models only allow pure shear action without any effect of bending on the sections, while FE models can consider the bending moment by adding distributed normal stress at two cross sections in order to maintain the static equilibrium. The SAFSM models are also developed using the computer program **bfinst7R.cpp** to investigate the effect of different boundary conditions on the shear buckling capacity. Both computer programs were developed by Professor Gregory J. Hancock at the University of Sydney.

The results of shear buckling analyses are used to perform a further parametric study. The relationships between shear buckling coefficient and the aspect ratios (AR) in terms of different flange width to depth ratios (b_2/b_1) from FE models are compared with those from the current design rules in AS/NZS 4600:2018. The current equations in the standard can be used for b_2/b_1 greater than 0.3 only. Using these existing equations can result in a significant over-estimation when predicting the value of k_v for sections with narrow flanges due to twisting effect.

The research has found that the shear buckling mode for sections with very narrow flanges is governed by twisting buckling, and it switches from twisting to shear local buckling with the gradual increase of flange sizes. This is related to the additional fixity provided by the flanges to the web panel. Finally, based on the research, a new explicit approach for determining the shear buckling coefficient of both lipped and un-lipped sections with narrow flanges in shear is introduced.

Keywords: Thin-walled structure, Channel sections, Shear elastic buckling, Narrow flange

Statement of Originality

This is to certify that to the best of my knowledge, the content of this thesis is my own work. This thesis has not been submitted for any degree or other purposes.

I certify that the intellectual content of this thesis is the product of my own work and that all the assistance received in preparing this thesis and sources have been acknowledged.

Thesis Authorship Attribution

This thesis contains material published or submitted for publication, based on the work presented in the thesis, for which I am the main author. This material is distributed throughout Chapters 3, 4, 5 and 6.

Journal Papers

"Elastic shear behaviour and design of thin-walled channel sections with narrow flanges in shear" in preparation.

In addition to the statements above, in cases where I am not the corresponding author of a published item, permission to include the published material has been granted by the corresponding author.

Name: Xuyang Chen

Date: 17/05/2023

As supervisor for the candidature upon which this thesis is based, I can confirm that the authorship attribution statements above are correct.

Name: Cao Hung Pham

Date:17/05/2023

Acknowledgements

I would like to sincerely thank my supervisor, Associate Professor Cao Hung Pham, for his continuous support during my M.Phil study, and for his guidance, motivation and immense knowledge.

A special thanks is also extended to Professor Gregory J. Hancock for his support to make the **bfinst7R.cpp** and **bfinst8R.cpp** available. These programs have significantly contributed to the research in this thesis.

I would also like to sincerely thank PhD candidate, Mr Duy Khanh Pham, for his enthusiastic help and support for my research during my candidature.

I wish to thank the School of Civil Engineering for providing the facilities such as ABAQUS, THIN-WALL, AUTO CAD, MATLAB and ENDNOTE software package for my research. Also, I would like to thank the software management staff from School of Engineering for technical supports.

I am grateful to Ms Daniela Entenmann, Postgraduate Administration Officer, who has supported me during my research periods.

I also wish to thank my friends and colleagues in the “Blue Room” (Room 360) for their friendship and the great moments we have shared.

I am greatly indebted to my family for their encouragement and support.

ABBREVIATIONS

ABM	:	Average Bending Moment
AR	:	Aspect Ratio
DSM	:	Direct Strength Method
FE	:	Finite Element
FEM	:	Finite Element Method
FSM	:	Finite Strip Method
reSAFSM	:	Resemi-Analytical Finite Strip Method
SAFSM	:	Semi-Analytical Finite Strip Method
SFSM	:	Spline Finite Strip Method

NOTATIONS

τ_{cr}	=	Elastic shear buckling stress (MPa)
$\tau_{cr,\ FEM}$	=	Elastic shear buckling stress from the FEM (MPa)
$\tau_{cr,\ reSAFSM}$	=	Elastic shear buckling stress from the reSAFSM (MPa)
v	=	Poisson's ratio
A_w	=	Cross-sectional area of web panel (mm^2)
a	=	Shear span of web panel(mm)
AR	=	Aspect ratio
AR_{tr}	=	Transition point
b_f	=	Depth of flat flange portion (mm)
b_1	=	Depth of web panel (mm)
b_2	=	Flange width (mm)
E	=	Young's modulus
f_y	=	Average yield stress (MPa)
h	=	Depth of flat web portion (mm)
k_v	=	Elastic shear buckling coefficient
k_{LCB}	=	Elastic shear buckling coefficient of lipped channel beams
k_{LSB}	=	Elastic shear buckling coefficient of LiteSteel beams
k_n	=	Coefficient of fixity level at web-flange juncture
k_{sf}	=	Elastic shear buckling coefficient of simple-fixed boundary condition
k_{ss}	=	Elastic shear buckling coefficient of simple-simple boundary condition
M	=	Bending moment (kNm)
t	=	Member thickness (mm)
t_f	=	Thickness of flange (mm)
t_w	=	Thickness of web (mm)
V	=	Shear force (kN)
V_{cr}	=	Shear buckling load (kN)
V_v	=	Nominal shear capacity (kN)
V_y	=	Shear yield load (kN)

CONTENTS

LIST OF FIGURES

LIST OF TABLES

CHAPTER 1 : INTRODUCTION

1.1 RESEARCH BACKGROUND AND PRESENT PROBLEM

Thin-walled structures such as cold-formed steel and cold-rolled aluminium structures have been commonly applied in the construction industry for both structural and non-structural components such as beams, columns, decks, girts, wall panels, joists and purlins. Thin-walled channel sections used in the building industry have many valuable advantages such as high strength-to-weight ratio, economy of transportation and handling, and ease of prefabrication, erection and installation compared to other conventional structures.

In thin-walled building structures, channel sections are usually used as flexural members such as floor joists and purlins as shown in **Figure 1.1.**. Therefore, identifying their flexural and shear capacities is indispensable in the design process. For thin-walled channel sections in shear, the elastic shear buckling is a major type of structural failure to affect their shear capacity. Thus, during the past decades, extensive research has focused on investigating the shear buckling behaviour of channel sections.

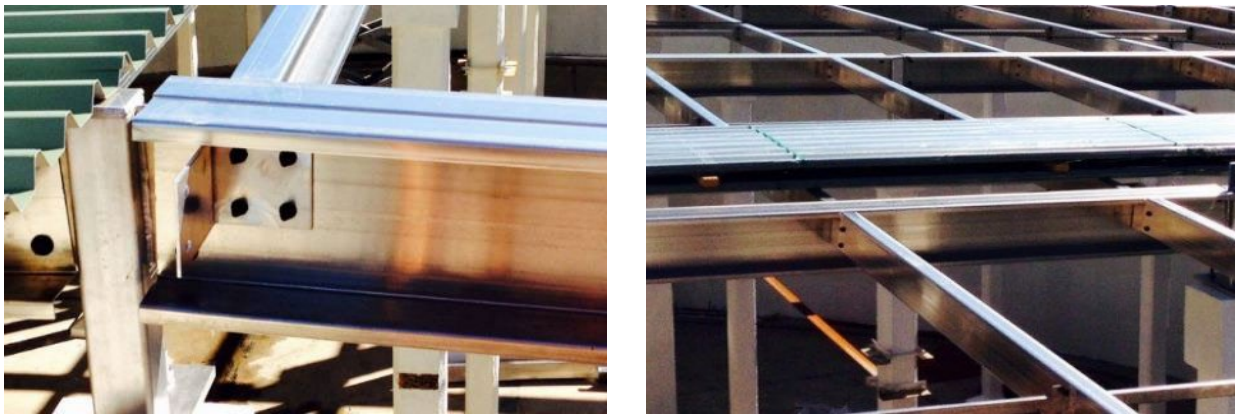

Figure 1.1: Channel sections used as flexural members. [1]

The traditional design method for shear buckling behaviour of channel sections is to consider the web element only without accounting for the effect of flange and lip rigidity. Pham and Hancock [2] have investigated the elastic shear buckling of both lipped and unlipped channel sections in shear using the

spline finite strip method (SFSM) developed by Lau and Hancock [3]. It involves four different cases of shear flow distribution and two types of boundary conditions, including the simply supported edges of the cross-sectional plane with and without lateral restraints along the two longitudinal edges of the web panels. Their investigation suggested that the flange can significantly affect the shear buckling capacity of thin-walled channel sections. Lack of lateral restraints for the channel sections with narrow flanges can also result in premature twisting and lateral buckling. Hancock and Pham [4] used the semi-analytical finite strip method (SAFSM) and resemi-analytical finite strip method (reSAFSM) to investigate the elastic shear buckling behaviour of channel sections with different boundary conditions. Pham and Hancock [5] investigated elastic shear buckling behaviour and conducted elastic buckling analyses of thin-walled channel sections with various flange and lip sizes subject to pure shear stress using the semi-analytical finite strip method and spline finite strip method. They used these two numerical approaches to investigate the effects of two different boundary conditions, including simply supported and free cross-section edges on the shear buckling capacity of channel sections. Their results showed that the flange stiffened by lips can improve the shear buckling stress of the channel sections. The shear buckling stresses obtained by the two methods are significantly different at short half-wavelength or member length due to the difference in boundary conditions. In addition, the results from the two methods also showed that channel sections with narrow flanges may buckle in a twisting mode.

However, Pham and Hancock [5] only studied the shear buckling behaviour of channel sections by varying the flange sizes without proposing a new equation for the design of shear buckling capacity. Therefore, Keerthan and Mahendran [6] investigated the shear buckling behaviour of lipped channel sections using the finite element method (FEM), which recognises the influence of flange rigidity on the web shear buckling. The study found that a flange width to depth ratio (b_2/b_1) greater than 0.3 can provide 23% fixity to the web panel. Based on the study, they have proposed new design methods for determining the shear buckling coefficient (k_v) for lipped channel sections standardized in the Australian Standard AS/NZS 4600:2018 [7].

Although the current design codes have been developed for determining the shear buckling coefficient for channel sections in shear, only design codes for lipped channels were included in AS/NZS 4600:2018 [7] and only were used to determine the value of k_v for a flange width to web depth ratio greater than 0.3. However, there is a gap in the current standard for channel sections

with b_2/b_1 smaller than 0.3. The channel sections with a small flange width to depth ratio are usually used to resist high shear forces but have less bending moment as shown in **Figure 1.2**. The continuous span beams are supported by multiple main beams and are subjected to concentrated loads transferred from the joists. In this scenario, the failure modes in the segments between the main beams and joists is likely to be governed by high shear in regions of high moment gradient (double curvature segment) **Table 1.1** and **Table 1.2** shows some typical standard cold-formed steel channel C sections manufactured by ExSteel [8] and ClarkDietrich [9] who have been manufacturing steel building components used in industrial, commercial, creational and institutional projects across North America and around the world. It can be found that the ratios of flange width to depth of these sections are smaller than 0.3. Thus, from a practical perspective, a full understanding of the elastic shear buckling behaviour of channels with narrow flanges is necessary for engineers to design thin-walled structures in shear.

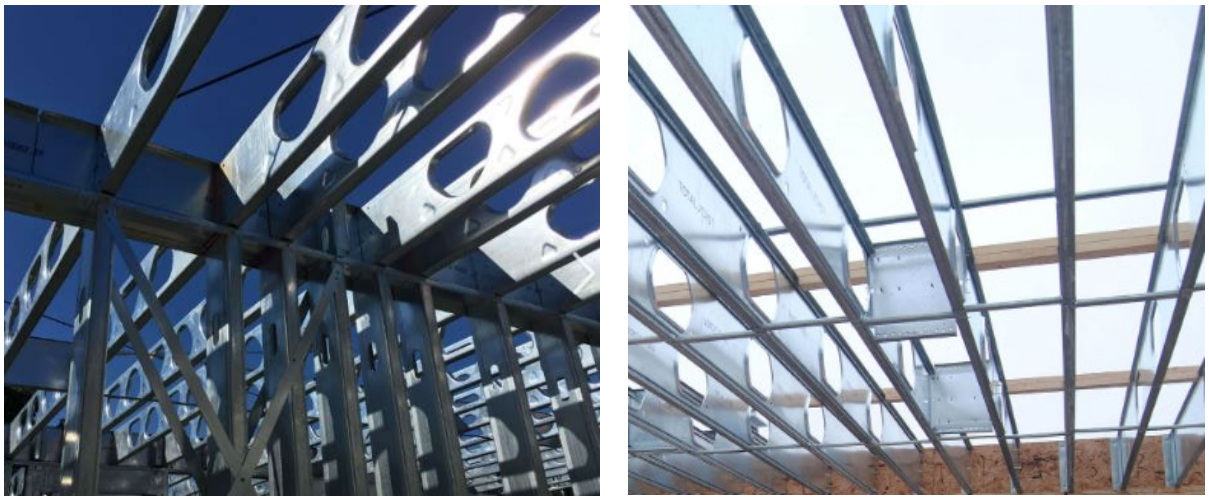

Figure 1.2: Channel section with narrow flanges used in cold-formed framing.[10] [11]

Table 1.1: The typical section dimensions of channel C sections manufactured by ExSteel (Table courtesy of ExSteel Building Components Company). [12]

Section	Depth of section d (mm)	Flange width b (mm)	Thickness t (mm)	Ratio of flange width to depth
12C13	305	85.9	2.28	0.282
12C12	305	85.9	2.66	0.282
14C13	356	88.9	2.28	0.250
14C12	356	88.9	2.66	0.250
16C13	406	88.9	2.25	0.219
16C12	406	88.9	2.66	0.219

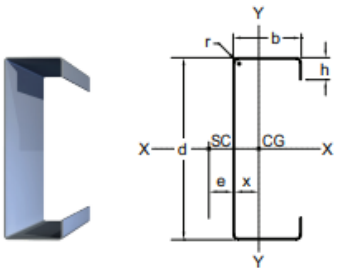

Table 1.2: The typical section dimensions of channel C sections by ClarkDietrich. [13]

Section	Depth A (mm)	Flange width B (mm)	Thickness t (mm)	A/B
725TDJ24-175-43	184	44.5	1.16	0.24
800TDJ24-175-43	203	44.5	1.16	0.22
925TDJ34-175-43	235	44.5	1.16	0.19
1125TDJ24-175-54	286	44.5	1.44	0.16
1000TDW24-200-54	254	50.8	1.44	0.2
1200TDW24-200-54	305	50.8	1.44	0.17

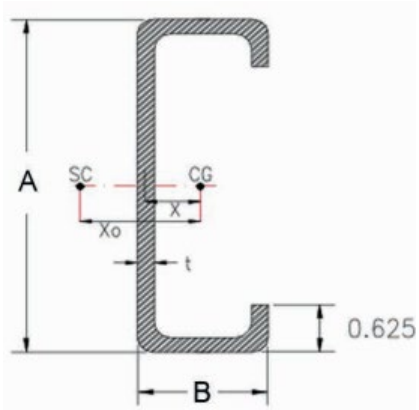

1.2 RESEARCH SCOPE AND OBJECTIVE

The main objective of this thesis is to provide a full understanding of the elastic shear behaviour of thin-walled channel sections with narrow flange width in shear by using different numerical approaches. Three different numerical methods, the finite element method, semi-analytical finite strip method and resemi-analytical finite strip method, are used to conduct shear buckling analyses to investigate the shear buckling coefficient of channels by changing the flange width to depth ratios. Furthermore, a detailed parametric study is conducted to study how the change in flange width can affect the shear buckling coefficients of channel sections with narrow flanges. Finally, a new explicit approach for the determination of k_v is proposed for both lipped and unlipped channel sections. The main tasks in this thesis are:

(1) To conduct shear elastic buckling analyses by developing finite element models of both lipped and unlipped channel sections with different flange widths and the aspect ratios subjected to the predominantly shear.

(2) To develop a series of semi-analytical finite strip simulations of channel sections with various flange widths including the influence of unrestrained boundary condition on the shear buckling behaviours of channel sections.

(3) To develop a series of semi-analytical finite strip simulations for shear buckling analyses of channel sections with a variety of flange sizes in pure shear excluding the influence of bending on the shear capacity of the channel sections

(4) To conduct a detailed parametric study on the basis of the shear buckling analyses results using three different methods to investigate the shear buckling behaviour of channels with narrow flanges and evaluate the applicability of the current design codes by comparing the value of k_v from buckling analyses results and the current proposals.

(5) To propose a new explicit approach for shear to predict the shear buckling coefficient of both lipped and unlipped channel sections with narrow flange widths under predominantly shear.

1.3 RESEARCH METHODOLOGY

For shear elastic buckling analyses of channel sections with different size flanges, nonlinear finite element simulation using the finite element package ABAQUS 6.14 is employed to develop finite element models of both lipped and unlipped channel sections. The results of buckling analyses and the shear buckling mode shapes can be generated by the BUCKLE procedure in ABAQUS. The results can then be used to calculate the shear buckling stresses and shear buckling coefficients. After that, parametric studies are conducted based on the results of the buckling analyses to investigate the elastic shear behaviours of channel sections with different flange sizes. In addition, the results obtained from the finite element models are benchmarked by finite strip methods to ensure the reliability of the outcomes.

Finite strip method, semi-analytical finite strip method and resemi-analytical finite strip method are employed to investigate the effects of different boundary conditions on the shear buckling behaviours of channel sections with different flange widths. The results are also used to benchmark the results generated by the finite element method. The semi-analytical finite strip simulation using the computer program **bfinst7R.cpp** is employed to develop the finite strip models where the section ends of the models are unrestrained and free to distort. By contrast, the resemi-analytical finite strip simulation is employed using the computer program **bfinst8R.cpp** where the boundary conditions of the models are simply supported.

The results from shear elastic buckling analyses by three different numerical methods are collected to compare the shear buckling coefficients influenced by changing the narrow flange widths. Based on the buckling analysis results a new explicit approach for the determination of shear buckling

coefficient for both lipped and unlipped channel sections under predominantly shear is proposed to predict the shear buckling stress of channels with narrow flange widths.

The thesis is structured as follows. Chapter 2 presents the literature review to describe the previous investigations contributing on the elastic shear buckling of thin-walled structures. Chapter 3 mainly describes the details of numerical models including the SAFSM, reSAFSM and FEM. Chapter 4 presents the results of buckling analyses using the three methods. Chapter 5 presents a detailed parametric study and the new explicit approach for determining the elastic shear buckling coefficient. Chapter 6 mainly concludes all contents presented in this thesis and provides some recommendations for future studies.

CHAPTER 2 : LITERATURE REVIEW

2.1 ELASTIC SHEAR BUCKLING OF PLATES

The shear buckling of flat rectangular plates has been investigated for many decades. For a slender flat plate with length a, depth b_1 and thickness t and simply supported along all four edges, shear buckling usually governs its ultimate strength. When the plate buckles out of its original plane due to shear stresses distributed uniformly along the four edges, the stresses are equal to the elastic buckling value τ_{cr}. Timoshenko and Gere [14] have developed the following equation to estimate the elastic shear buckling stress of a rectangular flat plate:

$$\tau_{cr} = k_v \frac{\pi^2 E}{12(1-v^2)} \left(\frac{t}{b_1}\right)^2 \tag{2-1}$$

where E is the Young's modulus, v is Poisson's ratio, b_1 is the depth of the plate, t is the plate thickness and k_v is the shear buckling coefficient of the plate depending on the boundary conditions and the aspect ratio of the plate a/b_1. For simply supported rectangular plates, an approximate prediction for k_v can be a function of the aspect ratio of the plates and is given as:

$$k_v = 5.34 + \frac{4}{\left(\frac{a}{b_1}\right)^2} \tag{2-2}$$

According to the formulae, as the plate is shortened, the value of k_v for the plate simply supported on all four edges will increase from 5.34 for an infinite long plate to 9.34 for a square plate.

2.2 ELASTIC SHEAR BUCKLING FOR COMPLETE THIN-WALLED CHANNEL SECTIONS

The traditional approach to designing the web shear buckling behaviour is considered in isolation without considering the influence of flange rigidity. LaBoube and Yu [15] have investigated the shear strength of cold-formed steel lipped channel beam, where the edge support conditions were provided by the flanges with different flat width to thickness ratios. However, most tests only considered a constant aspect ratio of 1.0. Their experiments did not recommend local or distortional buckling

failures since the specimens consisted of a couple of lipped channel beams, and angle sections and rectangular bars were used to connect two beams at their compression and tension flanges. In addition, LaBoube and Yu [15] just assumed that the web-flange juncture of lipped channel beams was simply supported. In order to prevent any torsional loading and web crippling, a single web side plate was used at the end supports and the loading point.

Pham and Hancock [2] demonstrated that the common design approach for a complete thin-walled channel section assumes that the web panel is treated as a flat plate simply supported on four edges. However, this traditional method does not consider whether adjacent elements can influence shear buckling stress. Therefore, their study employed the spline finite strip method (SFSM) to investigate the effect of adjacent plate elements on shear buckling stress and buckling modes for complete channel sections. Both lipped and unlipped channels with various section geometry have been investigated. Three different cases have been used to incorporate three different shear stresses in the thin-walled sections, including pure shear in the web only, pure shear in the web and flanges, and a shear distribution to allow the occurrence of practical section shear flow. The shear stress distribution performed in this study has been divided into four cases, as shown in **Figure 2.1** and **Figure 2.2.**

In Case A, only the web plate of the channel section is loaded by uniformed pure shear stress along its four edges. In addition, two longitudinal edges of the channel section are restrained laterally in order to prevent twisting. Case B is the same as Case A but without lateral restraints along the longitudinal edges. For Case C, the pure shear stress is applied not only throughout the web plate but also to flanges and lips. This case is mainly used to investigate the effects of flanges on the shear buckling behaviour of a whole cold-formed steel channel section. Case D is considered the most practical because it simulates a shear flow distribution caused by a shear force parallel to the web.

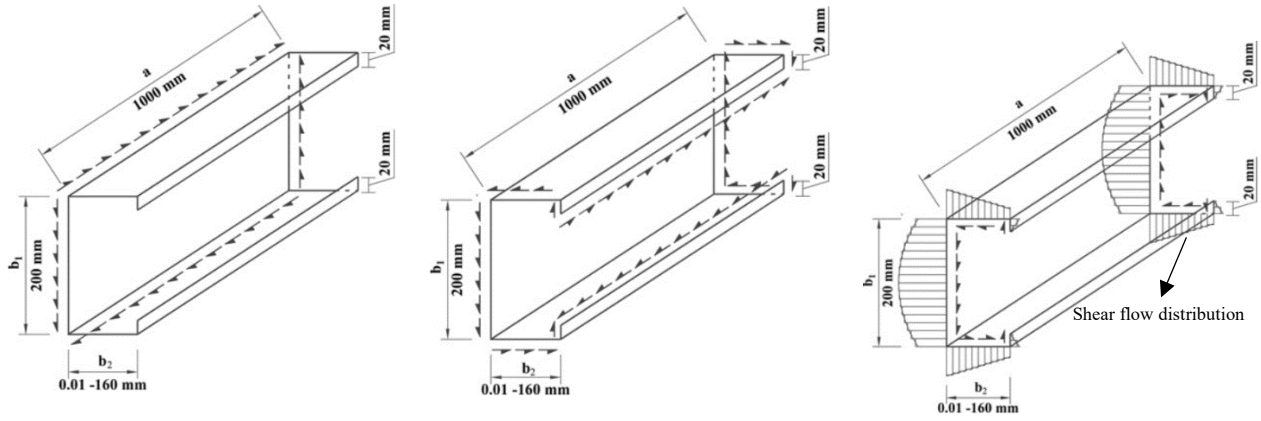

(a) Cases A & B (b) Case C (c) Case D

Figure 2.1: The shear stress distributions in lipped channel [2].

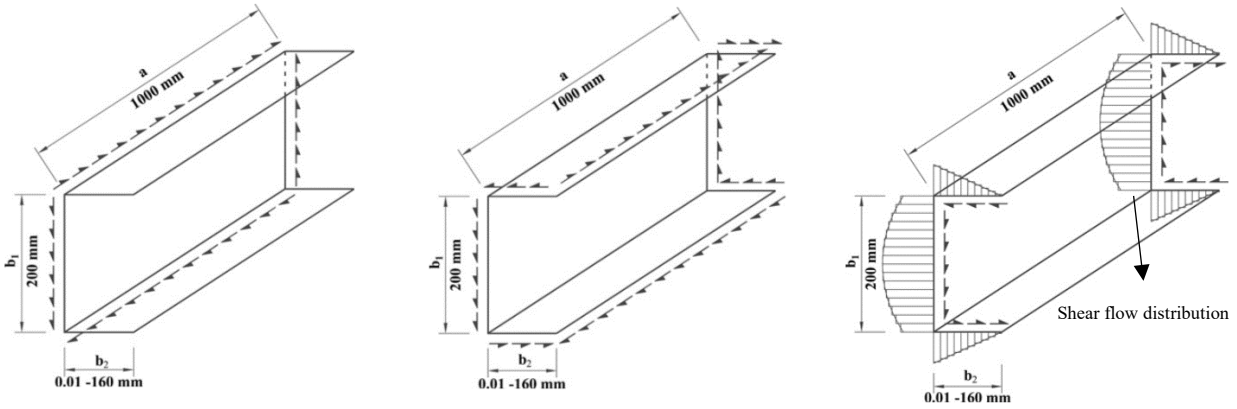

(a) Cases A & B (b) Case C (c) Case D

Figure 2.2: The shear stress distributions in unlipped channel [2].

As a result, the relationship between the ratio of flange and web width (b_2/b_1) and the shear buckling coefficient for both unlipped and lipped channel sections with an aspect ratio ($AR = a/b_1$) of 0.2 are plotted in **Figure 2.3** and **Figure 2.5**, and the corresponding shear buckling mode shapes are shown in **Figure 2.4** and **Figure 2.6**. This study has provided an insight into how the shear buckling behaviour of channel sections can be affected by differing section geometries and how shear buckling capacity can be improved due to the presence of flanges and lips. The outcomes can be summarised in three points: Firstly, the shear buckling capacity of channel sections with narrow flanges is much lower than those with large flange due to the occurrence of twisting and lateral buckling. This is because the narrow flanges cannot provide enough lateral restraint to the longitudinal edges of the web. As the ratio of b_2/b_1 exceeds 0.3, the shear buckling coefficient curve of Case B nearly matches that of Case A. This is because the flanges are wide enough to provide full lateral restraints to the channel sections. Secondly, channel sections with very large flanges will reduce the shear buckling

capacity due to the effect of flange slenderness. As the flange width is small, the effect of flange slenderness on the shear buckling capacity is little and can be ignored. However, for channel sections with greater flange width, the effect of flange slenderness is quite considerable. Furthermore, by comparing the shear buckling coefficient curve of lipped and unlipped channel sections, it can be found that the values of k_v of the lipped channel are higher than for the unlipped channel. The explanation is that the presence of lips can improve the shear buckling capacity of channel section members.

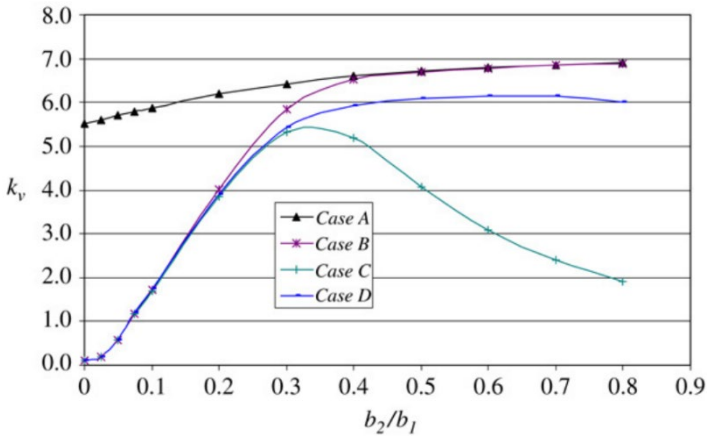

Figure 2.3: The ratio of flange widths and web depth and shear buckling coefficients for unlipped channel $a/b_1 = 5.0$ [2].

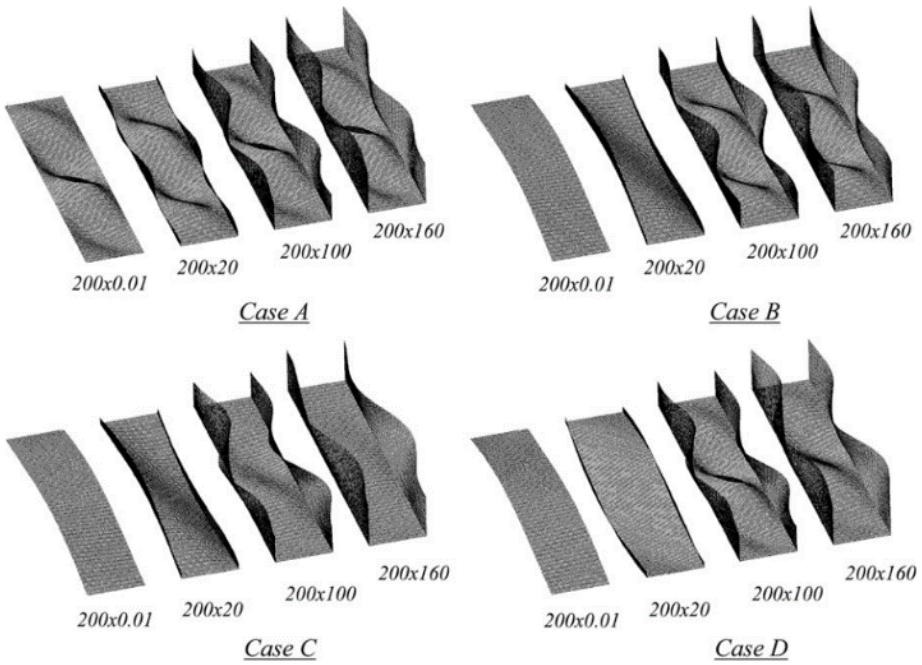

Figure 2.4: The shear buckling mode shape of unlipped channel $a/b_1 = 5.0$ [2].

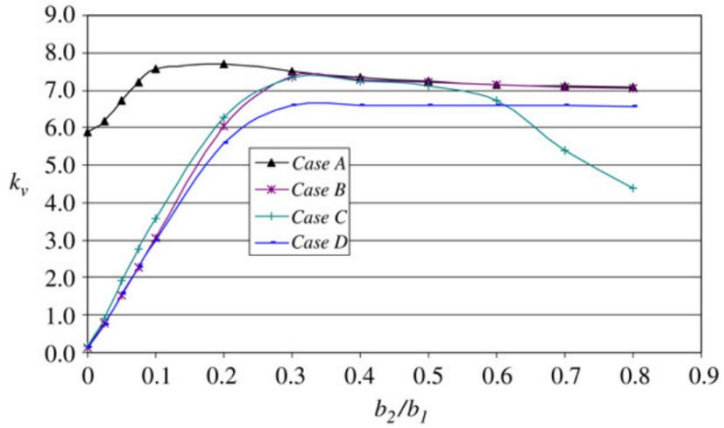

Figure 2.5: The ratio of flange widths and web depth and shear buckling coefficients for lipped channel a/b_1 =5.0 [2].

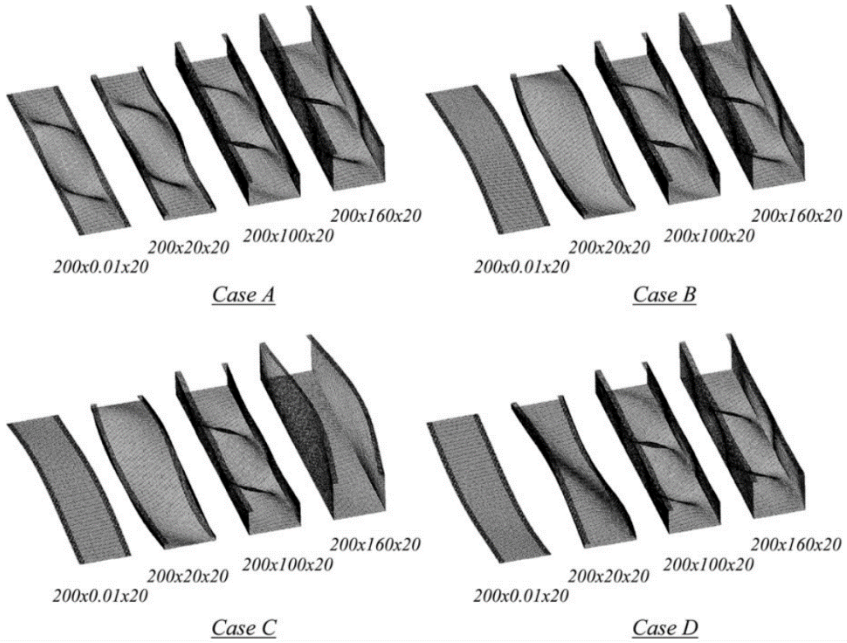

Figure 2.6: The shear buckling mode shape of lipped channel a/b_1 =5.0 [2].

Pham and Hancock [2] found that the flange can significantly affect the shear buckling capacity of channel sections. A twisting and lateral buckling can occur in channel sections with narrow flanges due to a lack of lateral restraints. Hence, further research to extend the data range for the shear buckling analysis of channel sections with different geometries has been conducted by Pham and Hancock [16] based on the spline finite strip method. In order to investigate how shear buckling capacity can be influenced by varying geometry properties, more variables have been taken into consideration, including the flange widths, member length and lip sizes. The boundary conditions at two cross-sectional ends are simply supported. This study uses a shear distribution that allows section shear flow to incorporate the practical shear stress distribution in thin-walled channel sections.

The results of this study have been plotted in **Figure 2.7** (a), (b) and (c), which indicates that the member length and flange width can significantly influence the shear buckling capacity of the thin-walled channel sections. The detailed outcomes can be summarised in several points: Firstly, it can be seen that the value of the shear buckling coefficient for a member length of 200 mm (a/b_1= 1.0) is much higher than other lengths. This indicates that flanges with lips and a short member length can considerably enhance the shear buckling coefficient of the channel sections. Secondly, increasing flange width can enforce channel sections to buckle into local buckling with multiple half-waves for a longer member length instead of twisting due to the improvement of lateral restraint from flanges. **Figure 2.8** demonstrates the buckling mode shapes of lipped channel sections for a member length of 2000 mm (a/b_1 = 10). As the flange width increases, the buckling mode of the section transfers from twisting to local buckling. This can indicate that the flange can significantly contribute to the improvement of shear buckling capacity. Thirdly, it is suggested that the lips can also play an indispensable role in improving the shear capacity of channel sections since the value of the shear buckling coefficient for lip size of 20 mm is higher than that for lip size of 10 mm and 0.01 mm.

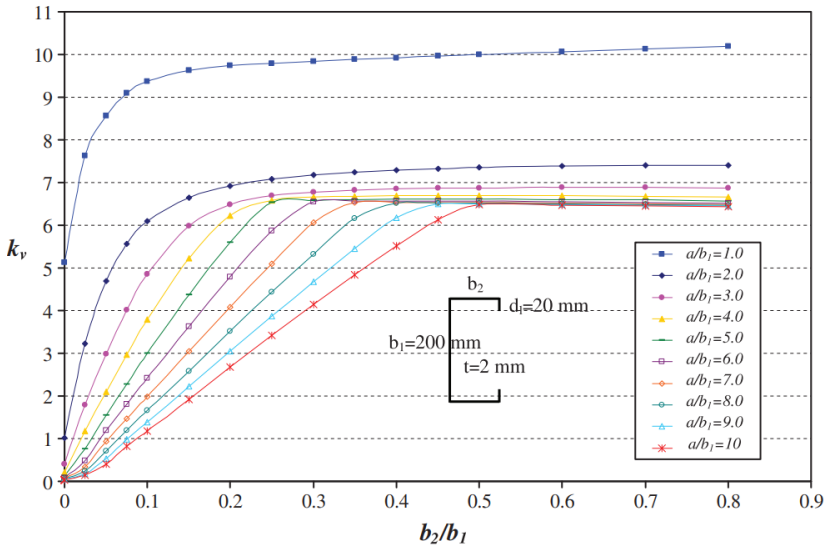

(a) The ratio of flange and web depth and the shear buckling coefficient for lip size of 20 mm.

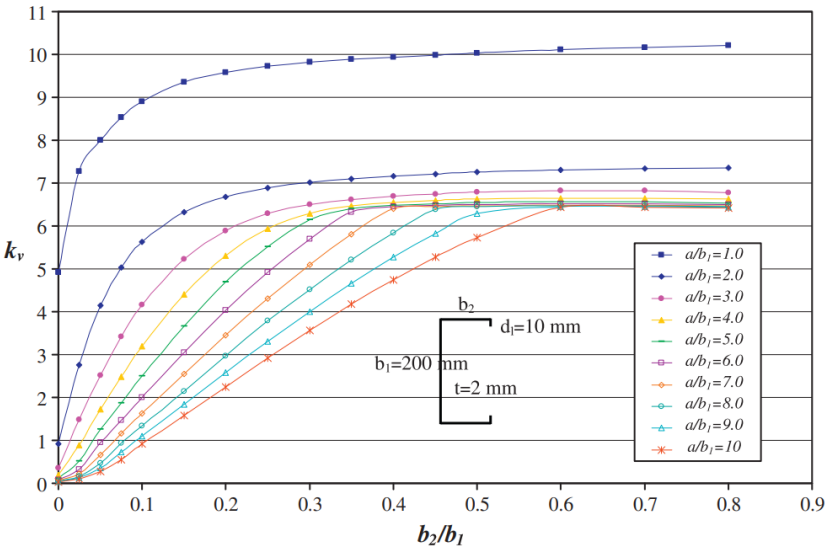

(b) The ratio of flange and web depth and the shear buckling coefficient for lip size of 10 mm.

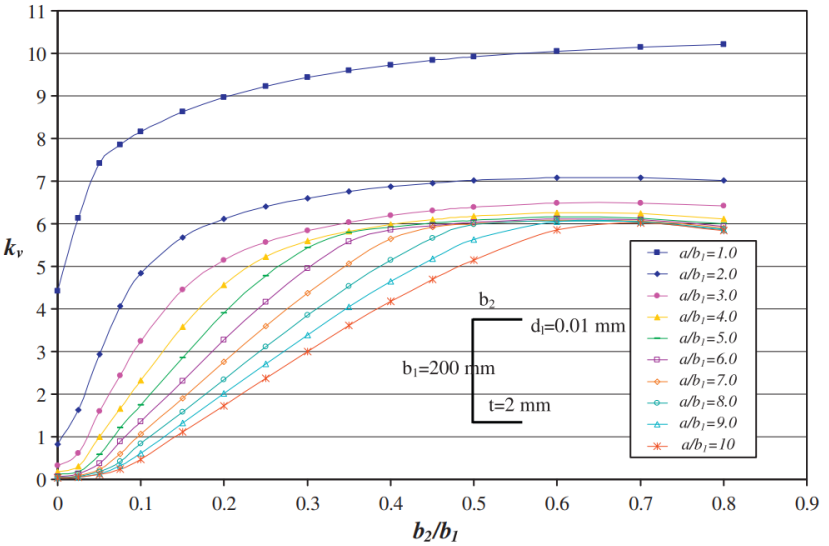

(c) The ratio of flange and web depth and the shear buckling coefficient for lip size of 0.01 mm.

Figure 2.7: The relationship between the ratio of flange and web depth and the shear buckling coefficient for various lip sizes [16].

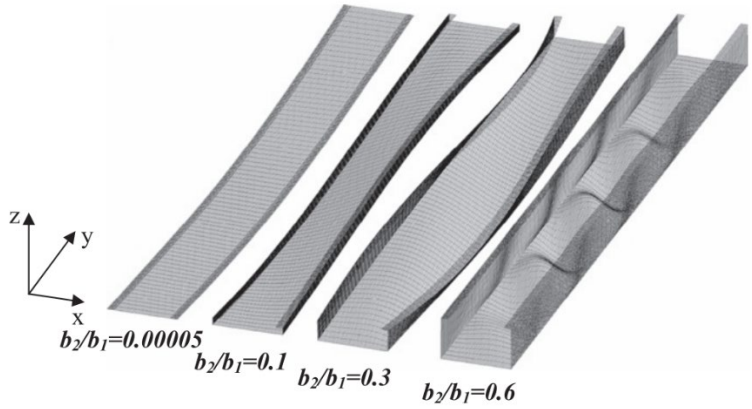

Figure 2.8: Buckling mode shapes of lipped channel sections for a member length of 2000 mm in terms of various ratio of b_2/b_1 [16].

Consequently, the study concluded that the shear buckling capacity of the thin-walled channel section could be significantly improved by flange with lips. When the channel member is long, the member with a narrow flange can present a twisting buckling mode. However, as the flange becomes wider, the buckling mode will transfer from twisting to distortional buckling. When the flange is wide enough to give lateral and torsional restraint to the longitudinal edges of the web, the channel will buckle in mainly local buckling mode.

Although the previous studies have identified that the flange and lip can improve the shear buckling capacity of the channel sections, there were no simple equations to approximate the shear buckling coefficient of channel sections provided in those studies. Therefore, Keerthan and Mahendran [6] have conducted elastic shear buckling analyses using suitable finite element models of lipped channel beams based on ABAQUS. Their studies have also focused on how the shear buckling coefficient can be affected by varying flange width to clear web height ratios. It is suggested that estimation of boundary conditions at the web-flange juncture of lipped channel sections can play a significant role in approximating the elastic shear buckling coefficient. The flange can give additional fixity to the web panel at the web-flange juncture, and actual boundary condition at the juncture of the flange and web elements should be somewhere between simple and fixed conditions. However, the previous studies and design standards usually assumed it as simply supported or a fixed condition due to a lack of means to evaluate it rationally. For example, Basler [17] and Porter et al. [18], in the case of plate girders, have assumed that the boundary condition of the plate juncture was simply supported, whereas Chern and Ostapenko [19] assumed it as fixed supports to obtain the ultimate strength. However, Sharp and Clark [20] have suggested that the juncture of web to flange should be halfway between simply supported and fixed conditions. Lee et al. [21] indicated that the boundary condition at the flange to web juncture is much closer to fixity for plate girders in practical design since the assumption of the simply supported condition can result in a significant underestimation of the elastic shear buckling stress. Lee et al. [21] have proposed the following equations **Eq (2-3)** to **(2-8)** for determining the shear buckling coefficient of plate girder web panels based on a detailed numerical study of plate girders. The equations for predicting the shear buckling coefficient of plate girders take account of web plates with simple-simple (k_{ss}) and simple-fixed (k_{sf}) boundary conditions. The latter case indicates that the web panel has fixed boundary conditions at the web-flange juncture and simply supported conditions at the other two edges.

For $\frac{1}{2} < \frac{t_f}{t_w} < 2$ $$k_v = k_{ss} + \frac{4}{5}\left(k_{sf} - k_{ss}\right)\left[1 - \frac{2}{3}\left(2 - \frac{t_f}{t_w}\right)\right] \quad (2\text{-}3)$$

For $\frac{t_f}{t_w} > 2$ $$k_v = k_{ss} + \frac{4}{5}\left(k_{sf} - k_{ss}\right) \quad (2\text{-}4)$$

For $\frac{a}{d_1} < 1$ $$k_{ss} = 4 + \frac{5.34}{(a/b_1)^2} \quad (2\text{-}5)$$

For $\frac{a}{b_1} \geq 1$ $$k_{ss} = 5.34 + \frac{4}{(a/b_1)^2} \quad (2\text{-}6)$$

For $\frac{a}{b_1} < 1$ $$k_{sf} = \frac{5.34}{(a/b_1)^2} + \frac{2.31}{(a/b_1)} - 3.44 + 8.39\,(a/b_1) \quad (2\text{-}7)$$

For $\frac{a}{b_1} \geq 1$ $$k_{sf} = 8.98 + \frac{5.61}{(a/b_1)^2} - \frac{1.99}{(a/b_1)^3} \quad (2\text{-}8)$$

where t_w and t_f are the thickness of the plate girder web and flange elements, a is the shear span of the web and a/b_1 is the aspect ratio.

Keerthan and Mahendran [22] conducted a series of elastic buckling analyses based on the finite element method computer program ABAQUS to develop a new equation for the determination of the shear buckling coefficients of LiteSteel beams. LiteSteel beam is a new cold-formed steel channel beam with a pair of rectangular hollow flanges produced by OneSteel Australian Tube Mills. The elastic buckling analysis results are shown in **Table 2.1**, which includes the shear buckling coefficients for 13 LiteSteel beams with varying geometry properties based on the aspect ratio of 1.0.

Table 2.1: The shear buckling coefficients of LiteSteel beams with different sections [22].

Section	k_{ss}	k_{sf}	k_{LSB}
125 x 45 x 1.6	9.34	12.60	12.58
125 x 45 x 2.0	9.34	12.60	12.59
150 x 45 x 1.6	9.34	12.60	12.57
150 x 45 x 2.0	9.34	12.60	12.58
200 x 60 x 1.6	9.34	12.60	12.19
200 x 60 x 2.0	9.34	12.60	12.57
200 x 60 x 2.5	9.34	12.60	12.58
250 x 60 x 2.0	9.34	12.60	12.45
250 x 75 x 2.5	9.34	12.60	12.58
250 x 75 x 3.0	9.34	12.60	12.59
300 x 60 x 2.0	9.34	12.60	12.41
300 x 75 x 2.5	9.34	12.60	12.43
300 x 75 x 3.0	9.34	12.60	12.45

$$k_{LSB} = k_{ss} + 0.87\left(k_{sf} - k_{ss}\right) \tag{2-9}$$

The proposed equation for the determination of the shear buckling coefficient of LiteSteel beams by Keerthan and Mahendran [22] is shown in **Eq (2-9)**, indicating that the boundary condition at the web-flange juncture is equivalent to 87% fixed condition. The factors k_{ss} and k_{sf} can be determined by **Eq (2-5)** to **Eq (2-8)** The study also conducted elastic buckling analysis of LiteSteel beams with an aspect ratio equal to 1.5 to confirm the proposed equation is applicable for all the aspect ratios.

Keerthan and Mahendran [6] investigated the elastic shear buckling behaviour of lipped channel sections by developing the finite element models of 20 lipped channel beams (LCB) based on the commonly used sizes to improve the equation for the higher elastic shear buckling coefficient of lipped channel beams.

The investigation results have compared the shear buckling coefficients obtained from the elastic shear buckling analyses with the reference buckling coefficients k_{ss} and k_{sf} determined by **Eq (2-5)** to **Eq (2-8)** for an aspect ratio of 1.0 as shown in **Table 2.2**. It is suggested that the shear buckling coefficient of lipped channel beams is not close to the simple-fixed boundary condition k_{sf} as compared with LiteSteel beams. However, it is relatively higher than k_{ss}, which means that the realistic support condition of lipped channel beams at the juncture of the web to flange is more rigid than simply supported boundary condition.

Keerthan and Mahendran [6] also conducted further buckling analyses to investigate the effect of flange width to clear web height ratio (b_2/b_1) on the shear buckling behaviour of lipped channel beams.

Table 2.2: Effect of flange width to clear web height ratio on the shear buckling coefficients of [6].

LCB Section	k_{LCB}	k_{ss}	k_{sf}	Web-Flange Fixity Level	b_2/b_1
200x20x20x2.0	9.39	9.34	12.6	1.5%	0.1
200x40x20x2.0	9.98	9.34	12.6	20%	0.2
200x60x20x2.0	10.13	9.34	12.6	24%	0.3
200x80x20x2.0	10.20	9.34	12.6	26%	0.4
200x100x20x2.0	10.24	9.34	12.6	28%	0.5
200x120x20x2.0	10.27	9.34	12.6	29%	0.6
500x50x30x2.0	9.56	9.34	12.6	6.7%	0.1
500x100x30x2.0	9.94	9.34	12.6	18.4%	0.2
500x150x30x2.0	10.08	9.34	12.6	23%	0.3
500x200x30x2.0	10.14	9.34	12.6	25%	0.4
500x250x30x2.0	10.17	9.34	12.6	26%	0.5
500x300x30x2.0	10.19	9.34	12.6	26%	0.6

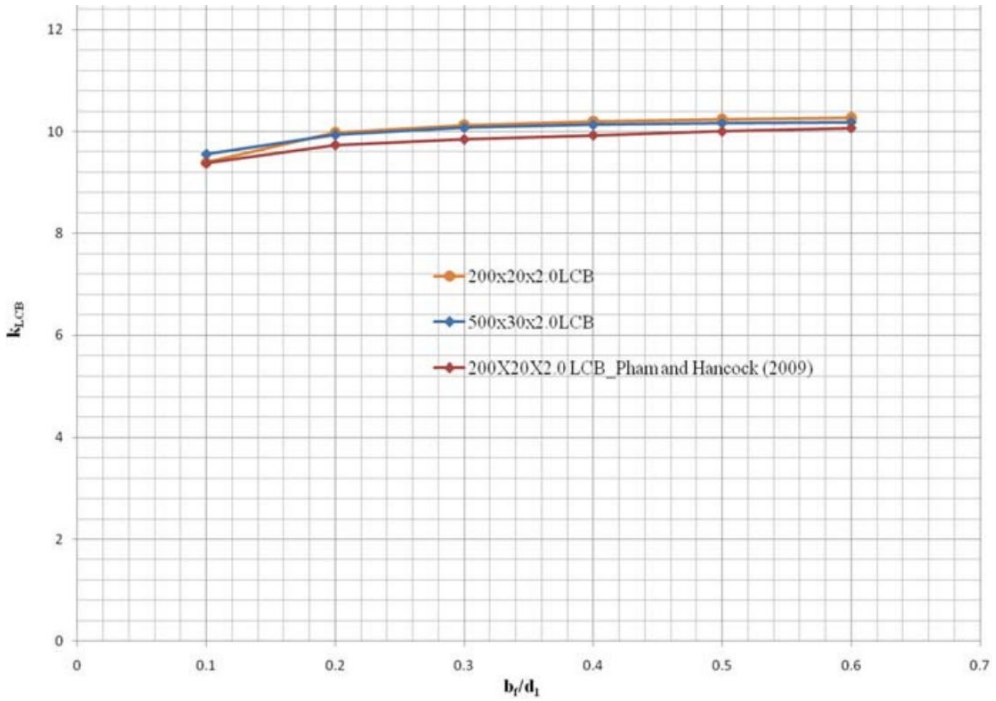

Figure 2.9: Effect of flange width to clear web height ratio on the shear buckling coefficients of LCBs [6].

Table 2.2 and **Figure 2.9** compared the elastic buckling coefficients of LCBs with varying flange width to clear web height ratios. 200x20x2.0LCB means the lipped channel beam with 200mm depth, 20mm of lip and 2.0mm of thickness. It is demonstrated that the elastic shear buckling coefficient of

LCBs can increase rapidly as the flange width to clear web height ratio increases up to 0.3. However, the coefficient did not change significantly when the flange width to clear web height ratio was greater than 0.3. Therefore, the flange width to clear web height ratio should be increased to 0.3 to obtain around a 23% fixity level at the web-flange juncture.

The improved equations for determination of shear buckling coefficient of LCBs have been proposed by Keerthan and Mahendran [6] based on the new finding of the fixity level at the web-flange juncture of LCBs.

For $b_f/d_1 \geq 0.3$

$$k_{LcB} = k_{ss} + 0.23\left(k_{sf} - k_{ss}\right) \tag{2-10}$$

For $b_f/d_1 \leq 0.3$

$$k_{LcB} = k_{ss} \tag{2-11}$$

where b_f and d_1 are the flange width and clear web height

Pham and Hancock [5] used both the spline finite strip analysis and semi-analytical finite strip analysis to investigate the effect of flange widths and lip sizes of the channel sections on the elastic shear buckling stress. This study provided the comparison between the semi-analytical finite strip method and the spline finite strip method for whole plan channel sections including various flanges and lips subjected to pure shear parallel to the web as shown in **Figure 2.10** and **Figure 2.11**. The semi-analytical finite strip method is limited to a single half-wavelength, while the spline finite strip method can allow multiple buckles in the entire length of the member.

The study has used the channel consisting of web depth of 200 mm, a flange width of 0.01 mm to 160 mm, a lip size of 0.01 mm to 20 mm and a thickness of 2 mm. The member was subdivided into 40 strips in the longitudinal direction including 16 strips in the web, 10 strips in each flange and 3 strips in each lip. The case of shear stress distribution was based on Case D referred to in the study of Pham and Hancock [2] for the purpose of achieving the most practical condition. Even though this shear distribution was not in equilibrium longitudinally as this can only be achieved by way of a moment gradient, it effectively isolates the shear from the bending to identify the pure shear buckling loads.

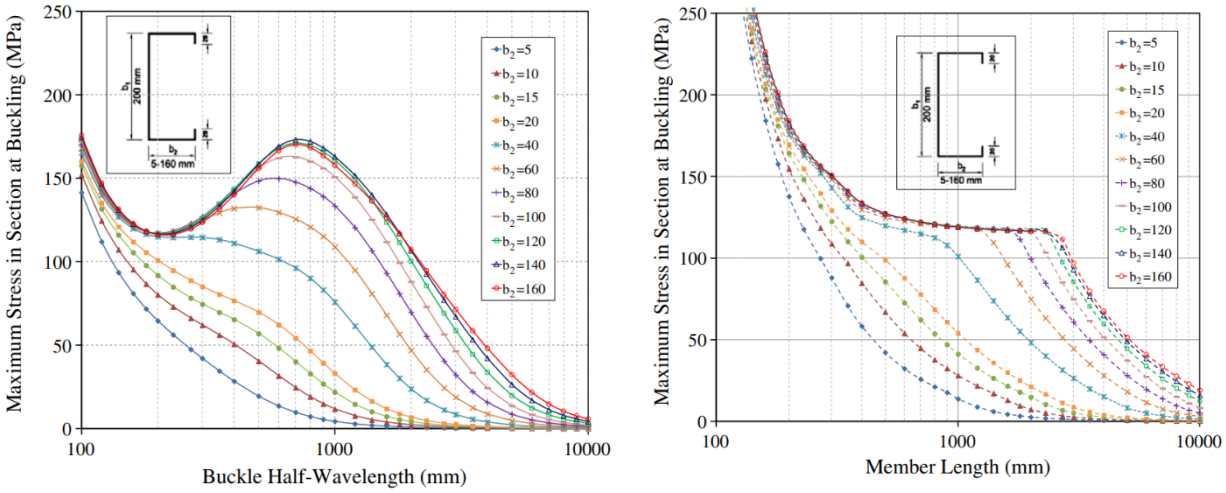

(a) Semi-analytical finite strip method (b) Spline finite strip method

Figure 2.10: Shear buckling stress versus length/half-wavelength from the SAFSM and SFSM for lipped channel sections with lip size of 20 mm [5].

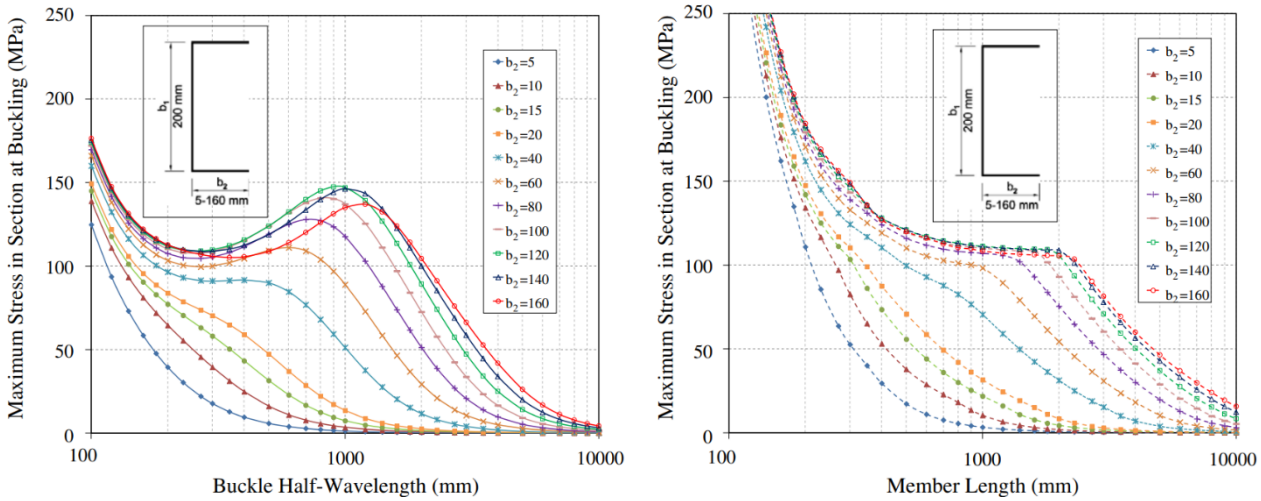

(a) Semi-analytical finite strip method (b) Spline finite strip method

Figure 2.11: Shear buckling stress versus length/half-wavelength from the SAFSM and SFSM for lipped channel sections with lip size of 10 mm [5].

As a result, by varying the flange widths and lip sizes, the analysis results show that the flanges with lips can significantly improve the shear buckling stress of the channel sections. When the flange width is small, the two relationship curves of the two methods can have a similar behaviour. The shear buckling stresses drop rapidly as the half-wavelengths or lengths of the channel increase. A significant difference of the shear buckling stresses for the two methods can be at short half-wavelengths or lengths due to different boundary conditions at the two end sections. At longer half-wavelengths or lengths, the SFSM curves drop closer to those of the SAFSM, which implies less effect of the end

boundary conditions. In addition, channel sections with a very narrow flange may buckle in a twisting mode.

In practice, sections are often restrained at their section ends or by transverse stiffeners, leading to obvious changes of the shear buckling modes and a significant increase of the buckling loads. However, the SAFSM analysis only assumes that the buckle is part of a very long section with unrestrained section ends so that the section ends are free to distort. Although Pham and Hancock [2] and Pham and Hancock [16] used the SFSM to investigate the channel sections with simply supported ends in pure shear, it still needs substantial computer resources to generate the results. Hancock and Pham [4] have further developed a resemi-analytical finite strip method (reSAFSM) based on the previous shear buckling analysis by Anderson and Williams [23] to understand simply supported end conditions for sections in pure shear, which is performed by a new computer program bfinst8.cpp written in Visual Studio C++. SAFSM employs the longitudinal harmonic series for shear so that the ends of the half-wavelength are free to distort, and the buckle is part of very long length without end restraints. However, reSAFSM is a new version of the SAFSM developed by Hancock and Pham [2] to accomplish the buckling analysis of thin-walled channels with simply supported end conditions. The method is called reSAFSM to reflect the restrained ends. The method uses multiple series terms to allow for producing multiple buckle half-waves as the sections become longer.

The results of the study are demonstrated in **Figure 2.12** which compares the buckling stress against the length/half-wavelength from the SAFSM (bfinst7.cpp) and the reSAFSM (bfinst8.cpp). Obviously, the curve of the reSAFSM is shifted to the right compared to the SAFSM for the seam value of shear buckling stress due to the difference of the boundary conditions. In conclusion, the study indicated that the restrained section ends can significantly improve the shear buckling capacity of the channel sections in shear.

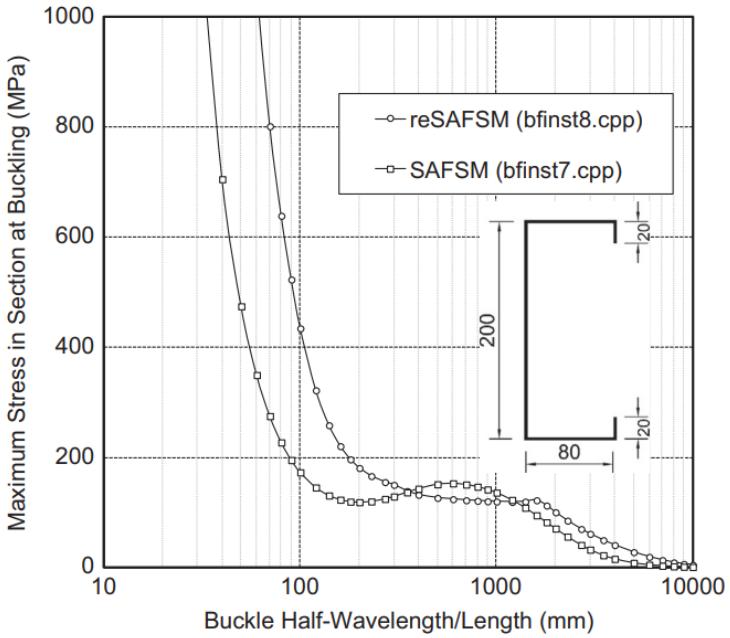

Figure 2.12: Buckling stress versus length/half-wavelength from SAFSM (bfinst7.cpp) and reSAFSM (bfinst8.cpp) for lipped channel sections [4].

Pham et al. [24] have conducted elastic buckling analysis to investigate the local buckling of lipped and unlipped thin-walled channel sections subjected to the interaction of bending and shear using the finite element method. By varying the ratios of bending moments resulting from the longitudinal stress, different types of interactions have been studied during the buckling analyses. In addition, an explicit approach for determining local buckling loads for both lipped and un-lipped channel sections under different combinations of bending and shear has been developed for practical design use.

In Pham et al. [24], three different methods including the SAFSM/bfinst7.cpp, restrained SAFSM/bfinst8.cpp and the FEM analyses have been used in the buckling analyses to benchmark the results from the FEM models. It has been indicated that the boundary condition at the section ends can affect the shear buckling capacity of the channel sections. Compared to the SAFSM/bfinst7 models with free section ends, the FEM and reSAFSM/bfinst8.cpp models having simply supported conditions have shown a higher shear buckling capacity as shown in **Figure 2.13**. Furthermore, the study also found that the FEM results at longer members are under predominantly shear, and the local buckling mainly occurs in bending at two ends, leading to a lower shear buckling stress of the FEM models at long members than the those from the bfinst8.cpp.

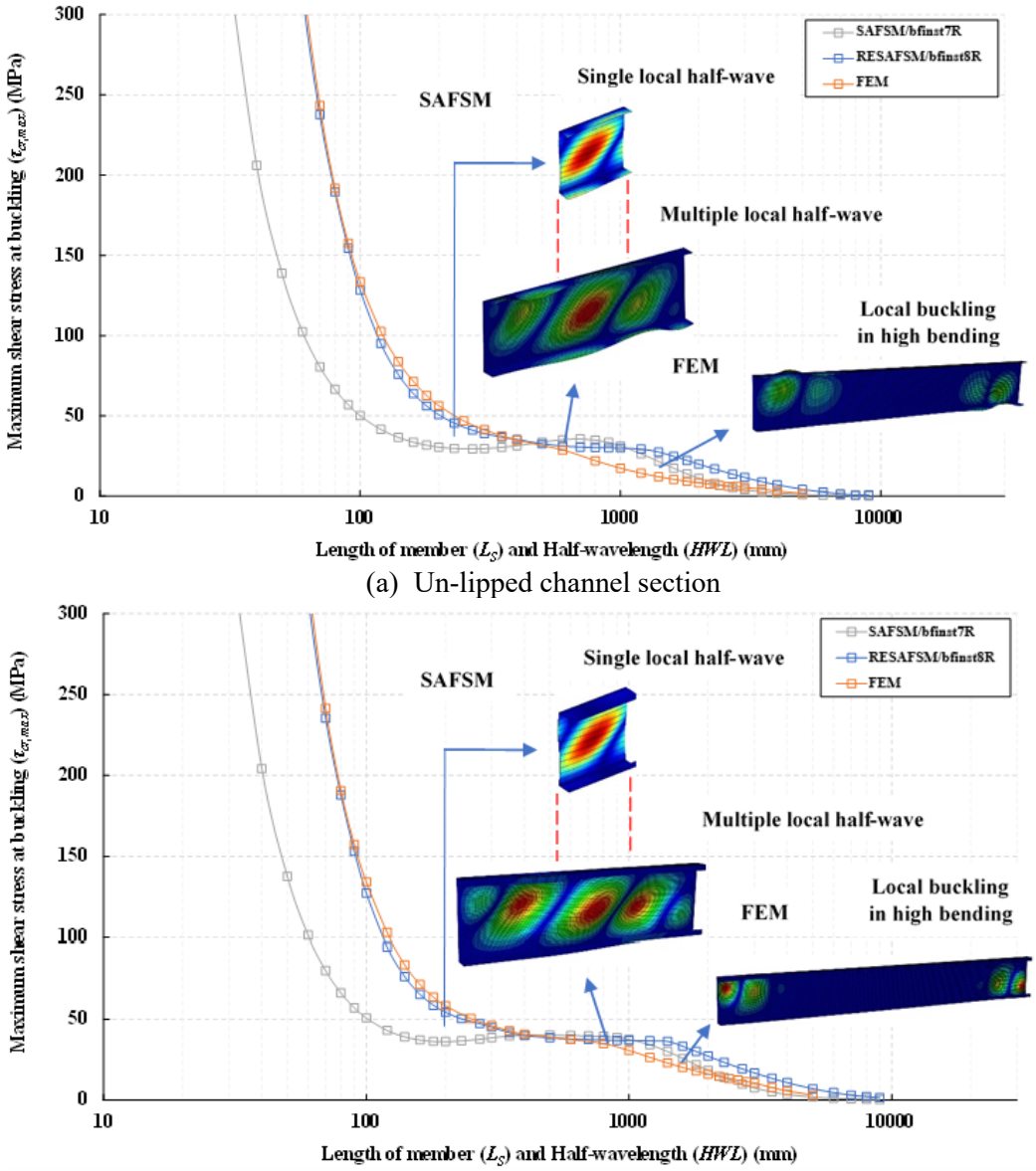

(a) Un-lipped channel section

b) Lipped channel section C200-40-15 (t = 1.0 mm)

(b) Lipped channel sections

Figure 2.13: The comparison of three different numerical approaches for buckling analysis of channel sections [24].

A new proposal for determination of the shear buckling coefficient for both un-lipped and lipped channel sections under combined bending and shear has been introduced by Pham et al. [24]. To provide a prediction of the shear buckling coefficient (k_v) for a full range of aspect ratio, this study combined two approximation curve parts. The first part is the current curve of elastic shear buckling determined according to AS/NZS 4600:2018 [7] Appendix D3, mainly predicting the shear buckling coefficient in the range of local shear buckling in the web panels. The second part mainly used to approximate the reduced shear buckling coefficients resulted from the effect of high bending moments at two section ends at higher aspect ratio. The intersection of two curve segments is implied

as a transition point ($AR_{m\text{-}v}$), at which the interaction of the local shear buckling in web and local bending moment in compressed flange can be observed at two ends of members under predominantly shear. The value of $AR_{m\text{-}v}$ can be determined by the following equations:

For lipped channel:
$$AR_{m\text{-}v} = 1.55 + 13.65\frac{b_f}{h} - 14\left(\frac{b_f}{h}\right)^2 \quad (2\text{-}12)$$

For un-lipped channel:
$$AR_{m\text{-}v} = 0.75 + 0.47\frac{b_f}{h} \quad (2\text{-}13)$$

where b_f is the flat portion of the flange, and h is the flat portion of the web.

For the case of aspect ratio (AR_0) $\leq AR_{m\text{-}v}$, the value of the shear buckling coefficient can be determined by AS/NZS 4600:2018 [7] directly. For the case of $AR_0 \geq AR_{m\text{-}v}$, the shear buckling coefficient can be determined as follows:

$$k_{v\text{-}0} = \left[C_1 - C_2\left(\frac{1}{AR_0{}^2}\right)^n\right]\left(\frac{1}{AR_0{}^2}\right)^n \quad (2\text{-}14)$$

where factor C_1 is equal to the value of the shear buckling coefficient at the transition point, which can be calculated according to AS/NZS 4600:2018 [7] Appendix D3. Factor C_2 can be determined as follows:

$$C_2 = \frac{C_1 - \dfrac{C_1}{\left(\dfrac{1}{AR_{m\text{-}v}{}^2}\right)^n}}{\left(\dfrac{1}{AR_{m\text{-}v}{}^2}\right)^n} \quad (2\text{-}15)$$

For lipped channel:
$$n = 0.3 \quad (2\text{-}16)$$

For un-lipped channel:
$$n = 0.2{+}0.9\frac{b_f}{h} \quad (2\text{-}17)$$

This explicit approach was developed based on the FEM buckling analysis and a new concept of average bending moment (ABM) for the elastic local buckling interaction, which can effectively provide an accurate prediction of the shear buckling coefficient accounting for both lipped and un-

lipped channels with combined bending and shear behaviour under predominantly shear. However, this approach cannot address the shear buckling coefficients of channel sections with narrow flanges. A channel with relatively narrow flanges may lead to twisting and lateral deformation instead of local bucking when it is under predominantly shear due to lack of lateral restraints.

2.3 NUMERICAL METHODS IN THIN-WALLED STRUCTURE ANALYSIS

In previous research, several numerical methods have been used to investigate the elastic shear buckling of thin-walled structures, including the semi-analytical finite strip method, the spline finite strip method and the finite element method. The SAFSM and SFSM are two common types of finite strip method, which involves subdividing the whole member into finite longitudinal strips. Both methods use polynomial functions for the transverse displacements. However, the SAFSM uses harmonic functions to estimate the longitudinal displacements, whereas the SFSM uses spline functions to allow more complex boundary conditions to be investigated.

2.3.1 Semi-analytical finite strip method

The semi-analytical finite strip was developed by Cheung [25] and Cheung [26] and was originally mainly used for the stress analysis of isotropic and orthotropic variable thickness plates with simply supported conditions in bending. Przmieniecki [27] applied this method to analyse the buckling stress of plate assemblies under biaxial compression. The application of this method was further extended into analysis of buckling behaviour of thin-walled cross-sections under longitudinal and transverse compression, longitudinal in-plane bending and shear by Plank and Wittrick [28]. Hancock [29] identified local, distortional and lateral -torsional buckling modes of beams by using the SAFSM. He also used this method to investigate the relationship between the buckling stress and buckle half wavelength for a beam known as the signature curve.

Recent research by Hancock and Pham [30], Hancock and Pham [31] has extended the SAFSM to analyse the pure shear buckling for channel sections. The studies use complex mathematical techniques to develop a computer program “bfinst7.cpp” to accomplish the SAFSM for shear buckling analysis. Pham SH, Pham CH and Hancock [32] [33] investigated the elastic shear buckling of lipped channel sections with complex web stiffeners by using the SAFSM. Pham and Hancock [4] also use the SAFSM analysis to investigate the effect of flange widths and lip sizes of the channel sections on the elastic shear buckling stress.

2.3.2 Spline finite strip method

The Spline finite strip method was developed based on the SAFSM by Cheung [25] by using spline functions in the longitudinal direction to replace the single half sine wave along the member length. The SFSM is characterised by an advantage that it allows more complex types of boundary conditions to be easily studied and buckling in shear can also be accounted for. The initial use of the SFSM was for the linear structural analysis of folded plate structure by Fan and Cheung [34]. The method involves subdividing a thin-walled member into several strips longitudinally, and each strip is free to deform both in plane and out of its plane. The ends of the section are normally free to deform in the longitudinal direction but are not allowed to deform in a cross-sectional plane.

The SFSM was used in investigations by Pham and Hancock [2] [35] and Pham and Hancock [16] to study the elastic buckling of thin-walled channel sections and thin-walled channel sections with intermediate web stiffeners in pure shear. These studies give insightful knowledge and an effective tool to determine the elastic shear buckling stress which is one of the essential inputs for the proposed direct strength method [36]. Pham and Hancock [5] have compared both the SAFSM and the SFSM to investigate the effect of flange width and lip size on the shear buckling stress of the lipped channel sections. Pham [37] has also provided solutions to determine the shear buckling of loading of the plate and thin-walled channel sections with holes using the SFSM analysis.

2.3.3 Finite element method

The FEM is a powerful and reliable tool with many functions to perform the most practical simulation and to produce numerical models. FEM software such as ABAQUS and ANSYS is commonly used to validate the experiments results, extend the test database and optimise the designs for tests. Keerthan and Mahendran [22] and Keerthan and Mahendran [6] have employed the FEM analysis to investigate the effect of flange width on elastic shear buckling stress of the LiteSteel sections and lipped channel beams respectively, and a series of equations for determination of shear buckling coefficients for these two types of sections have been developed based on the FEM buckling analysis results.

Pham [37], Pham, [38], Pham, [39] have also used the FEM and SFSM to investigate the shear buckling load of plate and thin-walled channel sections with holes as shown in **Figure 2.15**. In the FEM modelling, a shear flow distribution resulting from a shear force parallel with the web was applied at two section ends to simulate the practical condition. In addition, longitudinal stresses

caused by a couple of bending moments ($M/2 = V\,a/2$) are applied at two ends of the sections in the same direction in order to maintain equilibrium as shown in **Figure 2.14**. Pham, et al. [24] also used this shear stress distribution in the FEM simulation to investigate elastic local buckling of thin-walled channels under combined bending and shear.

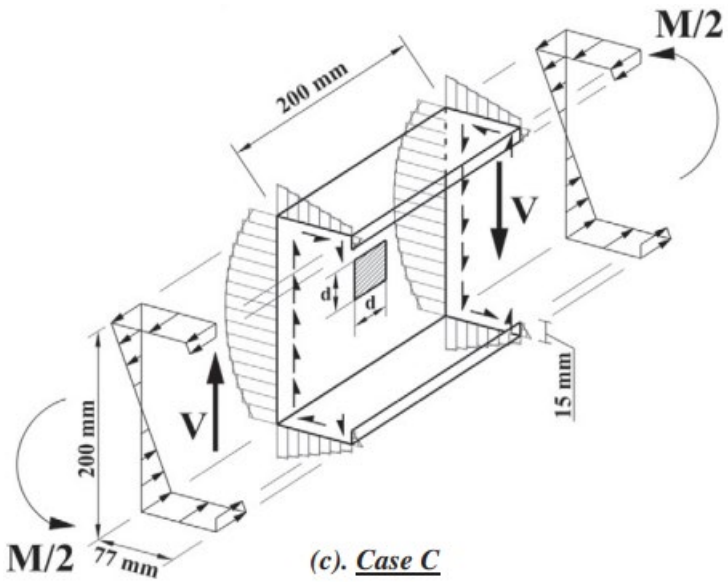

Figure 2.14: Stress distribution of lipped channel with central square [37].

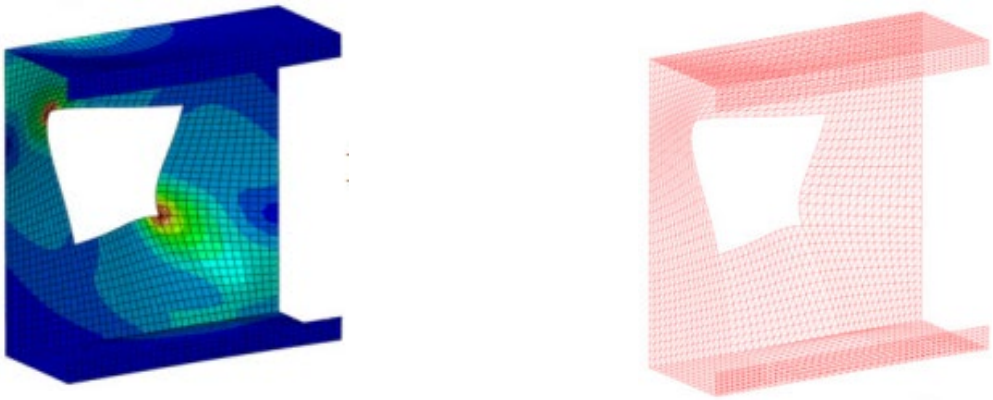

(a) FEM (b) SFSM

Figure 2.15: Shear buckling mode shapes from the FEM and SFSM [37].

2.4 SHEAR ELASTIC BUCKLING STRESS TO AUSTRALIAN STANDARD

AS/NZS 4600:2018 [7] specifies the design approach of elastic shear buckling of cold-formed steel members in its Appendix D3 based on the investigation of Keerthan and Mahendran [6]. The elastic shear buckling force (V_{cr}) of the web panel of members in shear can be determined as follows:

$$V_{cr} = \frac{\pi^2 E A_w k_v}{12(1-v^2)\left(\frac{b_1}{t}\right)^2} \tag{2-18}$$

where E is the modulus of elasticity of steel, v is the Poisson's ratio of steel, b_1 is the depth of the flat portion of web measured along the plane of the web panel and t is the thickness of web. k_v is the shear buckling coefficient calculated with respect to the following different conditions:

(a) For un-reinforced web, k_v should be equal to 5.34.

(b) For webs with transverse stiffeners

When $a/d_1 < 1.0$

$$k_v = 4.00 + \frac{5.34}{\left(\frac{a}{d_1}\right)^2} \tag{2-19}$$

When $a/d_1 \geq 1.0$

$$k_v = 5.34 + \frac{4.00}{\left(\frac{a}{d_1}\right)^2} \tag{2-20}$$

Where a refers to the shear panel length of an un-reinforced web element or clear distance between transverse stiffeners of reinforced web elements. d_1 is the clear web depth.

(c) For webs restrained at the top and bottom edges by flanges, the shear buckling coefficient can be determined as follows:

$$k_v = k_{ss} + k_n(k_{sf} - k_{ss}) \tag{2-21}$$

where k_{ss} and k_{sf} is the shear buckling coefficients of plates with simple-simple and simple-fixed boundary conditions calculated in accordance with **Eq (2-5)** to **Eq (2-8)** based on Keerthan and Mahendran [6] study.

k_n is the additional level of fixity at the web-flange juncture provided by flanges defined in **Table 2.3** below:

Table 2.3: Coefficient kn for open and hollow flange steel beams [7]

Section	k_n	
Lipped channel	0.23	$b_2/b_1 \geq 0.3$
Hollow flange channel	0.87	$b_2/b_1 \geq 0.3$
Triangular hollow flange beam	0.9	$b_2/b_1 \geq 0.3$
Rectangular hollow flange beam	$(0.82\ t_w/t_f - 0.41)$ $0.5 \leq t_w/t_f < 1.6$	$b_2/b_1 \geq 0.4$
	$0.90\ t_w/t_f \geq 1.6$	$b_2/b_1 \geq 0.4$

2.5 DIRECT STRENGTH METHOD FOR MEMBERS SUBJECT TO SHEAR

Elastic shear buckling force is one of the essential inputs in the direct strength method (DSM) to determine the nominal member shear capacity (V_v) when designing thin-walled members subject to shear. AS/NZS 4600:2018 [7] provides a detailed DSM approach to design the nominal shear capacity of beams without transverse web stiffeners, which follows the equation below:

For $\lambda_v \leq 0.815$:

$$V_v = V_y \tag{2-22}$$

For $0.815 \leq \lambda_v \leq 1.227$:

$$V_v = 0.815\sqrt{V_{cr} V_y} \tag{2-23}$$

For $\lambda_v \geq 1.227$:

$$V_v = V_{cr} \tag{2-24}$$

where:

$$\lambda_v = \sqrt{\frac{V_y}{V_{cr}}} \tag{2-25}$$

$$V_y = 0.6 A_w f_y \tag{2-26}$$

where A_w is the cross-sectional area of the web element, f_y is the design yield stress and V_{cr} is the elastic shear buckling force determined by **Eq (2-18)**.

CHAPTER 3 : NUMERICAL SIMULATION

3.1 CHAPTER INTRODUCTION

This chapter describes non-linear numerical simulations of shear elastic buckling analysis based on the finite element method (FEM) using the software package ABAQUS/Standard. This study has developed a series of finite element models in order to investigate the shear buckling behaviour of both lipped and un-lipped channel sections with narrow flange under predominantly shear using the *BUCKLE procedure in ABAQUS. The shear buckling loads V_{cr} can be generated from the models for different cases of flange widths and aspect ratios (AR). Furthermore, the shear buckling load can then be used to calculate the shear buckling coefficients for each case. Usings the results of the buckling analyses, a new explicit approach is developed to predict the shear elastic buckling coefficient of channel sections with narrow flanges.

This chapter also provides detailed finite strip models including the semi-analytical finite strip method and the resemi-analytical finite strip method. The buckling results from the FEM models are benchmarked against the buckling results from the SAFSM models and reSAFSM models using computer programs bfinst7R.cpp and bfinst8R.cpp respectively. The major difference between the SAFS models and the reSAFSM models is the boundary conditions. In the SAFSM model, the boundary conditions at two section ends are free to distort and allow unrestrained shear buckling. Whereas the reSAFSM models are developed to account for simply supported boundary conditions. The major difference between the FE models and reSAFSM is the effect of high bending moments at the two end sections which are in equilibrium with the shear action in the FEM analysis. The detailed comparisons of the shear buckling behaviours and the shear buckling mode between the different methods are discussed later in this chapter. The reference section geometry properties of sections for all the three models are the same. Specifically, the web depth of the channels is 200 mm, the lip size is 20 mm, The flange size varies from 5 mm (very narrow flanges) to 120 mm (wide flanges). The length of the channel varies from 30 mm to 9000 mm to observe the transition of different buckling modes depending upon the member lengths. The thickness for all cases is 2 mm. It can be noted that the dimensions used in the sections are all centreline and not overall. Young's modulus for elasticity (E) of 200000 MPa and Poisson's ratio (μ) of 0.3 are taken.

3.2 FINITE ELEMENT MODELLING

To investigate the influence of different flange widths on the elastic shear buckling behaviour of thin-walled channel sections, finite element method (FEM) models using ABAQUS/Standard (ABAQUS 6.14-2) are developed for elastic buckling analysis. The deformable 4-node doubly curved shell element with reduced integration known as S4R with a relatively fine mesh size of 5x5 mm is used for the whole channels modelling. S4R is the small-membrane strain shell element using a Mindlin-Reissner plate type of flexural theory that includes transverse shear.

As shown in **Figure 3.1**, simply supported boundary conditions of the channel sections are modelled by restraining the two ends of cross-sectional planes in X and Y directions to prevent the sectional deformation occurring at the two ends while allowing displacements to happen in the Z direction. To prevent the longitudinal movement of the whole model happening in the Z direction, a restraint is attached at the mid-point of one section end. In addition, there is no lateral restraint applied along the longitudinal edges of the web panels so that the flange twisting of the channels is likely to be observed.

For the elastic buckling analysis using ABAQUS/Standard, the distribution of shear and normal stress, which are caused by the shear force balanced with the end bending moments, are modelled by using distributed shell edge loads on the two ends of the sections. The loading conditions for the FE model in this study refer to the stress distribution case provided by [37], [40] and [24] as shown in **Figure 3.2.** The shear flow distributed in web, flanges and lips caused by a couple of shear forces is added at two sectional ends. The resulting longitudinal stresses from a couple of bending moments ($M=V \times a/2$) in the same direction are applied at both end section in an opposite way in order to balance with the moment caused by two coupling shear forces which is automatically generated by the simply supports at two section ends. The moment gradients which can generate a shear force in the FEM models are modelled by the distributed edge loads in Abaqus. The shear elastic buckling loads and their corresponding shear buckling modes can be generated through the *BUCKLE procedure in ABAQUS/Standard.

Using the FEM models for elastic buckling analysis, the linear eigenvalue buckling process can generate the magnitudes of shear actions at buckling. The eigenvalue can be used to calculate the

buckling loads by multiplying the reference loads, and then the buckling stress can be back-calculated by the obtained buckling load.

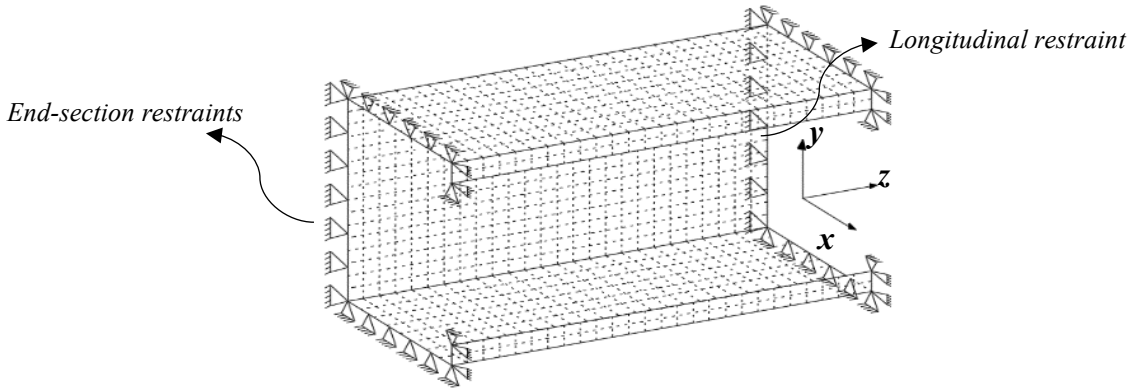

Figure 3.1: Simply supported boundary conditions at two section ends of a channel.

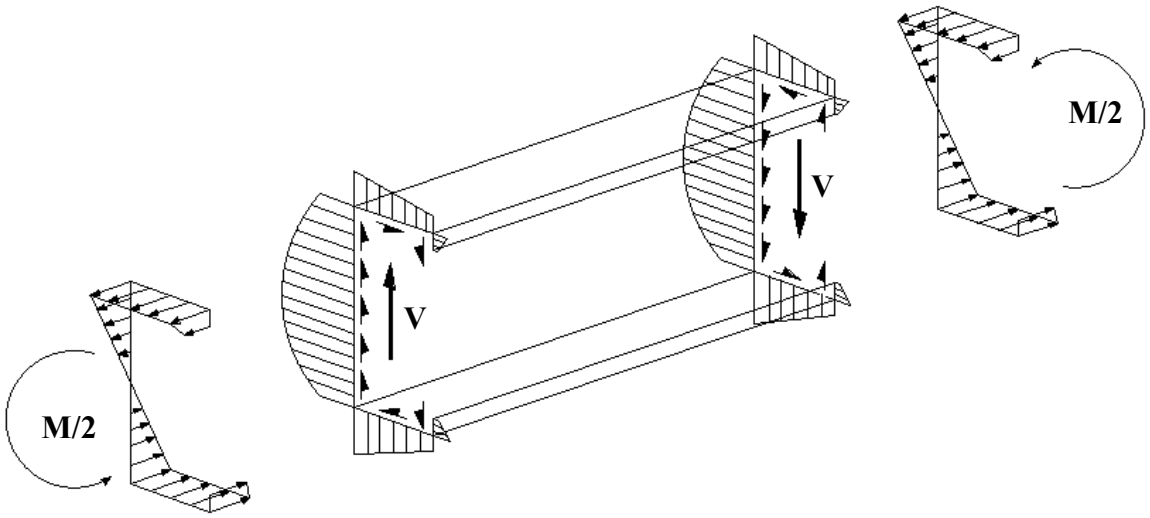

Figure 3.2: Stress distributions of the channel section.

3.3 MESH CONVERGENCE

The mesh convergence study is performed to determine the optimal mesh size used for finite element modelling in buckling analyses. Using this size of element can ensure the accuracy of the model but prevent excessive use of computational resources. **Figure 3.3** indicates the relationship between the number of elements of a single channel model and the shear buckling stress.

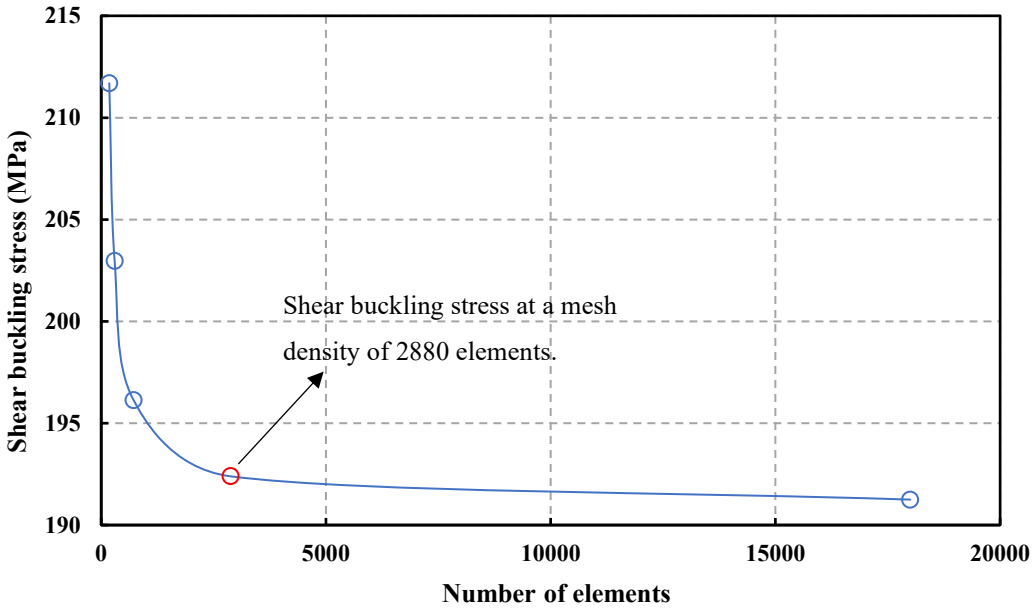

Figure 3.3: Mesh convergence study.

A mesh density of 2880 elements corresponding to a mesh size of 5 x 5 mm is the optimal mesh size to provide an accurate result without a considerable consumption of time and computational resources. When the mesh size reduces from 20 x 20 mm to 5 x 5 mm, the shear buckling stress presents a significant change by 10.03%. However, when further reducing the mesh size to 2 x 2 mm, the shear buckling stress only changes by 0.59%. Therefore, the mesh size of 5 x 5 mm is selected in the study for finite element modelling.

3.4 SEMI-ANALYTICAL AND RE-SEMI-ANALYTICAL FINITE STRIP MODELLING

To assess the performance of the FEM models and achieve a more comprehensive elastic buckling analysis for channels under predominantly shear, the elastic buckling results from the FEM models and those from the SAFSM and reSAFSM are compared.

The semi-analytical finite strip method embedded in the computer program (bfinst7.cpp in Thinwall 2) is used to investigate the channels whose section ends are free to distort. The resemi-analytical finite strip method based on a computer program bfinst8R.cpp in Thinwall 3 is used to investigate the effect of simply supported section ends on the elastic shear buckling, which is also consistent with the end boundary conditions in the FEM models.

The geometry of the channel sections used in both SAFSM and reSAFSM is the same as that in the FEM model. For both the SAFSM and reSAFSM analyses, all the members with different flange widths are subdivided into 36 strips including 8 strips in web, 4 strips in flanges and 5 strips in lips. The member length for the channels for both methods vary in a wide range from 30 mm to 9000 mm.

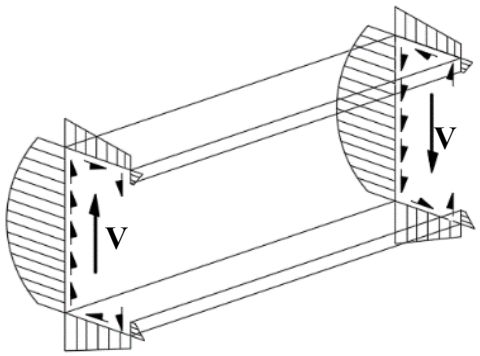

(a) Shear stress distribution for both the SAFSM and reSAFSM models

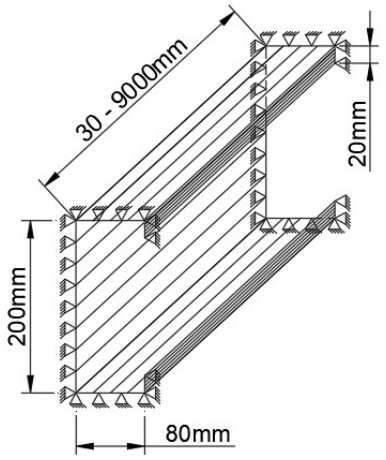

(b) Boundary condition and loading in reSAFSM

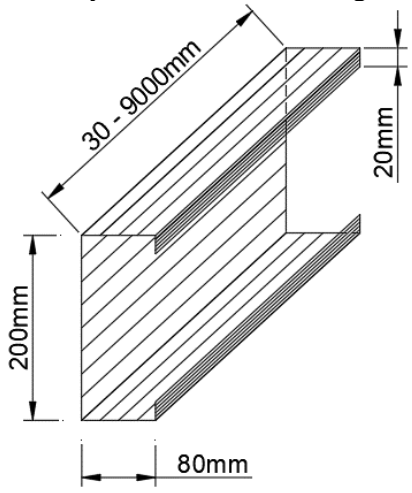

(c) Boundary conditions and loading in SAFSM

Figure 3.4: The loading and boundary conditions for the SAFSM and reSAFSM models.

The shear stress distribution and boundary conditions for both SAFSM and reSAFSM models are shown in **Figure 3.4**. The channel section is subjected to a couple of parallel shear forces at the two section ends. Because the SAFSM can only solve elastic buckling analyses with uniform longitudinal stress distribution, the computer software incorporating the SAFSM only allows pure bending or pure shear actions rather than creating a moment gradient for static equilibrium of the section undergoing the more practical actions of combined bending and shear. Therefore, there is no action of bending at the ends of the channel sections. There is a major difference in boundary conditions of the SAFSM and reSAFSM. In the SAFSM models, the channel is free to distort at two section ends. Whereas all edges of the end cross-sections of the reSAFSM channel are simply supported in order to prevent cross-sectional deformation. For the longitudinal direction, the SAFSM and reSAFSM can allow the plates to underdo twisting and lateral deformations along the channel member.

3.5 FINITE ELEMENT MODEL VALIDATION BY FINITE STRIP METHOD

The reliability of the finite element models for shear elastic buckling analyses is validated by comparing the shear buckling results and the corresponding shear buckling mode shapes generated from the finite element models and reSAFSM models. Both the FEM and reSAFSM models use the simply supported boundary conditions, which eliminates the effect of different boundary conditions on the shear buckling results. The most significant difference between these two methods is that the finite element models consider static equilibrium of the section by using bending moment to balance the shear force. However, the reSAFSM models only allow pure shear actions without any effect of bending moment on the section.

The shear buckling mode shapes for both lipped and un-lipped channel sections obtained from the finite element model with flange widths of 5 mm, 40 mm and 120 mm are compared with those from the reSAFSM models shown in **Figure 3.5** and **Figure 3.6** below. It can be seen that the two methods can generate very similar buckling mode shapes for both lipped and un-lipped channels. More specifically, diagonal shear buckle bands can be observed across the shear span in the case of flange width of 40 mm and 120 mm. Whereas a clear twisting buckling mode shape can be observed in the case of a very narrow flange.

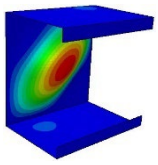

(a) Buckling mode shape for 120 mm flange width by FEM

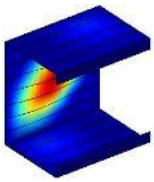

(b) Buckling mode shape for 120 mm flange width by reSAFSM/bfinst8.cpp

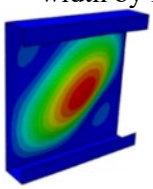

(c) Buckling mode shape for 40 mm flange width by FEM

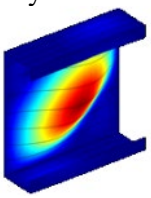

(d) Buckling mode shape for 40 mm flange width by reSAFSM/bfinst8.cpp

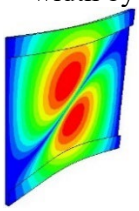

(e) Buckling mode shape for 5 mm flange width by FEM

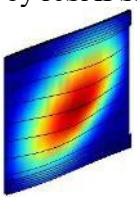

(f) Buckling mode shape for 5 mm flange width by reSAFSM/bfinst8.cpp

Figure 3.5: Shear buckling mode shapes of lipped channels with flange width of 120 mm, 40 mm and 5 mm.

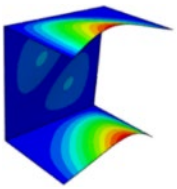

(a) Buckling mode shape for 120 mm flange width by FEM

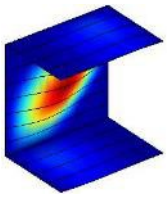

(b) Buckling mode shape for 120 mm flange width by reSAFSM/bfinst8.cpp

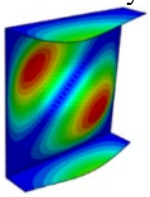

(c) Buckling mode shape for 40 mm flange width by FEM

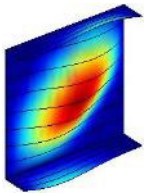

(d) Buckling mode shape for 40 mm flange width by reSAFSM/bfinst8.cpp

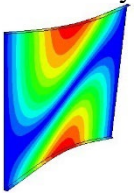

(e) Buckling mode shape for 5 mm flange width by FEM

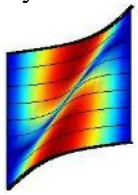

(f) Buckling mode shape for 5 mm flange width by reSAFSM/bfinst8.cpp

Figure 3.6: Shear buckling mode shapes of un-lipped channels with flange width of 120 mm, 40 mm and 5 mm.

Table 3.1, **Figure 3.7**, **Figure 3.8** and **Figure 3.9** compare the shear buckling stress generated by the FEM buckling analyses ($V_{cr,\ FEM}$) and the reSAFSM/bfinst8.cpp models ($V_{cr,\ reSAFSM}$) for both lipped and unlipped channel sections in terms of the flange widths of 5 mm, 40 mm and 120 mm at member lengths from 200 mm to 400 mm. To compare the shear buckling stress by both methods under predominantly shear, the member lengths are selected from 200 mm to 800 mm to minimise the effect of bending on the shear buckling stress. It can be seen that the values of shear buckling stresses obtained by the finite element models and reSAFSM/bfinst8.cpp are very close to each other. However, several significant differences can be found in the group of C200120 sections at medium long member lengths. For lipped channel section C200120, the shear buckling stress by the finite element model is much lower than that of the reSAFSM/bfinst8.cpp when the section has a member length of 800 mm. Meanwhile, a similar result can be found in unlipped channel section C200120 at the member lengths from 400 mm to 800 mm. This because the finite element models take account of the bending moment to maintain the static equilibrium of the sections, which can have significant effect on the shear buckling stress of channels with a large flange. A more significant difference between the two resulting curves can be seen in the unlipped channels as shown **Figure 3.9** (b) because the wider flanges without lips to stiffen the other longitudinal edge of the flange will buckle much easier. More detailed explanation is discussed later. In conclusion, by comparing the shear buckling stress obtained from two different methods, the finite element models can be approved as providing a series of reliable buckling analyses to investigate the buckling behaviour of both lipped and unlipped channels with narrow flanges under predominantly shear.

Table 3.1: Shear buckling stresses by FE models and reSAFSM/bfinst8.cpp models.

Designation	Lipped channel		Un-lipped channel	
	$\tau_{cr,\ FEM}$ (MPa)	$\tau_{cr,\ reSAFSM}$ (MPa)	$\tau_{cr,\ FEM}$ (MPa)	$\tau_{cr,\ reSAFSM}$ (MPa)
C2005-200	138.62	136.81	79.56	88.47
C2005-400	52.38	59.53	16.59	16.64
C2005-600	25.74	32.97	6.81	6.47
C2005-800	15.09	21.61	3.64	3.43
C20040-200	185.64	179.18	184.11	165.53
C20040-400	125.07	126.85	113.32	112.61
C20040-600	114.92	118.85	92.73	94.78
C20040-800	108.265	114.17	71.91	84.14
C200120-200	189.46	184.93	183.47	184.69
C200120-400	134.58	134.92	60.58	129.48
C200120-600	122.38	125.69	35.37	118.28
C200120-800	107.83	122.28	24.67	114.15

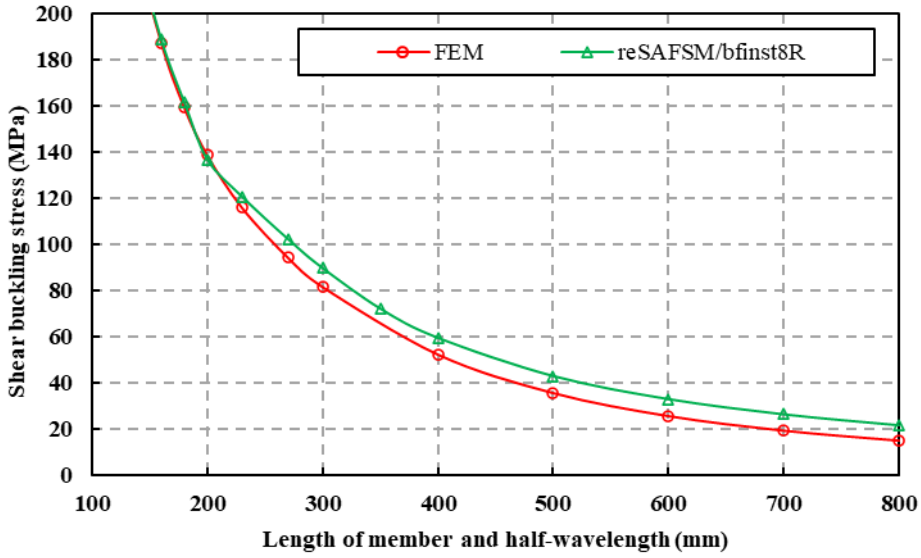

(a). Lipped channel section C200-5-20 (t = 2.0 mm)

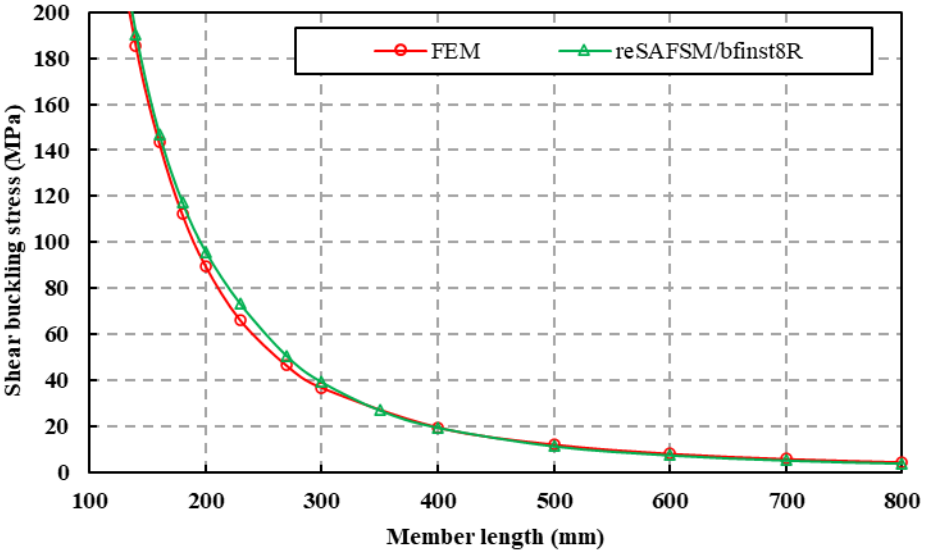

(b). Un-lipped channel section C200-5 (t = 2.0 mm)

Figure 3.7: Comparison of elastic buckling results from three different methods for a narrow flange width.

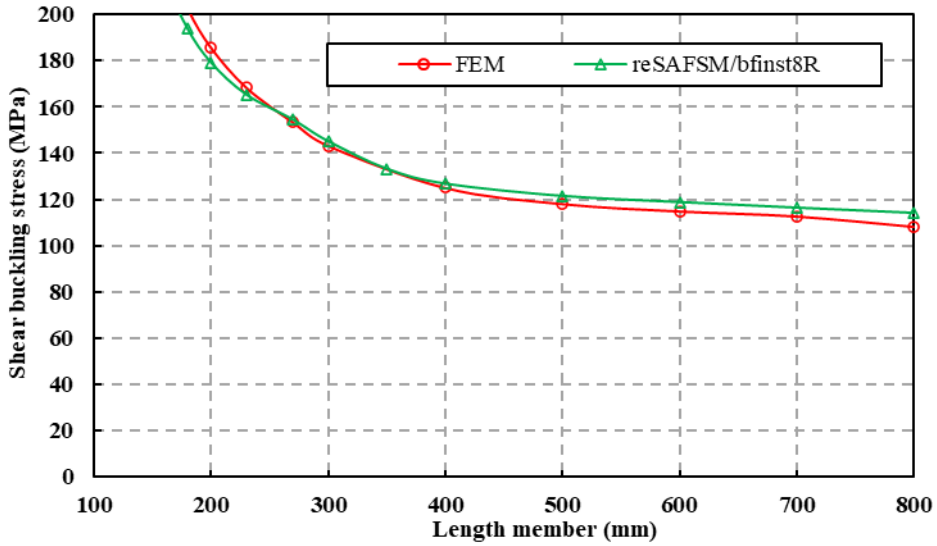

(a). Lipped channel section C200-40-20 (t = 2.0 mm)

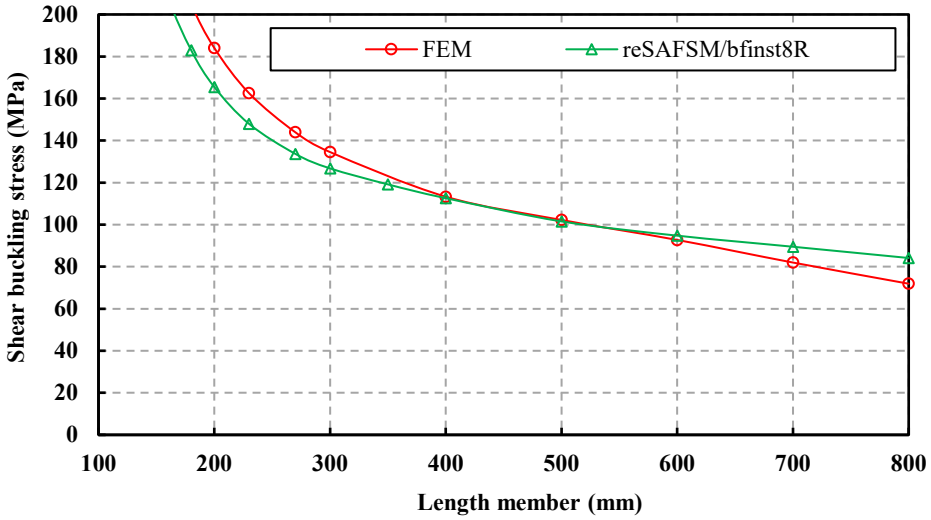

(b). Unlipped channel section C200-40 (t = 2.0 mm)

Figure 3.8: Comparison of elastic buckling results from three different methods for a medium flange width.

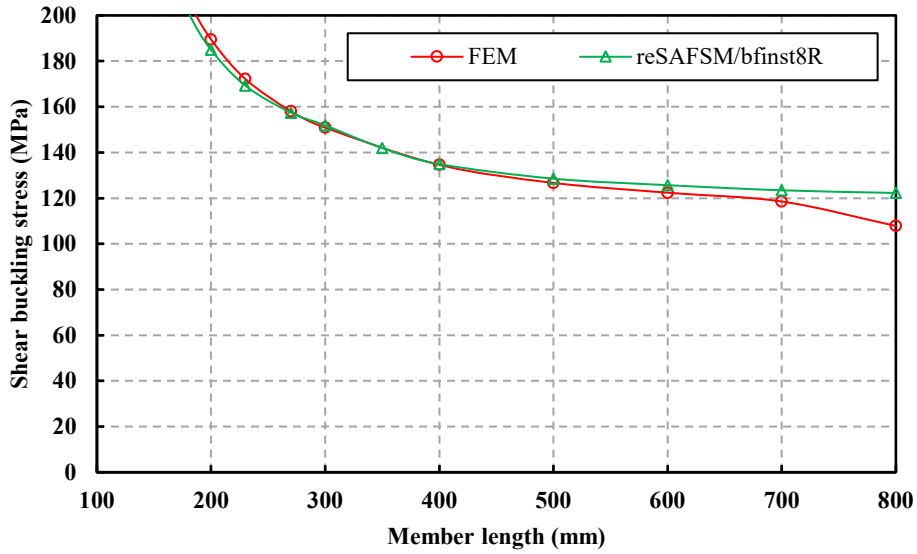

(a). Lipped channel section C200-120-20 (t = 2.0 mm)

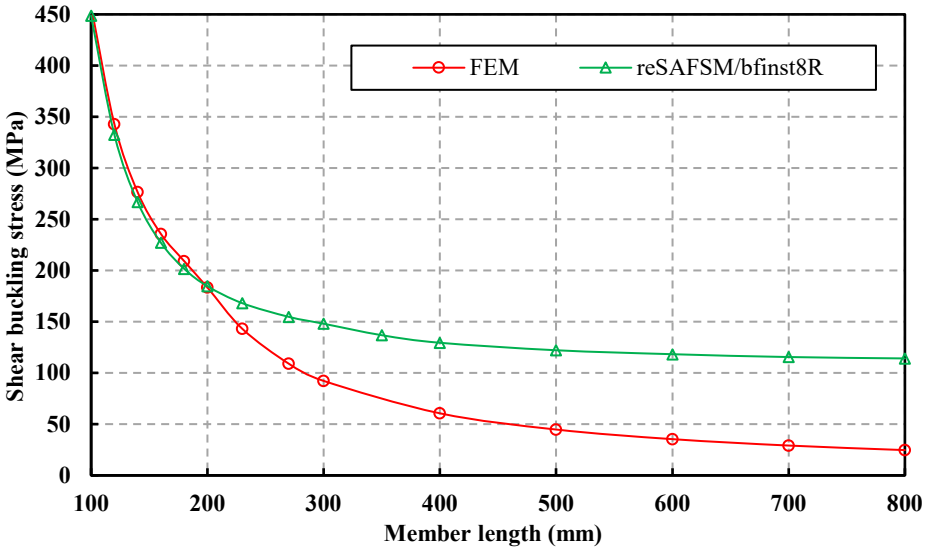

(b). Unlipped channel section C200-120 (t = 2.0mm)

Figure 3.9: Comparison of elastic buckling results from three different methods for a large flange width.

3.6 CHAPTER CONCLUSION

This chapter described the numerical modelling developed using the FEM, SAFSM and reSAFSM to study the elastic shear buckling behaviour of lipped and un-lipped channel sections for a full range of flange sizes. In the FEM models, the simply supported boundary condition is used at two section ends to prevent cross-sectional deformation. The shear and normal stress, caused by the shear force balanced with the end bending moments are modelled by using distributed shell edge loads. The bending moment is considered in the FEM models to maintain the static equilibrium of the whole section.

The SAFSM and reSAFSM models are also developed to benchmark the shear buckling results obtained from the FEM. In SAFSM models, the section ends are not restrained and are free to distort, while the simply supported condition is used in the reSAFSM models. The shear stress distribution is modelled by a couple of parallel shear forces at the two section ends, and no action of bending is involved for both SAFSM and reSAFSM models.

The reSAFSM models are selected for validation of the FEM models because the same boundary condition is used. The shear buckling results and the corresponding shear buckling mode shapes generated by the reSAFSM models highly agree with those of the FEM models. In addition, an obvious reasonable difference can be observed between the FEM and reSAFSM results in the case of unlipped channels with large flange width. This is due to the significant influence of high bending moment on the large flange with an unstiffened longitudinal edge.

CHAPTER 4 : ELASTIC SHEAR BUCKLING BEHAVIOUR OF CHANNELS WITH FULL RANGE OF FLANGE WIDTHS BY DIFFERENT ANALYSIS MODELS

4.1 CHAPTER INTRODUCTION

This chapter provides a detailed parametric study of local elastic shear buckling behaviour of channel sections with a full range of flange widths based on the buckling analysis results using the finite element method (FEM), semi-analytical finite strip method (SAFSM) and resemi-analytical finite strip method (reSAFSM). The aim of the parametric study is to provide a deeper understanding of the elastic shear buckling behaviour of thin-walled channel sections in shear with various sizes of flanges and discuss the differences in the buckling analysis results produced by these three methods. The detailed buckling results from each method for both lipped and un-lipped channels are presented in **Appendix A** and **Appendix B**.

To observe the elastic shear buckling behaviour of lipped and un-lipped channels of 200 mm in depth with different sizes of flanges, from large (160 mm) to narrow flange (5 mm) width, three buckling analysis models are used: FEM (using ABAQUS), SAFSM (using bfinst7.cpp) and reSAFSM (using bfinst8.cpp). The elastic shear buckling strength and behaviour are investigated via the relationship between the elastic shear buckling coefficient (k_v) and the change in member lengths (from FEM and reSAFSM/bfinst8.cpp) and member half-wavelengths (HWL) (from SAFSM/bfisnt7.cpp). The range of member lengths and half-wavelength is from 100 mm (AR = 0.5) to 9000 mm (AR = 45). The equation for determination of k_v can be back-calculated from **Eq (4-1)** and is given as follows:

$$k_v = \frac{12\,(1-\nu^2)}{\pi^2\,E}\left(\frac{b_1}{t}\right)^2 \tau_{cr} \tag{4-1}$$

where E is the Young's modulus, v is Poisson's ratio, b_1 is the depth of the web panel, t is the thickness of the web and τ_{cr} is shear buckling stress. For the reSAFSM and SAFSM analyses, the shear buckling stress τ_{cr} can be calculated based on the outcomes of shear force multiplied by the load factor, which

is then divided by the cross-section area of the web panel A_w. For the FEM models, the shear force can be calculated by the initial bending moment in the sections divided by the member length. The outcomes are then multiplied by the eigenvalue from the FEM buckling analysis in order to obtain the shear buckling force. The value of τ_{cr} can be determined by the buckling force divided by A_w.

4.2 SEMI-ANALYTICAL FINITE STRIP METHOD USING BFINST7R.CPP

This section demonstrates the buckling behaviour for both lipped and un-lipped channels in shear using the semi-analytical finite strip method incorporated in the program bfinst7R.cpp. It is noted that the ends of the half-wavelength are free to distort, and the buckle half-wave can be understood as a part of a very long member without restraints from the end conditions.

4.2.1 Lipped channels

The relationship of the shear buckling coefficient (k_v) and half-wavelength is illustrated using traditional buckling signature curves for shear as shown in **Figure 4.1**. For narrow flange widths smaller than 40 mm ($b_2/b_1 < 0.2$), the buckling coefficient keeps dropping as an increase in half-wavelengths without a clear minimum point. This occurs because a narrow flange provides very limited lateral restraints along the two longitudinal edges of the web panel, so the great twisting of the web section can be clearly observed. Typical buckling modes for the lipped channel with a narrow flange width of 5 mm at half-wavelengths of 200 mm, 1000 mm and 2000 mm are shown in **Figures 4.2** (a), (b) and (c). It can be seen that the channel buckles in a twisting mode and both section ends are free to distort. In addition, for a short and medium half-wavelength (less than 1000 mm), the curves of greater flange widths shift up as the ratios of flange width to half-wavelength becomes higher as shown in **Figure 4.2**, but when the half-wavelength exceeds 1000 mm, all the curves drop and converge to 0.0 with the significant increase in the half wavelength. This behaviour indicates that the lateral restraints provided by the flanges have negligible effect on the shear buckling capacity of channels with very long half-wave lengths.

For the flange width of 40 mm ($b_2/b_1 = 0.2$), the curve drops dramatically within the half-wavelength range of 100 mm to 200 mm, and then remains almost flat in the half-wavelength range of 200 mm to 400 mm. This implies that the flange to web ratio of 0.2 is adequate to provide lateral restraints to the longitudinal edges of the web plate to prevent twisting buckling occur at short half-wavelengths. As shown in **Figure 4.2**(d), the clear local buckling failure mode can be observed in the channel

section at 200 mm half-wavelength since the flange with flange-web ratio of 0.2 can stiffen the web portion. However, the buckling mode shapes shown in **Figures 4.2**(e) and (f) prove that the flange-web ratio of 0.2 is inadequate to provide lateral restraint to the web at a medium or long half-wavelength longer than 1000 mm, leading to the channels buckling sideways.

For the lipped channels with flange widths larger than 40 mm ($b_2/b_1 > 0.2$), the signature curves show clear minimum points at the half-wavelength of 200 mm and all curves converge to around 6.56. Accordingly, the channel buckles in a pure local buckling mode because the wide flange can provide sufficient lateral restraint to prevent the channels from twisting. **Figure 4.2** (g) shows the clear local buckling modes of the channel with a flange width equal to 120 mm ($b_2/b_1 = 0.6$) at a half wavelength of 200 mm. However, as the half-wavelength exceeds 200 mm, the curves of wide flange widths increase until the half-wavelength reaches around 800 mm followed by a dramatic drop. The corresponding shear buckling modes of channels with a flange width of 120mm for a medium half-wavelength of 1000 mm and long half-wavelength of 2000 mm are shown in **Figures 4.2** (h) and (i), which indicates that the buckling modes switch from local buckling to distortional buckling as the half-wavelength becomes longer.

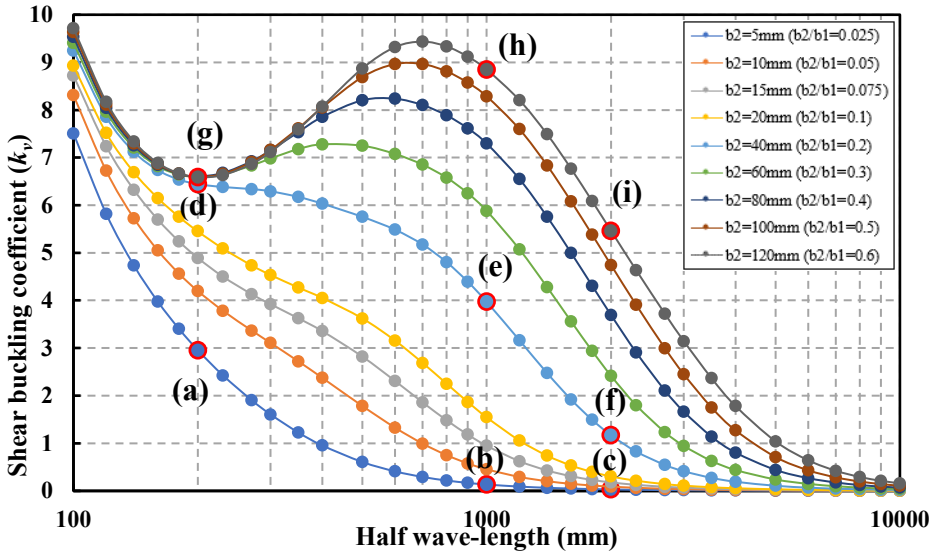

Figure 4.1: The behaviour of shear buckling coefficient against half-wavelength from bfinst7R.cpp.

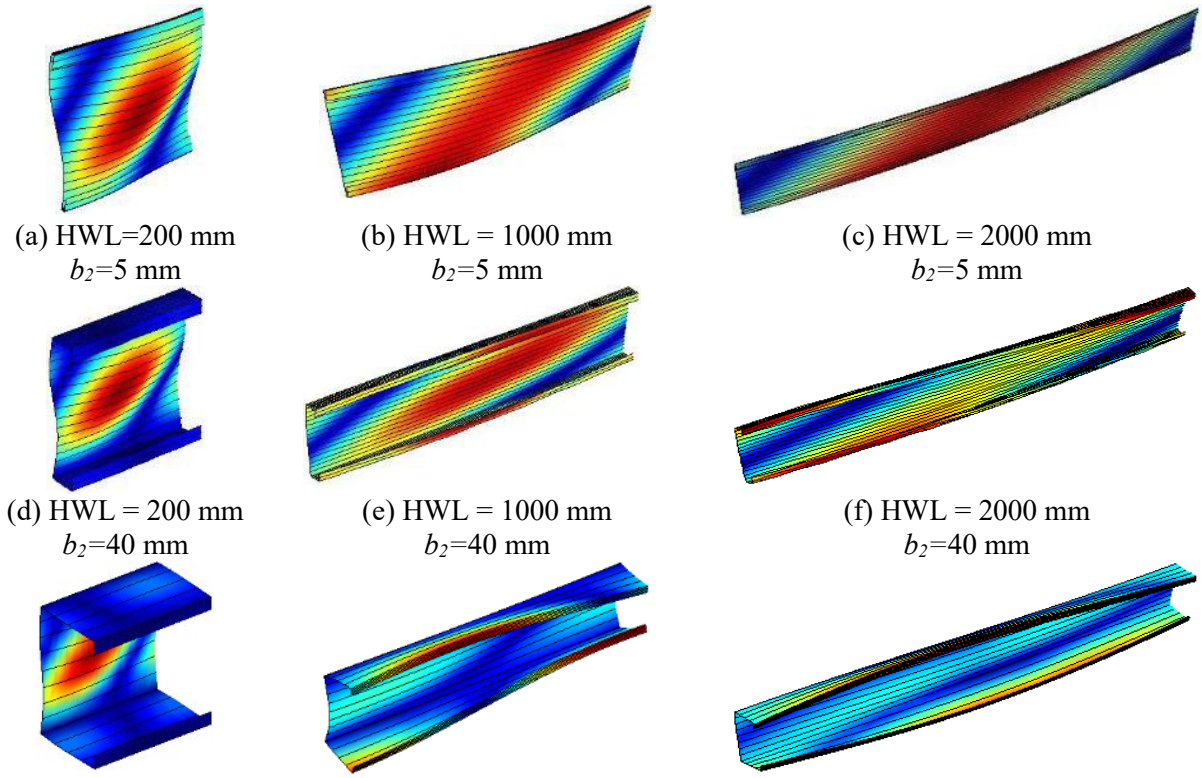

(a) HWL=200 mm b_2=5 mm | (b) HWL = 1000 mm b_2=5 mm | (c) HWL = 2000 mm b_2=5 mm

(d) HWL = 200 mm b_2=40 mm | (e) HWL = 1000 mm b_2=40 mm | (f) HWL = 2000 mm b_2=40 mm

(g) HWL = 200 mm b_2=120 mm | (h) HWL = 1000 mm b_2=120 mm | (i) HWL = 2000 mm b_2=120 mm

Figure 4.2: Shear buckling modes of lipped channels for flange width of 5 mm, 40 mm and 120 mm.

4.2.2 Un-lipped channels

Figure 4.3 presents the buckling analysis results of un-lipped channel sections using bfinst7R.cpp. It can be found that the shear buckling coefficient *kv* is lower than the lipped channel in a full range of half wavelengths. This is because the flange is unstiffened at one free edge and local buckling becomes easier to occur at the flange. Similar to lipped channels, the un-lipped channels with very narrow flanges also present twisting buckling for the full range of half-wavelengths as shown in buckling modes in **Figures 4.4** (a-c). The unlipped channels with flange width of 40 mm also show clear minimum points at the half-wavelength of 200 mm, which indicates the flange is wide enough to restrain the web plate and enable the web plate to buckle locally at small half-wavelengths as shown in **Figure 4.4**(d). When the half-wavelength increases to approximately 500 mm, the value of k_v drops dramatically and converges to 0.0 as the half-wavelength becomes extremely long. This is also because to the shear buckling modes switch from local to distortional buckling as indicated in **Figures 4.4** (e) and (f). For the unlipped channel with a flange size greater than 40 mm, the behaviour of signature curves is also similar to those of lipped channels, showing a clear twisting buckling as a result of a switch of buckling modes from local to distortional buckling as the increase of half-

wavelength. **Figures 4.4** (g-i) demonstrate the elastic shear buckling modes of un-lipped channels with a flange width of 120 mm at 200 mm, 1000 mm and 2000 mm. The channel at 200 mm presents a clear local buckling in the web. When the length increases to 1000 mm and longer, a clear twisting buckling can be observed in the entire channels.

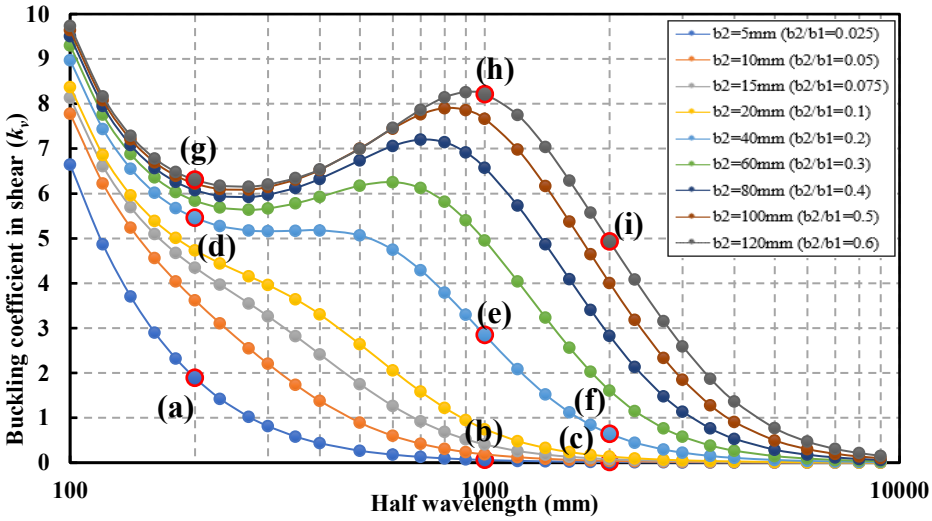

Figure 4.3: The behaviour of shear buckling coefficient against half wavelength from bfinst7R.cpp for un-lipped channels.

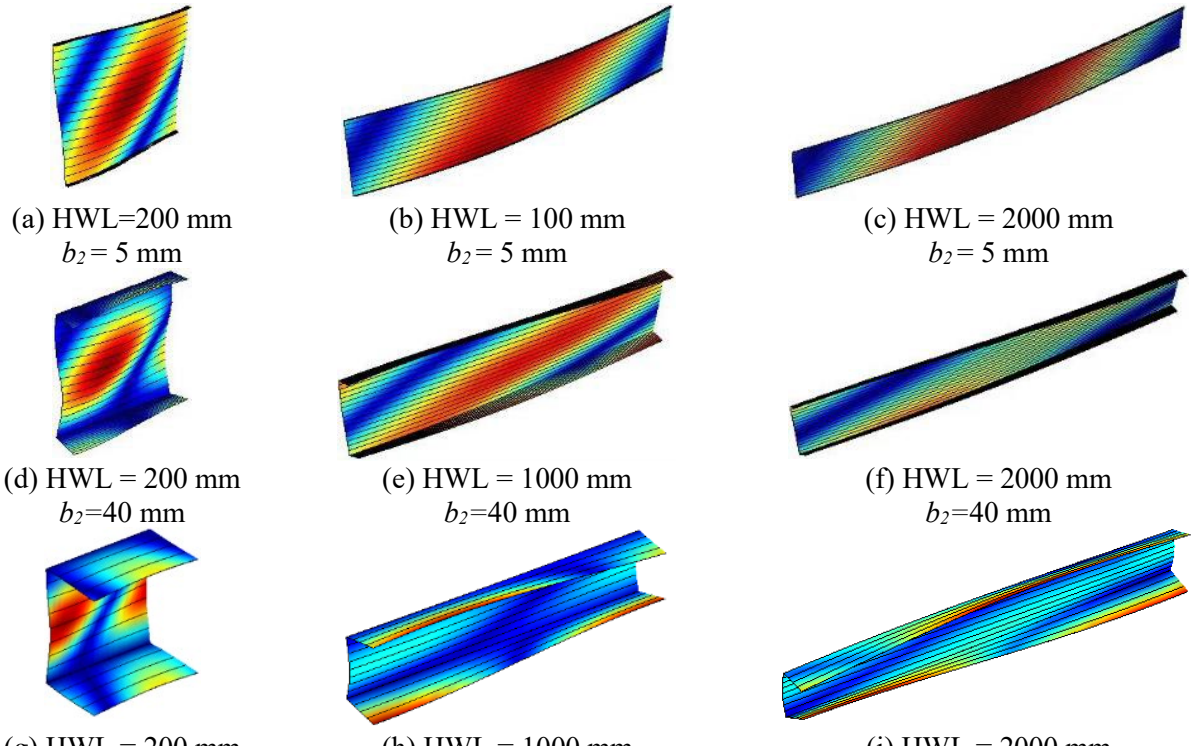

(a) HWL=200 mm b_2 = 5 mm
(b) HWL = 100 mm b_2 = 5 mm
(c) HWL = 2000 mm b_2 = 5 mm
(d) HWL = 200 mm b_2=40 mm
(e) HWL = 1000 mm b_2=40 mm
(f) HWL = 2000 mm b_2=40 mm
(g) HWL = 200 mm b_2=120 mm
(h) HWL = 1000 mm b_2=120 mm
(i) HWL = 2000 mm b_2=120 mm

Figure 4.4: Shear buckling modes of un-lipped channels for flange widths of 5 mm, 40 mm and 120 mm.

4.3 RESEMI-ANALYTICAL FINITE STRIP METHOD USING BFINST8R.CPP

This section describes the elastic shear buckling behaviour for both lipped and un-lipped channels in pure shear using the resemi-analytical finite strip method incorporated in the computer program bfinst8R.cpp. Specifically, the relationships between the shear buckling coefficient and member length of the channel sections with simply supported boundary conditions in a full range of flange widths are compared and explained.

4.3.1 For lipped channels

Figure 4.5 indicates the relationship between the shear buckling coefficient of the lipped channel and member length in terms of different flange widths from 5 mm to 160 mm obtained from the reSAFSM. For the narrow flange width ($b_2/b_1 < 0.2$), the shear buckling coefficients drop from around 22.0 and converge to 0.0 with the increase of the member length. The corresponding buckling modes in **Figures 4.6** (a-c) indicate that the channel sections at member lengths of 200 mm, 1000 mm and 2000 mm present a single buckle half-wave in a twisting mode between two restrained ends. It should be noted that the shear buckling mode of the channel section at the member length of 200 mm is governed by local buckling in the web panel. This is due to the presence of the 20 mm lip to stiffen the flange, making the section buckle locally rather than twisting at a short member length when it is under pure shear. When the member length becomes increasingly longer, the lipped flange cannot provide adequate lateral restraint, leading to the occurrence of the twisting buckling mode in the channels at long member length.

It can be noted that in the curve of 40 mm ($b_2/b_1 = 0.2$), the shear buckling coefficient drops rapidly from 23.3 to 6.72 at the channel length of 400 mm and then keeps flat until the length is up to 800 mm. The channel starts to exhibit a clear local buckling mode in this range as shown in **Figure 4.6** (d). This indicates that the flange width of 40 mm can provide enough lateral restraints to longitudinal edges of the web plate to avoid channel twisting and force the channel to buckle locally. However, as the length exceeds 800 mm, the shear buckling coefficient then decreases as a result of the buckling mode of the channel switching from local buckling to twisting buckling. It can be seen in **Figure 4.6** (e) that the channels at the length of 1000 mm have a mixed buckling mode combining the local buckling in the double buckle half-wave in the web panel with the twisting buckling mode in the flanges. As the length increases further from 1000 mm to 2000 mm, the channel buckles sideways as shown in **Figure 4.6** (f), indicating the ineffectiveness of the lateral restraint the flange to the web at a long member length.

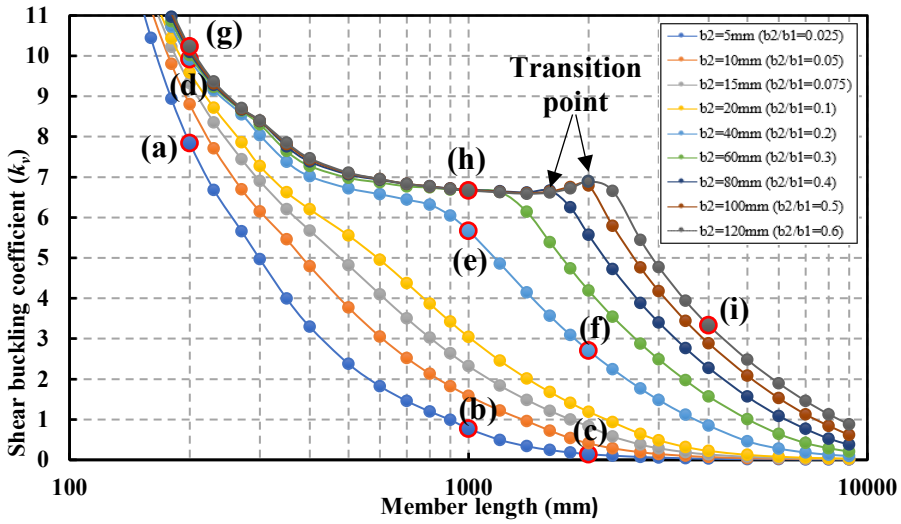

Figure 4.5: The behaviour of shear buckling coefficient against member length for lipped channels from bfinst8R.cpp.

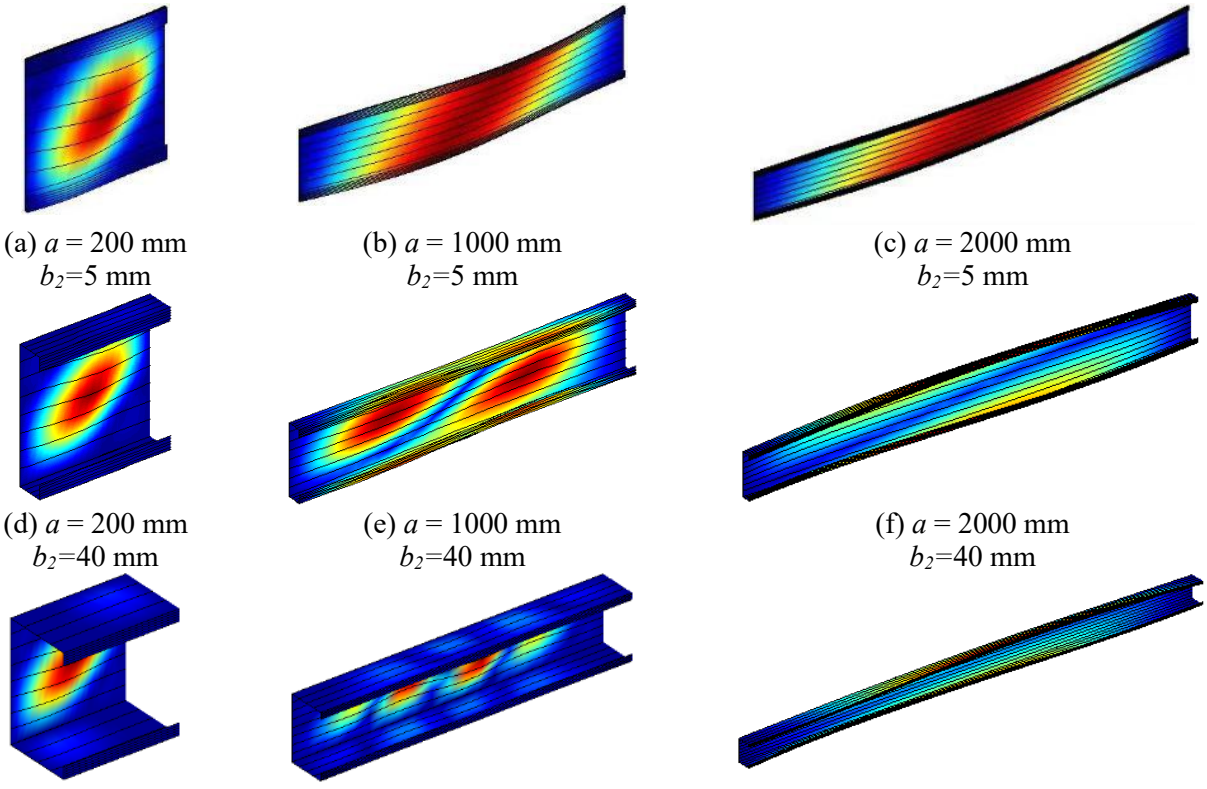

(a) a = 200 mm b_2=5 mm

(b) a = 1000 mm b_2=5 mm

(c) a = 2000 mm b_2=5 mm

(d) a = 200 mm b_2=40 mm

(e) a = 1000 mm b_2=40 mm

(f) a = 2000 mm b_2=40 mm

(g) a = 200 mm b_2=120 mm

(h) a = 1000 mm, b_2=120 mm

(i) a = 4000 mm b_2=120 mm

Figure 4.6: Shear buckling modes of lipped channel for flange widths of 5 mm, 40 mm and 120 mm by the reSAFSM.

For the channels with flange width larger than 40 mm (b_2/b_1 > 0.2), all the curves exhibit an almost identical behaviour and coincide with each other. However, as the length continues to increase, the curves will experience a dramatic reduction at the transition point. In addition, it can be seen that the

wider the flanges, the later the transition point will appear. This is because the greater flanges can provide more equivalent lateral restraints to the web when the channel is assumed only under pure shear. Therefore, the channel with greater flanges can be kept in local buckling mode for a longer length. **Figures 4.6** (g) and (h) exhibit the shear buckling modes of channel sections with a large flange width of 120 mm at member lengths of 200 mm and 1000 mm. It can be seen that the large flange widths can give more lateral restraints to the web, forcing the web panel to buckle locally in multiple half-waves. However, as the length exceeds approximately 3000 mm, the large flange fails to provide adequate lateral restraints, leading to the channel buckling sideways as shown in **Figure 4.6** (i).

4.3.2 For un-lipped channels

The buckling analysis results of reSAFSM for un-lipped channels are plotted in **Figure 4.7**, with very similar behaviour as the lipped channels. It can also be seen that the value of *kv* for un-lipped channels is lower than for the lipped channels due to the unstiffened free edge of the flange. Therefore, the lip can improve the shear buckling capacity of channels. **Figures 4.8** (a-c) show the shear buckling modes of un-lipped channels for flange widths of 5 mm obtained by reSAFSM. The twisting buckling in a single half-wave can also be found in the reSAFSM models for the narrow flange even though the member length is short.

As the flange becomes wider to 40 mm, lateral restraint can be provided to the longitudinal edges of the web, and the local buckling can be observed in the web and flanges at a short length of 200 mm as shown in **Figure 4.8** (d). When the length reaches 1000 mm, the channel has a double local buckle half-wave in the web and a twisting buckling in the flange as a result of gradually losing lateral restraint to the web as shown in **Figure 4.8** (e). The corresponding twisting buckling mode of the channel at 2000 mm is shown in **Figure 4.8** (f), which means the negligible lateral restraints provided by the flange at a long member length.

Figures 4.8 (g-h) show the shear buckling modes of the channels with a flange size of 120 mm. A clear local buckling can be observed at a length of 200 mm, and a multiple buckle half-wave can be seen in the channel at a length of 1000 mm. The transitional point can also be observed at around 2000 mm as the buckling failure mode transfers from local buckling to twisting buckling. **Figure 4.8** (i) shows that the channel buckles sideways at a length of 4000 mm.

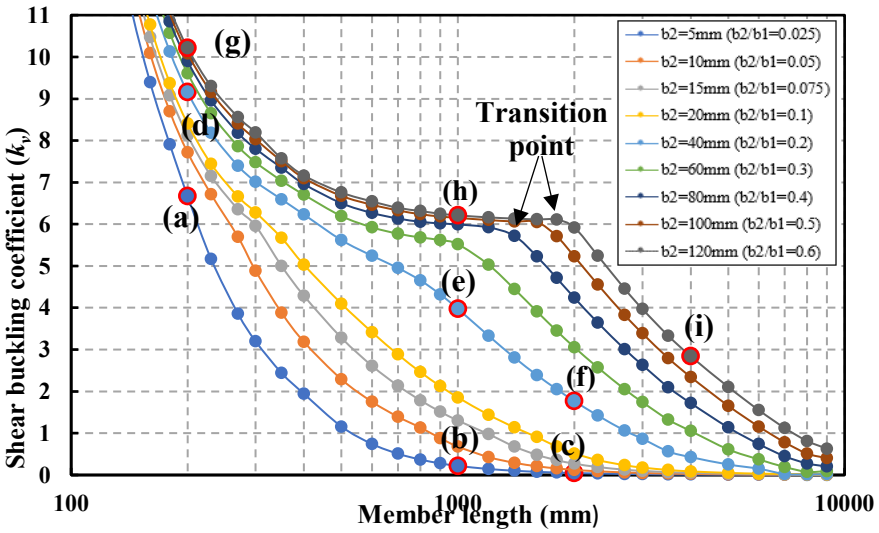

Figure 4.7: The behaviour of shear buckling coefficient against member length for un-lipped channels from bfinst8R.cpp.

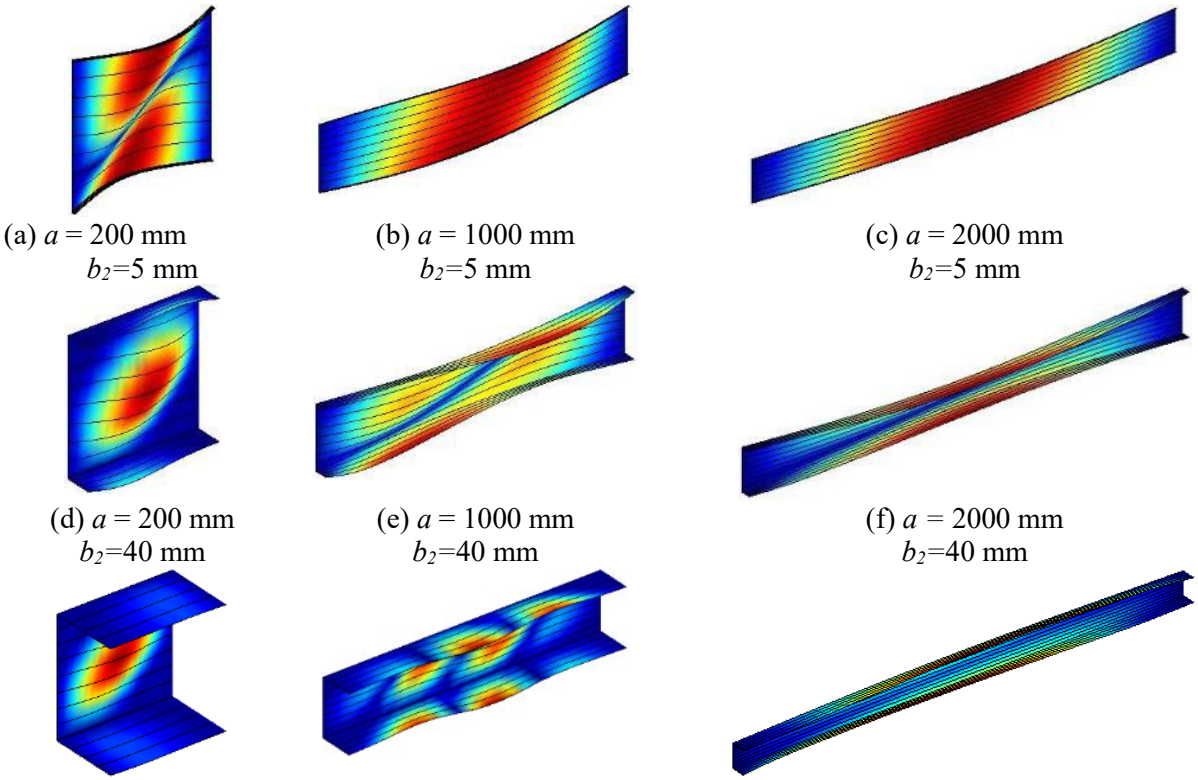

(a) a = 200 mm b_2=5 mm
(b) a = 1000 mm b_2=5 mm
(c) a = 2000 mm b_2=5 mm
(d) a = 200 mm b_2=40 mm
(e) a = 1000 mm b_2=40 mm
(f) a = 2000 mm b_2=40 mm
(g) a = 200 mm b_2=120 mm
(h) a = 1000 mm b_2=120 mm
(i) a = 4000 mm b_2=120 mm

Figure 4.8: Shear buckling modes of un-lipped channel for flange widths of 5 mm, 40 mm and 120 mm by the reSAFSM.

4.4 FINITE ELEMENT METHOD USING ABAQUS

This section demonstrates the elastic shear buckling behaviour for both lipped and un-lipped channels under predominantly shear using the finite element method incorporated in the software ABAQUS. The shear buckling analyses using the FEM can consider the effect of bending moment at the two end sections which are in equilibrium with the shear action. The first mode (the lowest eigenvalue) is used to calculate the shear buckling coefficient.

4.4.1 For lipped channels

Figure 4.9 demonstrates the buckling analysis results using FEM for lipped channels in shear with various flange width to depth ratios from 0.025 to 0.6. It can be seen that all curves of lipped channel sections are very close and decrease rapidly from the member length of 100 mm to 200 mm. This reveals that the aspect ratio in this range can significantly impact the buckling coefficient of lipped channel sections in shear. In contrast, the influence from different flange widths is not considerable. For the channels with flange width less than 40 mm ($b_2/b_1 < 0.2$), the curves decrease rapidly from 100 mm until the length increases to approximately 3000 mm, all the curves then coincide with each other and converge to 0.0. The reason is because the flange widths are too small to provide enough lateral restraints to the web plate. Hence, the channels with very small flanges will twist when they are under predominantly shear. As can be seen in **Figures 4.10** (a-c), the corresponding shear buckling modes for sections with a narrow flange of 5 mm exhibit a clear twisting at the member length of 200 mm, 1000 mm and 2000 mm. However, for the channels with a flange width greater than 40 mm ($b_2/b_1 > 0.2$), the curves stop dropping after around the member length of 300 mm and remain unchanged until the length reaches approximately 1000 mm, and then have an immediate decrease. For this range of flange width, the flanges are wide enough to restrain the web plate and force the whole section under predominantly shear to buckle by local buckling mode rather than twisting buckling. However, as the member length increases, the transition points will occur on each curve where an immediate drop of the buckling coefficient can be observed. This behaviour occurs because bending on the long-length channels reduces the shear buckling capacity of channels. As shown in **Figures 4.10** (g-i), the shear buckling mode of s short channel section has a clear local buckling. However, as the member length increases to a medium or long length (greater than 1000 mm), the local buckling can be observed in bending at two cross-sectional ends due to high bending moment. Furthermore, as the flange becomes larger than 80 mm, the curves shift to the left for the same value of the k_v. This result can be explained that a channel with too much large b_2/b_1 can reduce

the buckling capacity of channels in shear since a very wide flange under shear action will have local buckling before the web plate.

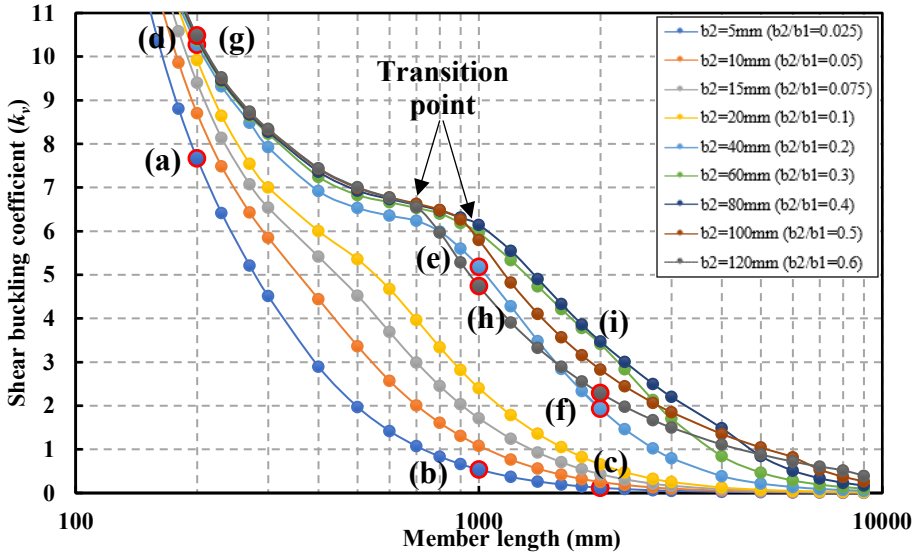

Figure 4.9: The behaviour of shear buckling coefficient against member length for lipped channels from FEM.

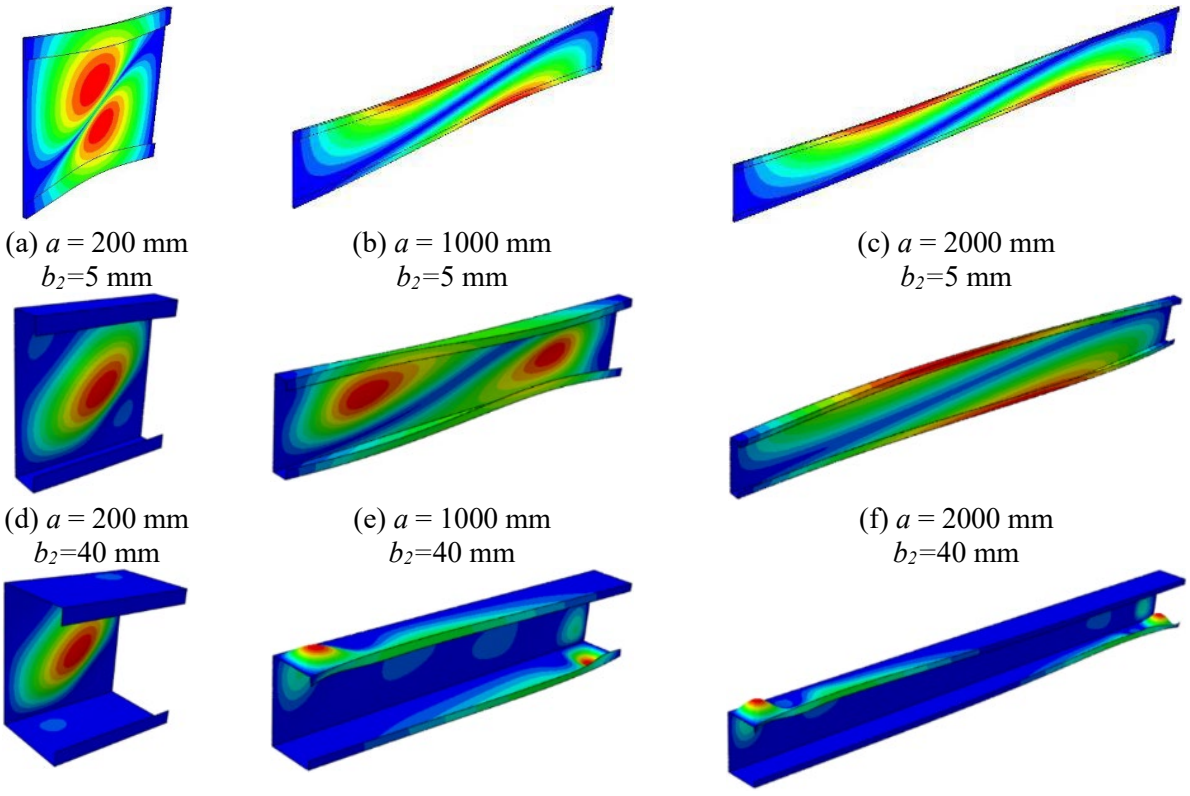

(a) a = 200 mm b_2=5 mm | (b) a = 1000 mm b_2=5 mm | (c) a = 2000 mm b_2=5 mm

(d) a = 200 mm b_2=40 mm | (e) a = 1000 mm b_2=40 mm | (f) a = 2000 mm b_2=40 mm

(g) a = 200 mm b_2=120 mm | (h) a = 1000 mm b_2=120 mm | (i) a = 2000 mm b_2=120 mm

Figure 4.10: Shear buckling modes of lipped channel for flange widths of 5 mm, 40 mm and 120 mm by the FEM.

4.4.2 For un-lipped channels

The results of the buckling analysis and the corresponding shear buckling modes for un-lipped channel from FEM are plotted in **Figure 4.11** and **Figure 4.12**. The twisting buckling mode can also be observed in those channels with very narrow flanges since the flanges cannot provide enough lateral restraint to the web plate as shown in **Figures 4.12** (a-c). Hence, the curves always decrease smoothly without any transitional point as the member length becomes longer. However, when the flange width increases to 40 mm, the transitional point can be observed at the member length of around 600 mm. The occurrence of the transition point can be attributed to the effect of the high bending moment at the two end sections. Therefore, it can be seen that the channel at 200 mm can have a local buckling mode as shown in **Figure 4.12** (d). However, as the length increases over the transition point, the local buckling occurs at both ends of the flange because of high bending moment. As the length increases further to 2000 mm, the local buckling mode of the channel switches from the local buckling to the twisting buckling as shown in **Figures 4.12** (e-f). As the flange width increases further from 40 mm to 120 mm, the curves shift to the left for the same value of the k_v. This can be attributed to the large flanges without the lips to stiffen one edge very easily buckle locally due to the high bending moment at the two section ends, leading to a reduction of the shear buckling capacity of the whole sections. As can be seen in **Figures 4.12** (g-i), the flange with a larger size of 120 mm always buckles earlier than the web at 200 mm, 1000 mm and 2000 mm.

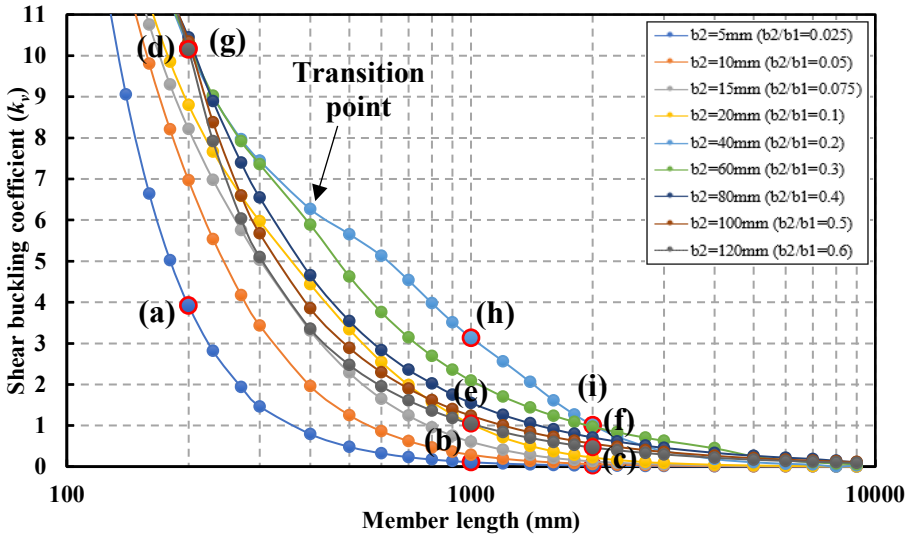

Figure 4.11: The relationship between the buckling coefficient and length in terms of various flange widths using FEM for un-lipped channels.

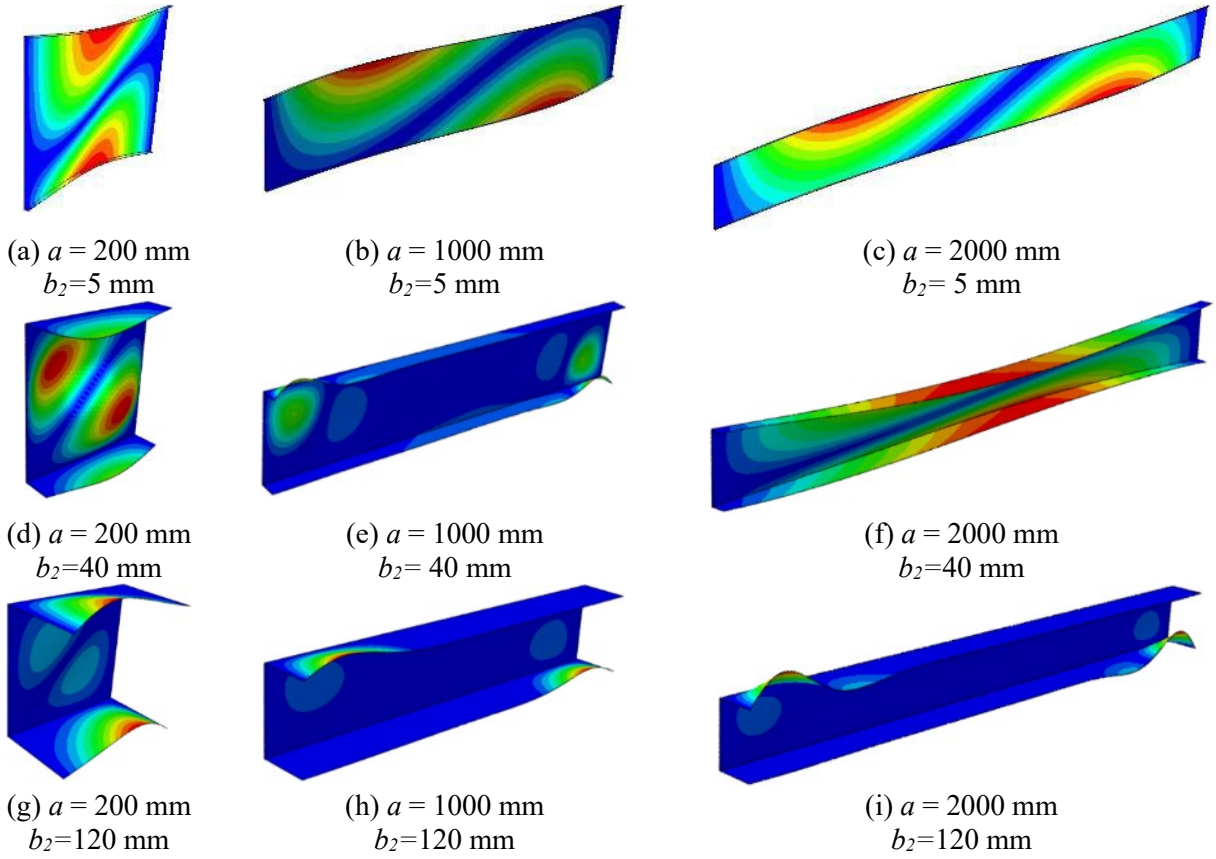

(a) a = 200 mm, b_2=5 mm; (b) a = 1000 mm, b_2=5 mm; (c) a = 2000 mm, b_2= 5 mm

(d) a = 200 mm, b_2=40 mm; (e) a = 1000 mm, b_2= 40 mm; (f) a = 2000 mm, b_2=40 mm

(g) a = 200 mm, b_2=120 mm; (h) a = 1000 mm, b_2=120 mm; (i) a = 2000 mm, b_2=120 mm

Figure 4.12: Shear buckling modes of un-lipped channel for flange widths of 5 mm, 40 mm and 120 mm by the FEM.

4.5 COMPARISON OF SHEAR BUCKLING RESULTS FROM THREE DIFFERENT METHODS

The elastic shear buckling behaviour of channel sections regarding the relationship between shear buckling coefficient and half wavelength or length from three different methods was explained previously. To compare the differences in the results from three different methods, three couples of buckling stress to member length (for the FEM and reSAFSM curves) or half wavelength curves (for the SAFSM curves) for both lipped and unlipped channel sections are shown in **Figure 4.13**, **Figure 4.14** and **Figure 4.15** with a very narrow flange width of 5 mm, a medium flange width of 40 mm and a large flange width of 120 mm. The signature curve generated by bfinst7R.cpp describes the relationship between buckling stress and a single buckling half-wavelength, whereas the curves from bfinst8R.cpp and the FEM are plotted with the relationship between buckling stress and member length which can contain multiple half-wavelengths.

For both lipped and unlipped channels, it can be seen that the curves from the reSAFSM/bfisnt8R and the FEM have very similar behaviour and are shifted to the right compared to the SAFSM/bfinst7R for a very narrow and medium flange width. This can be attributed to the difference in the boundary conditions mentioned previously. Both the section ends in the FEM and reSAFSM models are simply supported to avoid cross-sectional distortion, while the section ends in the SAFSM are free to distort. However, as the length or half-wavelength increases longer than 1000 mm, the three curves can start to converge together gradually. This is due to the reduced impact of restrained boundary conditions on the shear buckling capacity for long-length channels.

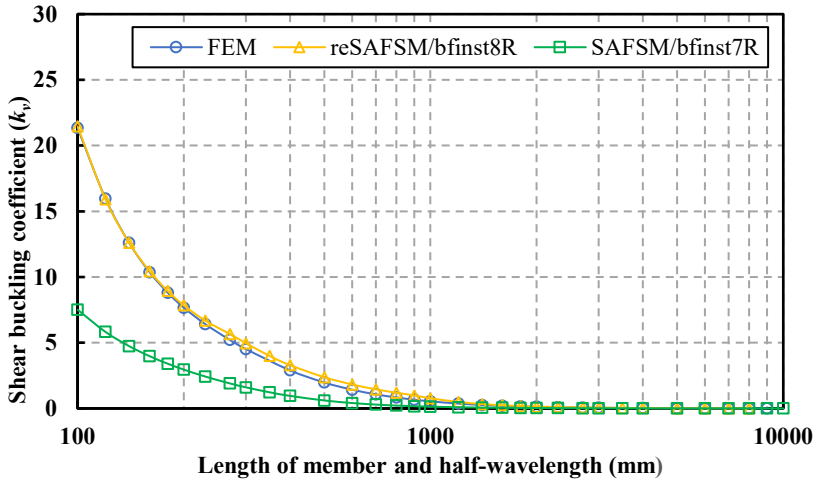

a). Lipped channel section C200-5-20 (t = 2.0 mm)

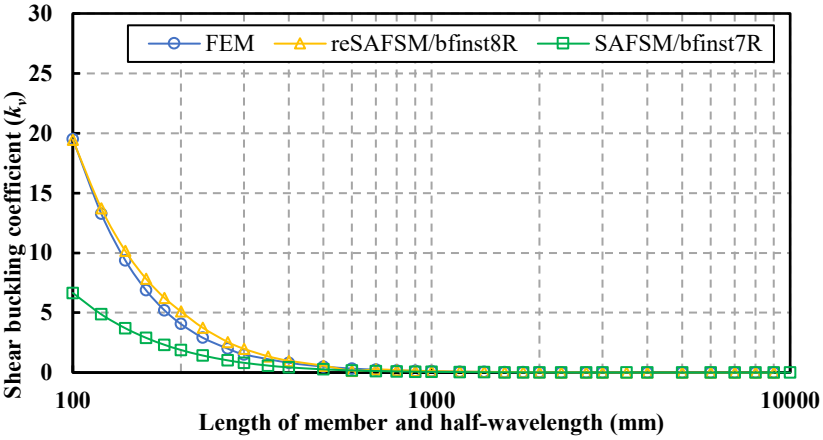

b). Un-lipped channel section C200-5 (t = 2.0 mm)

Figure 4.13: Comparison of elastic buckling results from three different methods for a narrow flange width.

In addition, when looking at the lipped channel with a large flange, the FEM curve can perform similarly to the reSAFSM curve for the member length shorter than 700 mm. However, as the member length exceeds 700 mm, the FEM curve starts to decrease rapidly while the reSAFSM curve remains

flat. For the FEM models at a longer member length under predominantly shear, the local buckling will occur at two section ends due to high bending moment. Thus, the shear buckling stress of the FEM models with longer member lengths is lower than those from the reSAFSM even though they have the same boundary condition. This is because the impact of a high bending moment at two section ends is in equilibrium with the shear action in the FEM models. This similar behaviour can also be observed in unlipped channels. The FEM curve can coincide with the reSAFSM curve before the member length exceeds 200 mm, which is then followed by a rapid decrease after 200 mm. This can be attributed to the fact that the flange without a lip to restrain another edge more easily has local buckling due to the high bending moment at two section ends. Therefore, the buckling analysis results obtained from the FEM are more accurate than the reSAFSM when the equilibrium of the whole member is considered.

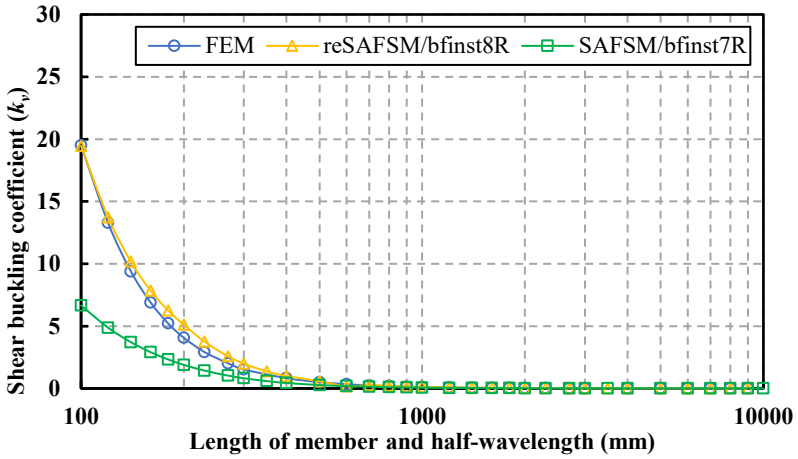

a). Lipped channel section C200-40-20 (t = 2.0 mm)

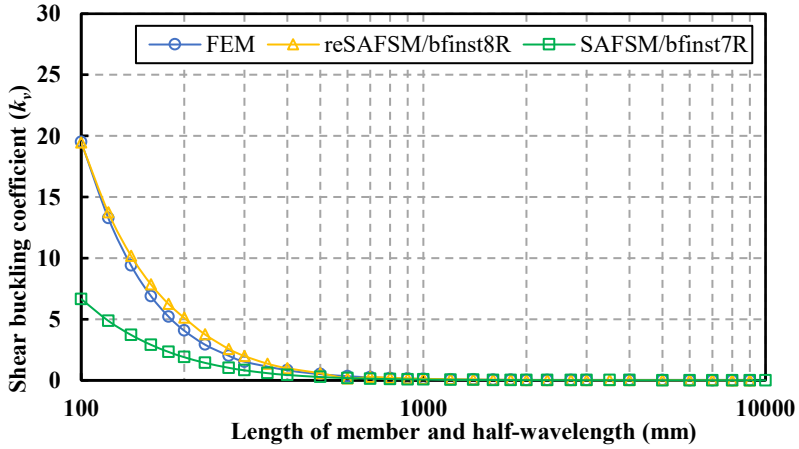

b). Unlipped channel section C200-40 (t = 2.0 mm)

Figure 4.14: Comparison of elastic buckling results from three different methods for a medium flange width.

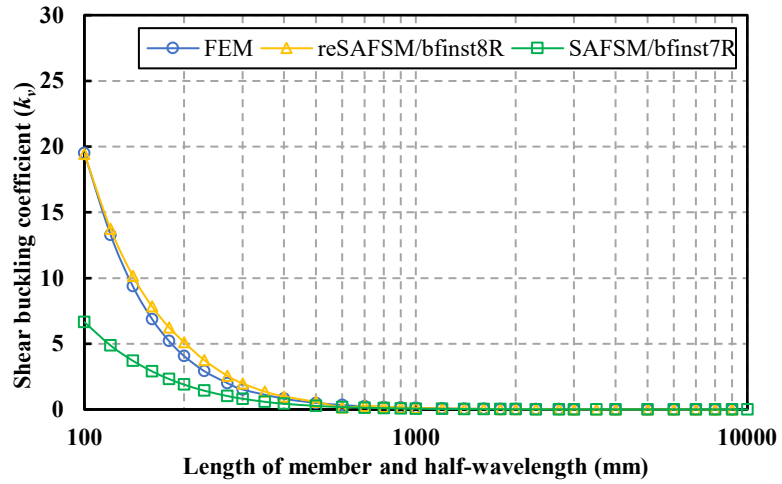

a). Lipped channel section C200-120-20 (t = 2.0 mm)

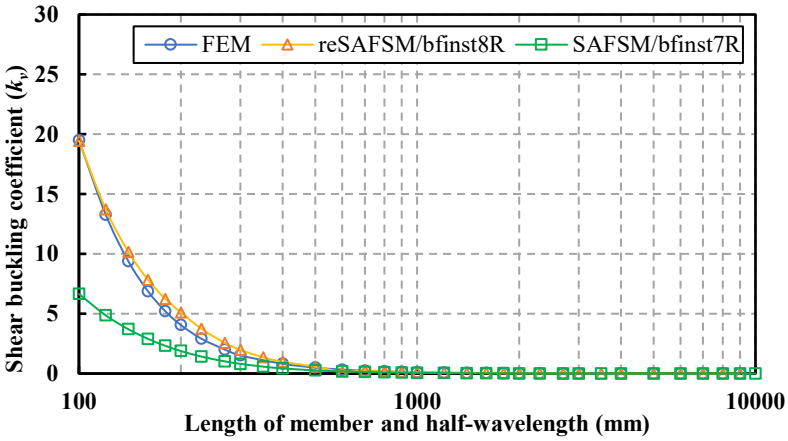

b). Unlipped channel section C200-120 (t = 2.0 mm)

Figure 4.15: Comparison of elastic buckling results from three different methods for a large flange width.

4.6 CHAPTER CONCLUSION

This chapter demonstrated the results of shear buckling analyses from the FEM, SAFSM and reSAFSM for both lipped and un-lipped channel sections with different flange width to depth ratios. The results mainly reveal the relationship between the shear buckling coefficient (k_v) and member length and half-wavelength for the full range of flange size and the corresponding shear buckling mode shapes.

First, all the results from the three different methods agree that the twisting buckling mode can occur in those sections with narrow flanges, and the local buckling can gradually govern the local buckling mode as the flange becomes wider. This is because the narrow flange cannot provide adequate fixity to the web, allowing the sections to buckle sideways. However, when the flange width to depth ratio exceeds 0.3, the local buckling can totally govern the shear buckling mode for the full range of length,

and varying flange size cannot affect the shear buckling coefficient significantly. This also proves the outcomes of Keerthan and Mahendran [6] that a flange width to depth ratio greater than 0.3 can provide almost the same fixity to the web.

This chapter also compared the results from different methods and suggested that the simply supported boundary conditions at section ends can improve the shear buckling capacity of the sections. In addition, the FEM analysis shows a lower shear buckling coefficient than the reSAFSM for large flange width due to the high bending moment. The flange is easier to get local buckling than the web when subject to a couple of high bending moments. Thus, the buckling analysis results obtained from the FEM are more accurate and practical than the reSAFSM when the equilibrium of the whole member is considered.

CHAPTER 5 : PARAMETRIC STUDY AND NEW PROPOSED EXPLICIT APPROACH

5.1 CHAPTER INTRODUCTION

The current design rules for the shear buckling coefficient (k_v) of lipped channel sections based on Keerthan and Mahendran [6] have been incorporated into the Australian/New Zealand Standard AS/NZS 4600:2018 [7] Appendix D3. This method, which was calibrated for the width to depth ratio (b_2/b_1) greater than 0.3 only, mainly requires three inputs: the shear buckling coefficients of plates with simple-simple and simple-fixed boundary (k_{ss}) and (k_{sf}) and the fixity coefficient (k_n) The value of k_v can be determined by

$$k_v = k_{ss} + k_n(k_{sf} - k_{ss}) \tag{5-1}$$

where for $a/b_1 < 1.0$

$$k_{ss} = 4 + \frac{5.34}{\left(\frac{a}{b_1}\right)^2} \tag{5-2}$$

$$k_{sf} = \frac{5.34}{(a/b_1)^2} + \frac{2.31}{(a/b_1)} - 3.44 + 8.39\left(\frac{a}{b_1}\right) \tag{5-3}$$

For $a/b_1 \geq 1.0$

$$k_{ss} = 5.34 + \frac{4}{\left(\frac{a}{b_1}\right)^2} \tag{5-4}$$

$$k_{sf} = 8.98 + \frac{5.61}{(a/b_1)^2} - \frac{1.99}{(a/b_1)^3} \tag{5-5}$$

Equations (5-1) to (5-5) are Equation D3 (4-8) in AS/NZS 4600:2018 [7]. where a is the shear span of web panel and b_1 is the depth of web. The value of k_n for b_2/b_1 greater than 0.3 is equal to 0.23. However, there is no value for k_n defined for b_2/b_1 smaller than 0.3.

This chapter conducts further parametric study for the shear buckling coefficient of channel sections with narrow flange under predominantly shear and introduces the new explicit approach for determination of the value of k_v.

First, this chapter compares the results of the shear buckling analysis and the current design methods provided by AS/NZS 4600:2018 [7]with aspect ratios from 1.0 to 4.0 to minimise the effect of the bending moment, finding that the current design codes can lead to an over-estimation of k_v for b_2/b_1 smaller than 0.3. Furthermore, Pham et al. [16] has investigated the shear buckling coefficient of channel sections with different thickness under combined actions of bending and shear and did not include the influence of thickness. Thus, this chapter also investigates the effect of different thickness on the value of k_v by varying the thicknesses from 1.0 to 3.0 mm.

This chapter also introduces the new approach for determination of k_v of channel sections with narrow flange under predominantly shear. The approach is developed through studying the change of shear buckling behaviours of sections by changing aspect ratios and width to depth ratios. The relationship between k_n and b_2/b_1 is also defined in this chapter.

5.2 COMPARISON OF SHEAR BUCKLING COEFFICIENT FROM FEM AND CURRENT DESIGN METHOD

The results obtained from the three different methods used in this study show that flange width can significantly affect the shear buckling behaviour of lipped channels with narrow flange under predominantly shear. The relationships between the elastic buckling coefficient and the aspect ratio of the web panel ($AR = a/b_1$) with a full range of b_2/b_1 are plotted in **Figure 5.1**. The aspect ratio is limited from 0.5 to 4.0 in this study to minimise the effect of bending moments on the flange and ensure the channels are subject to predominantly shear.

For the beams with relatively large flanges ($b_2/b_1 > 0.3$), all the curves coincide with each other, and the shear buckling coefficient cannot be affected by increasing the value of b_2/b_1. This fact indicates that the fixity provided by the flange cannot be enhanced by increasing the flange width when b_2/b_1 is greater than 0.3. In contrast, unlike the case of b_2/b_1 greater than 0.3 where all curves can behave similarly and coincide with each other, the curves under 0.3 can be changed by varying the value of b_2/b_1. Specifically, increasing the flange width to depth ratio can improve the shear buckling coefficient significantly when b_2/b_1 is lower than 0.3. As demonstrated in the results, the channels with very narrow flanges do not have enough lateral restraints to prevent the beams from twisting between the section ends under the shear. However, as the flanges become increasingly wider, the lateral restraints provided by the flanges along the longitudinal edges of the web panel can be enhanced adequately to stop twisting and force the channels to buckle locally.

The current design rules to determine the shear buckling coefficient have been described previously and are plotted in **Figure 5.1**. By comparing the FEM buckling results with the existing design codes, it can be found that the current equation for $b_2/b_1 > 0.3$ (the red dash line) can be well-fitted to the curves with the FEM buckling results since all curves have the same behaviour and coincide with each other. Nevertheless, for the case of $b_2/b_1 \leq 0.3$, the current design codes (the green dash line) cannot predict the buckling behaviour of the FEM results accurately. Using the current equation to calculate the elastic buckling coefficient for channels with narrow flanges may cause significant over-estimation of shear buckling capacity.

As a result, varying flange width can significantly affect the shear buckling coefficient of lipped channels with narrow flange ($b_2/b_1 \leq 0.3$). As mentioned before, defining the relationship between the fixity and the flange width to depth ratios can play a key role in ensuring the accuracy of prediction for the shear buckling coefficient. Increasing the flange width for the channels with narrow flanges can give more additional fixity to the web, leading to more lateral restraints to improve the shear buckling capacity of whole channel sections. The current equation based on Keerthan and Mahendran [6] takes 0.23 for the coefficient of fixity level (k_n)to calculate the shear buckling coefficient for b_2/b_1 greater than 0.3, which can successfully capture the FEM buckling results. However, the current design rules ignore the effect of changing b_2/b_1 on the fixity at the web-flange juncture and simply takes 0.0 for the k_n to estimate all curves under 0.3. Hence, the rules cannot provide an accurate and reliable prediction for the shear buckling coefficient for channels with narrow flanges.

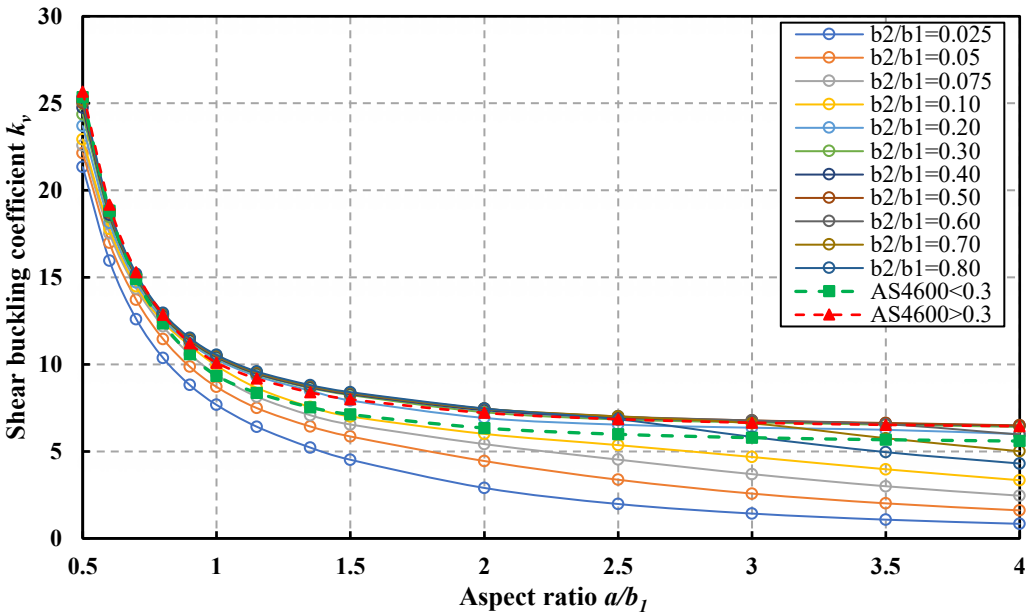

Figure 5.1: The relationship between the buckling coefficient and aspect ratio in terms of different flange widths compared with current standard codes.

5.3 Effect of Thickness of Channels on Shear Buckling Coefficient

It is known that the longitudinal boundary conditions, the aspect ratio (*AR*) of members and the flange width to depth ratio (b_2/b_1) can affect the shear buckling coefficient of channel members. This section investigates if the thickness of the channel section can impact the shear buckling coefficient.

The shear behaviour of channel members subjected to predominant shear concerning different thicknesses from 1.0 to 3.0 mm is plotted in **Figure 5.2**. It is demonstrated that the curves for all the thicknesses are almost identical for both lipped and unlipped channel sections. This implies that the sensitivity of the shear buckling coefficient to the thickness of channel sections is unimportant. Therefore, the member thickness can be ignored in determining the shear buckling coefficient.

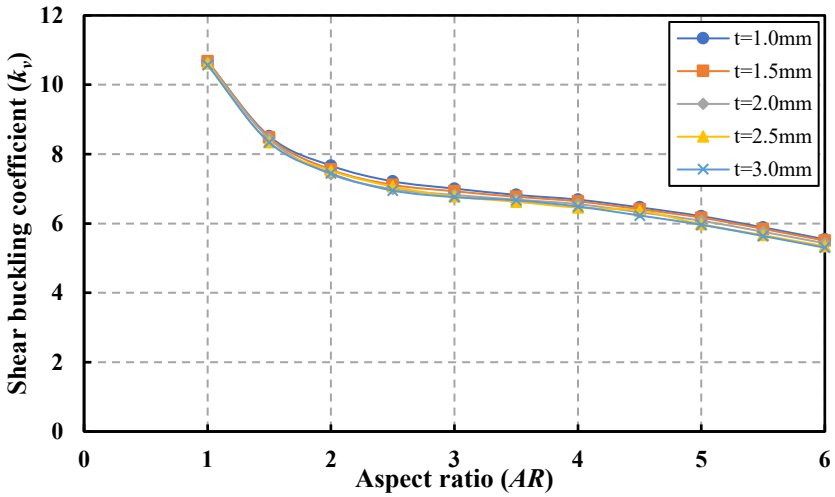

(a) Lipped channel section

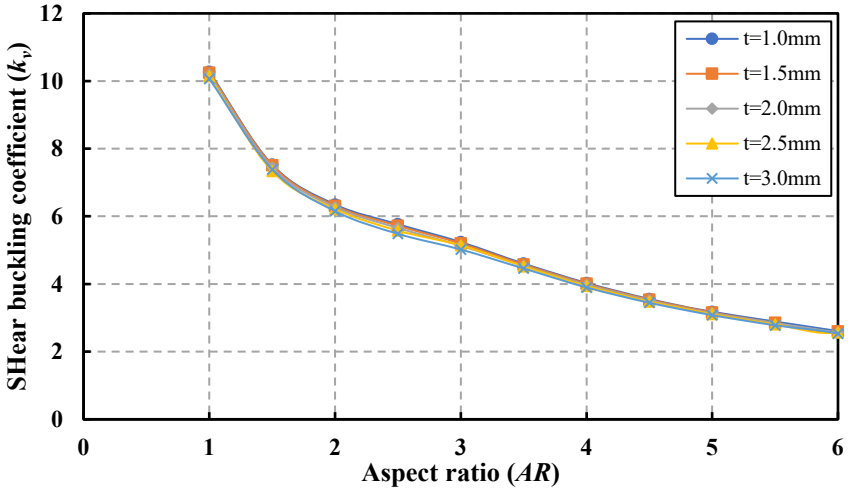

(b) Un-lipped channel section

Figure 5.2: Shear behaviour of channel members subjected to shear in terms of different thickness.

5.4 Definition of the Coefficient of Fixity for Narrow Flanges

As discussed in the previous section, the current design standards AS/NZS 4600:2018 [7] based on Keerthan and Mahendran [22] and Keerthan and Mahendran [6] are considered infeasible for predicting the shear buckling coefficient of a lipped channel section with narrow flanges due to a lack of definition of fixity coefficient k_n for b_2/b_1 lower than 0.3. As shown in **Table 5.1** provided by the current standard, the coefficient k_n at the juncture of web-flange is defined for the lipped channel, taking the fixed value of 0.23 for $b_2/b_1 \geq 0.3$. This means that the flange provides the equivalent 23% of fixed boundary conditions to the longitudinal web edges, and it will not be affected by changing b_2/d_1. However, for channels with narrow flanges, b_2/d_1 is considered a dominant factor influencing k_v since the degree of fixed boundary conditions can be improved by increasing the flange

width. Hence, developing new equations to express the relationship between b_2/b_1 and the coefficient k_n should be more reasonable for determining the shear buckling coefficient of channel sections with narrow flange than using a single fixed value to define k_n

Table 5.1: Coefficient k_n for open and hollow flange steel beams AS/NZS 4600:2018 [7].

Section	k_n	
Lipped channel (LC)	0.23	$\frac{b_2}{b_1} \geq 0.3$
Hollow flange channel (HFC)	0.87	$\frac{b_2}{b_1} \geq 0.3$
Triangular hollow flange beam (THFB)	0.90	$\frac{b_2}{b_1} \geq 0.3$
Rectangular hollow flange beam (RHFB)	$(0.82\ t_w/t_f - 0.41)$ $0.5 \leq t_w/t_f < 1.6$	$\frac{b_2}{b_1} \geq 0.4$
	$0.90\ t_w/t_f \geq 1.6$	$\frac{b_2}{b_1} \geq 0.4$

When b_2/b_1 is lower than 0.3, the degree of fixed boundary conditions at the juncture of the web to flange should be lower than 0.23 and continuously reduce until the twisting totally governs the buckling mode of the channels in the full range of aspect ratio in shear, the additional fixity can be considered equal to 0.0. At this stage the flange is not able to provide any lateral restraint to the web plate.

According to the results of the FEM buckling analysis, the shear buckling of lipped channel sections for b_2/b_1 lower than 0.3 can perform different behaviours, which can be divided into two groups as shown in **Figure 5.3**. For $0.1 < b_2/b_1 < 0.3$, the local buckling mainly governs the buckling mode of lipped channels under predominantly shear as shown in **Figure 5.3** (a), However, for the very narrow flange, the twisting can be found at low aspect ratios and continuously governs the buckling mode in the full range of aspect ratios as the decrease of flange width as shown in **Figure 5.3** (b). Therefore, b_2/b_1 equal to 0.1 is the critical point at which the flange will not provide any additional fixity to the web, and the coefficient k_n should be equal to 0.0. When b_2/b_1 continues to reduce lower than 0.1, the boundary condition at the juncture of the web to flange cannot satisfy 100% of the simply-to-simply boundary condition. Therefore, finding a new factor to estimate the degree of simply supported boundary conditions at the web-flange juncture that the narrow flange can reach is significant for b_2/b_1 lower than 0.1. As a result, the approximation equation for predicting the shear

buckling coefficient of lipped channel sections with b_2/b_1 lower than 0.3 should be divided into two conditions based on the different shear buckling behaviours.

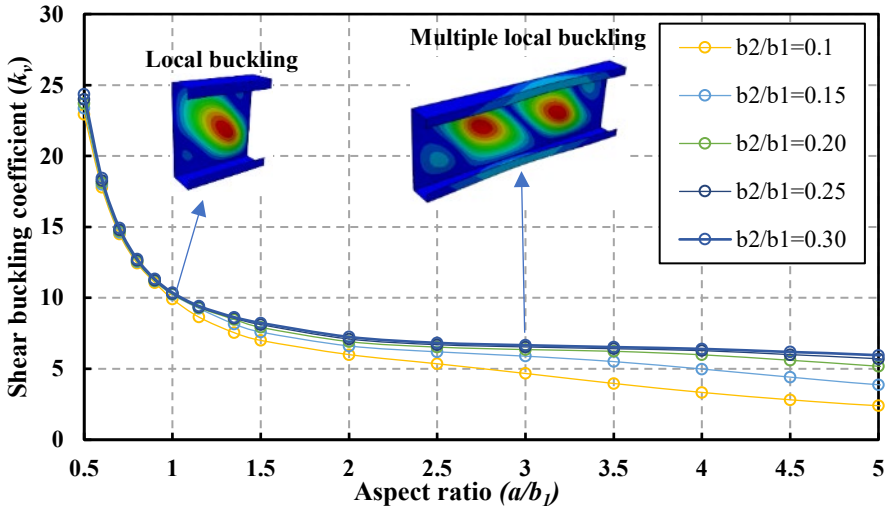

a) b_2/b_1 from 0.1 to 0.3

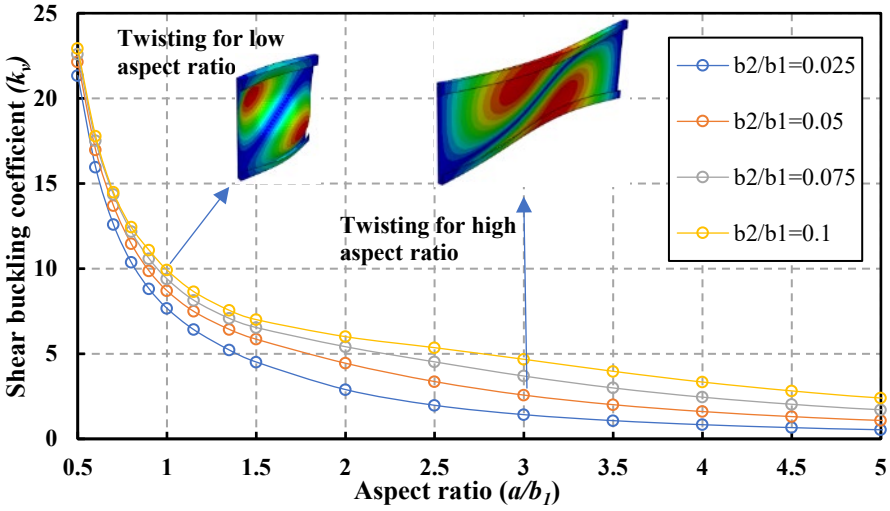

b) b_2/b_1 from 0.025 to 0.1

Figure 5.3: Two groups of different shear buckling behaviours for lipped channel sections with $b_2/b_1 \leqslant 0.3$.

For un-lipped channel sections, the FEM buckling analysis is shown in **Figure 5.4**. The effect of b_2/b_1 is more sensitive in affecting the shear buckling coefficient k_v of the channels under predominantly shear. Since there is no lip to stiffen another longitudinal edge of the flange, the flange with a great width to depth ratio will be more vulnerable to buckle in shear. The current standard AS/NZS 4600:2018 [7] does not provide specific design rules for predicting the shear buckling coefficient and defining the value of k_n for the un-lipped channel. Thus, the approximation for the value of k_v for un-lipped channels is based on the current design codes for lipped channels. At the same time, the

coefficient k_n for the fixity at the web-flange juncture should be identified according to the shear buckling behaviours.

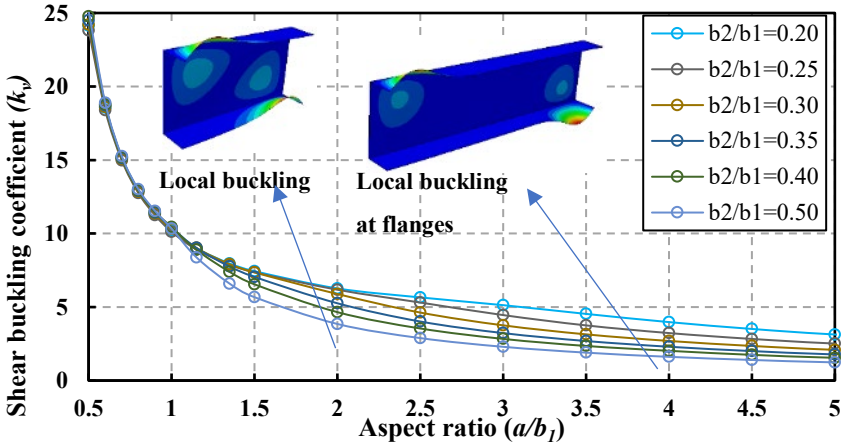

a) b_2/b_1 from 0.20 to 0.50

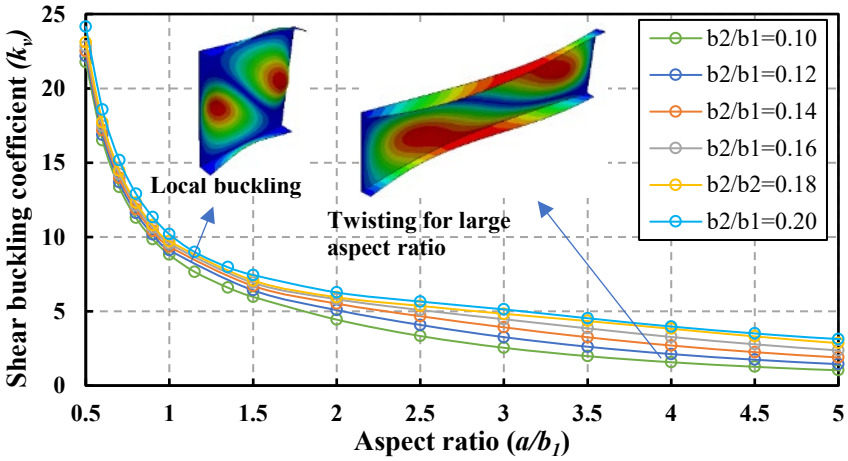

b) b_2/b_1 from 0.10 to 0.20

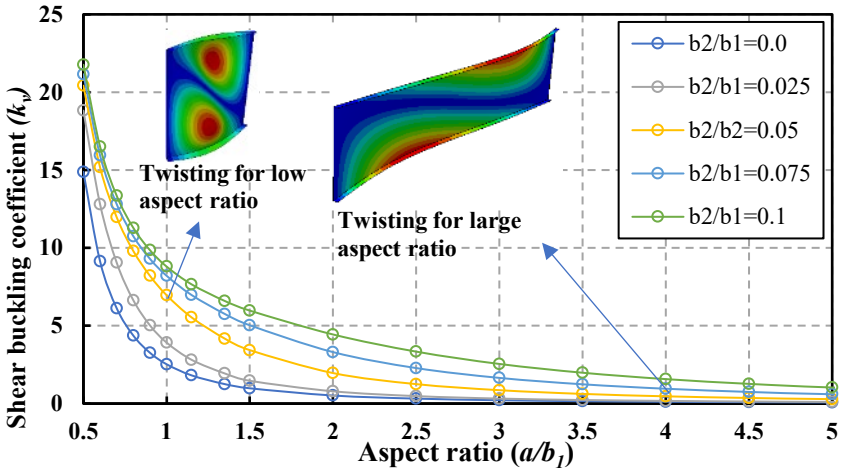

c) b_2/b_1 from 0.0 to 0.10

Figure 5.4: Two groups of different shear buckling behaviours for un-lipped channel sections with $b_2/b_1 \leqslant 0.5$.

In the group of b_2/b_1 from 0.2 to 0.5, it is clear that the curves of k_v are shifted downward as the increase of b_2/b_1. This is because the large flange without a lip to stiffen is more vulnerable when it is under predominantly shear, making the flange easier to buckle locally as shown in **Figure 5.4** (a). However, for the group of $0.1 < b_2/b_1 \leq 0.2$, local buckling mode can be found in the channel sections with a low aspect ratio, whereas twisting buckling can be observed in the channel sections with a high aspect ratio as shown in **Figure 5.4** (b). For the channels with very narrow flanges in a range of $0.0 \leq b_2/b_1 \leq 0.1$, the twisting buckling mode can be observed for the full range of aspect ratio under predominantly shear as shown in **Figure 5.4** (c).

5.5 EXPLICIT PROCEDURE FOR DETERMINATION OF SHEAR BUCKLING LOADS

The comparisons of shear buckling coefficients between the FEM and current design codes from Appendix D3 in AS/NZS 4600:2018 [7] for lipped channel sections under predominantly shear with b_2/b_1 in a range of 0.1 to 0.3 are shown in **Figure 5.5**

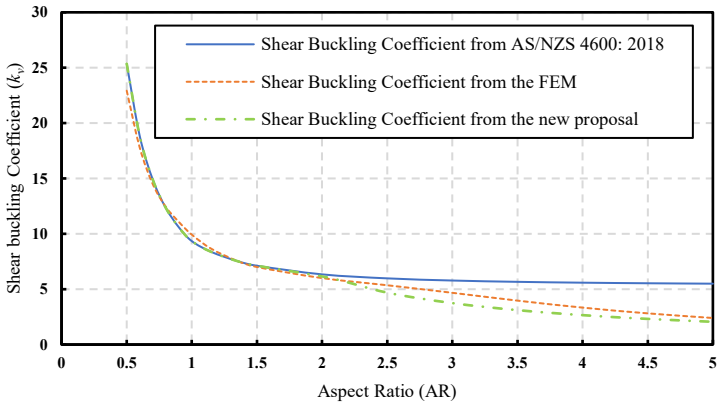

(a) $b_2/b_1 = 0.10$

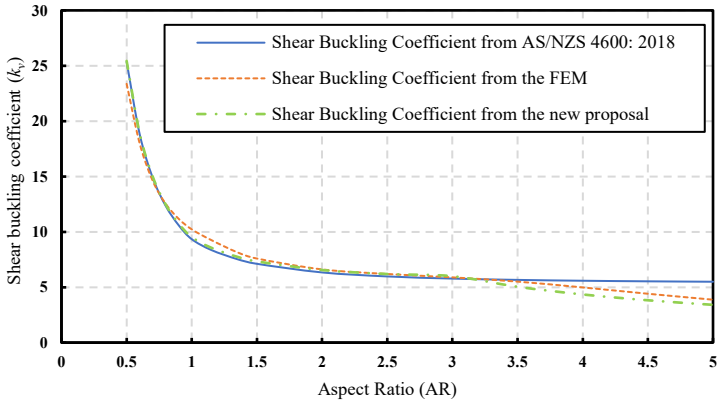

(b) $b_2/b_1 = 0.15$

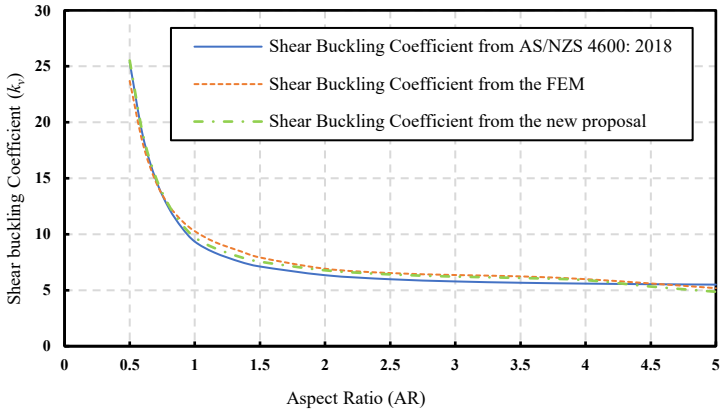

(c) b_2/b_1 = 0.20

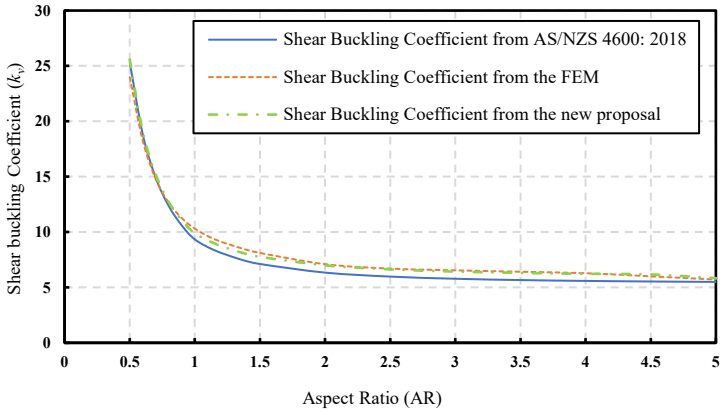

(d) b_2/b_1 = 0.25

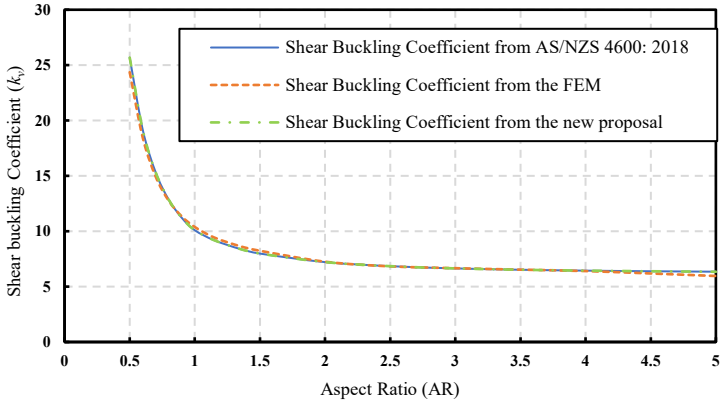

(e) b_2/b_1 = 0.3

Figure 5.5: Shear buckling coefficient of lipped channel sections with b_2/b_1 from 0.1 to 0.3.

It is clear that for cases of b_2/b_1 equal to 0.2 to 0.3, the current design codes for the determination of shear buckling coefficient can predict well the values from the FEM analyses. This is because the flange can provide a certain lateral restraint so that the local buckling mainly governs the buckling modes of the channel sections under predominantly shear at a short aspect ratio. However, for the cases of b_2/b_1 equal to 0.1 and 0.15, a significant reduction can be found when the aspect ratios are greater than 2.0 and 4.0 respectively. This is because the twisting buckling occurs due to the very narrow flanges not being able to stiffen the web plate.

The observation of the shear buckling coefficient for lipped channel sections under predominantly shear with b_2/b_1 in a range of 0.025 to 0.1 is shown in **Figure 5.6**. It is clear that the current design curves cannot accurately predict the shear buckling coefficient of channel sections in this range. Compared to the FEM results, the predictions using the current standard are always over-estimated when the aspect ratio becomes greater than 1.0. This is because the flanges are too narrow to restrain the longitudinal edges of the web plate, leading to twisting that can govern the buckling mode in the full range of aspect ratios of the sections.

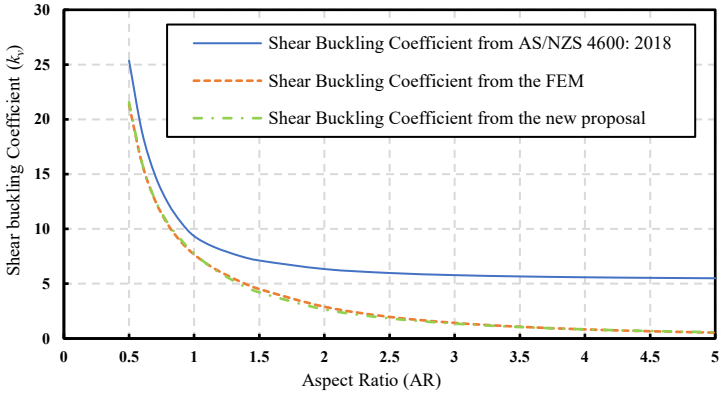

(a) $b_2/b_1 = 0.025$

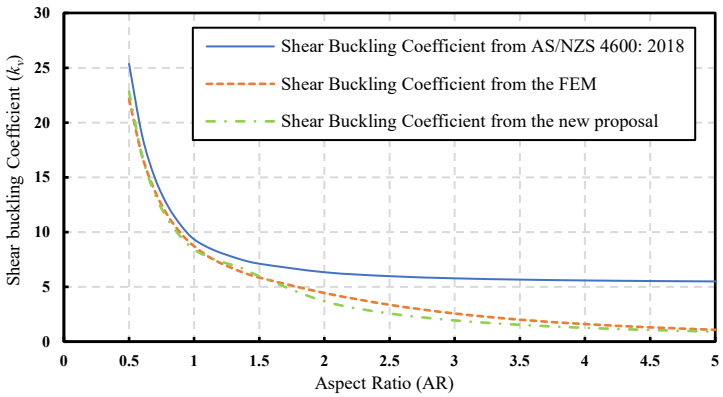

(b) $b_2/b_1 = 0.05$

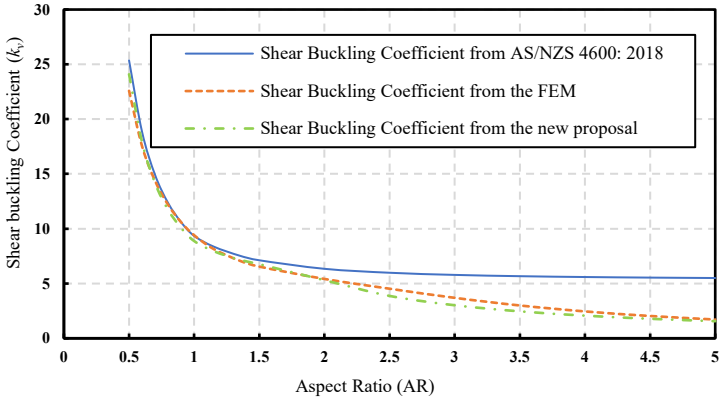

(c) $b_2/b_1 = 0.075$

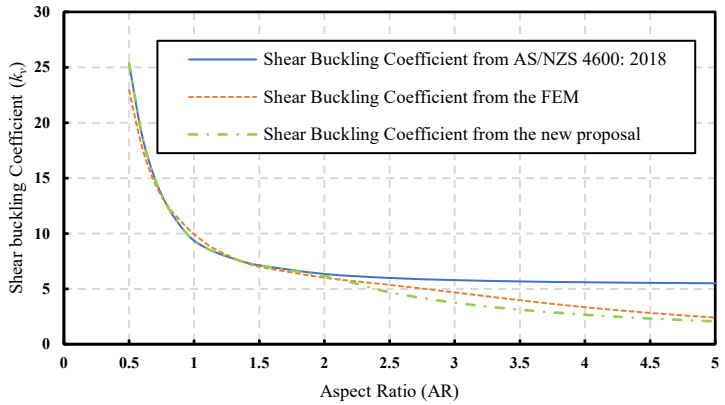

(d) $b_2/b_1 = 0.10$

Figure 5.6: Shear buckling coefficient of lipped channel sections with b_2/b_1 from 0.025 to 0.1.

The observation of the shear buckling coefficient for un-lipped channel sections under predominantly shear with the b_2/b_1 in a range of 0.0 to 0.1 is shown in **Figure 5.7**. It can be seen that the current standard curve cannot capture the FEM curve and has a considerable over-estimation of predicting the shear buckling coefficient in this range. This is because the twisting buckling totally governs the shear buckling mode in the full range of aspect ratios of the channel sections under predominantly shear due to the very narrow flange.

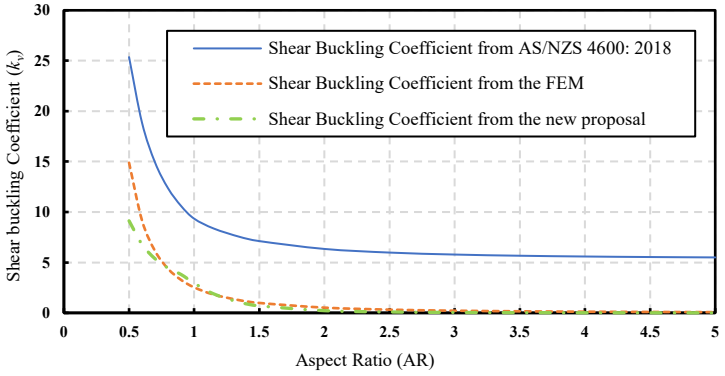

(a) $b_2/b_1 = 0.0$

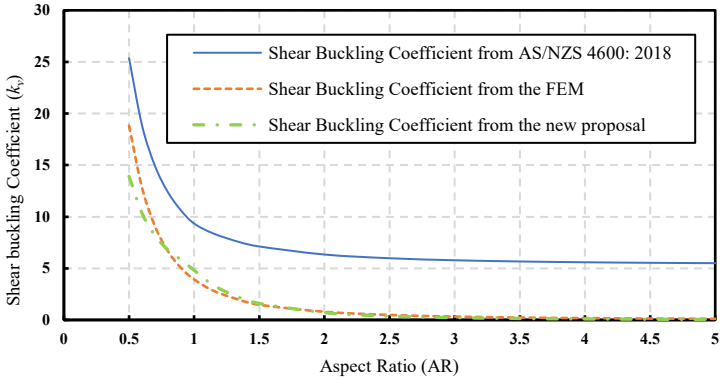

(b) $b_2/b_1 = 0.025$

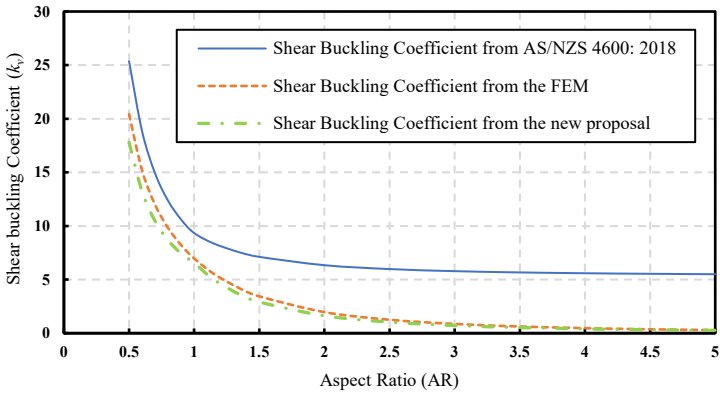

(c) b_2/b_1 = 0.05

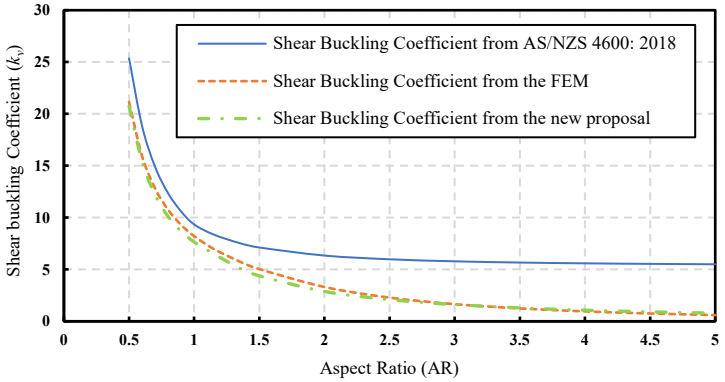

(d) b_2/b_1 = 0.075

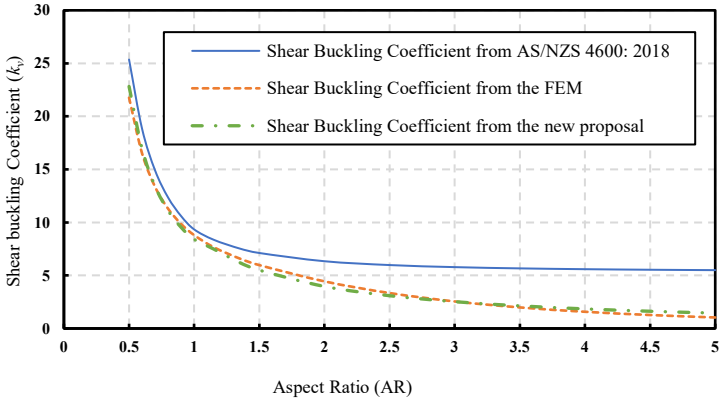

(e) b_2/b_1 = 0.10

Figure 5.7: Shear buckling coefficient of un-lipped channel sections with b_2/b_1 from 0.025 to 0.1.

The observation of the shear buckling coefficient for un-lipped channel sections under predominantly shear with b_2/b_1 in a range of 0.1 to 0.2 is shown in **Figure 5.8** . It is shown that the current shear buckling coefficient curve cannot be well fitted to the FEM curve. Even though the flange becomes increasingly greater, and local buckling would occur in the web of the member at a short aspect ratio, the current design curve still over-estimates the shear buckling coefficients for relatively large aspect ratios. This fact indicates that the current design codes for determination of the shear buckling

coefficient of a lipped channel section are not feasible for an un-lipped channel section and will generate an over-estimated prediction outcome.

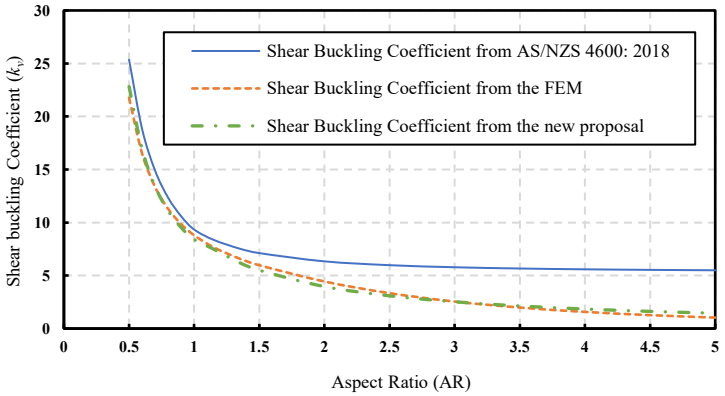

(a) $b_2/b_1 = 0.10$

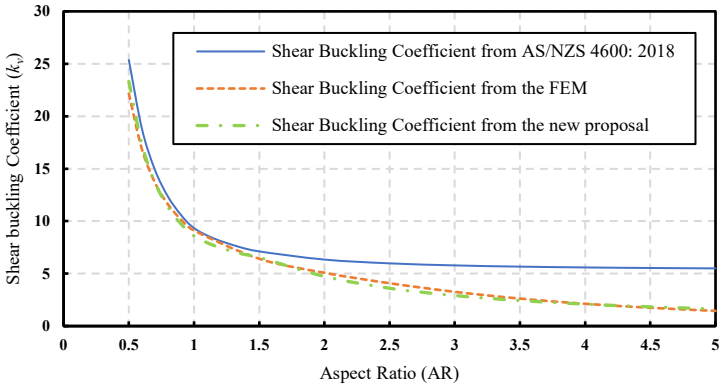

(b) $b_2/b_1 = 0.12$

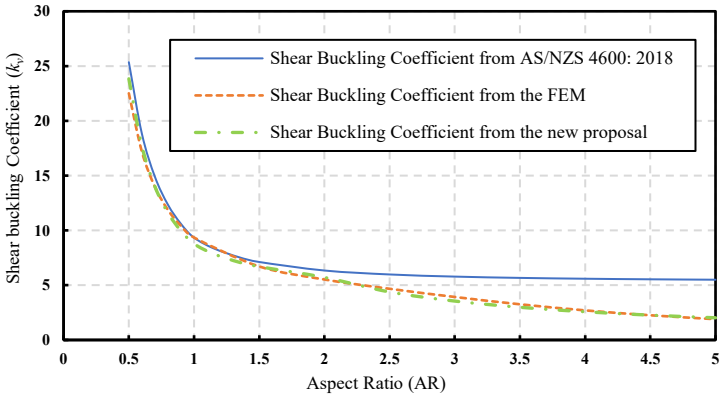

(c) $b_2/b_1 = 0.14$

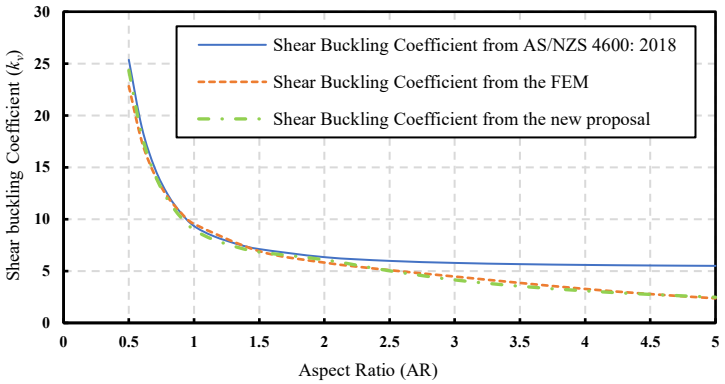

(d) b_2/b_1 = 0.16

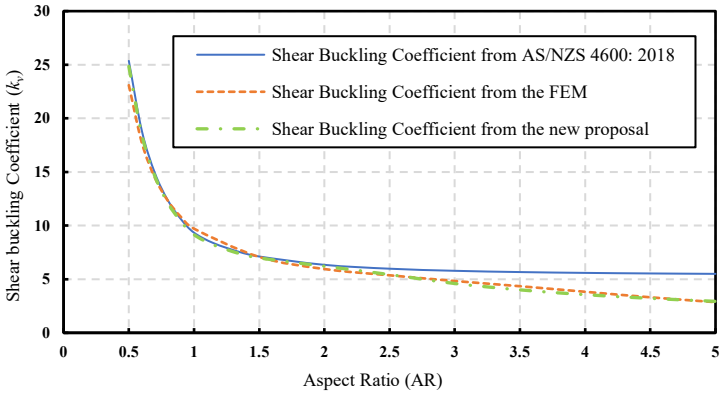

(e) b_2/b_1 = 0.18

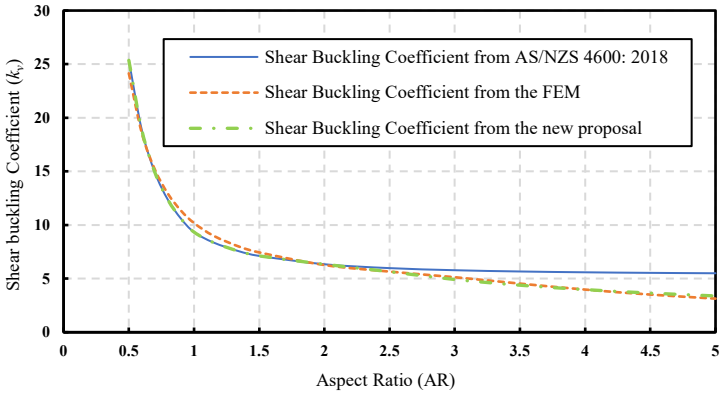

(f) b_2/b_1 = 0.20

Figure 5.8: Shear buckling coefficient of un-lipped channel sections with b_2/b_1 from 0.1 to 0.2.

Figure 5.9 compares the shear buckling coefficients between the current design method and the new proposal for un-lipped channel sections under predominantly shear with b_2/b_1 in a range of 0.2 to 0.5. It can be seen that as the b_2/b_1 increases, the shear buckling coefficient curves obtained by the FEM are shifted downward at relatively large aspect ratios. This is attributed to the fact that the flanges are unstiffened at one free edge, and the local buckling is easier to occur at the compression flange when the flange becomes wider. Hence, it is hard for the current design codes to capture the FEM curve,

and the significant over-estimated predictions of the shear buckling coefficient can be observed in this range of b_2/b_1.

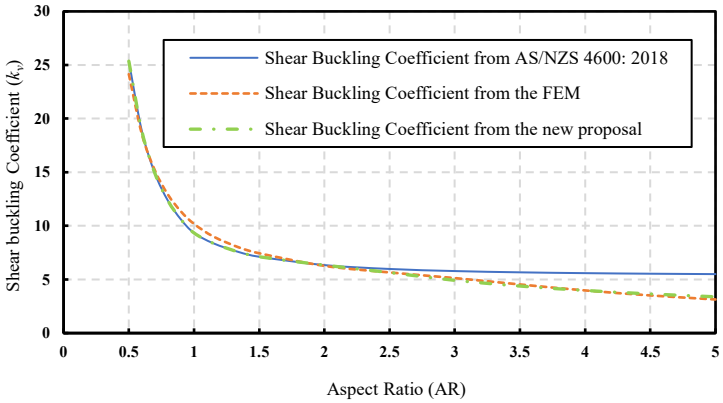

(a) $b_2/b_1 = 0.20$

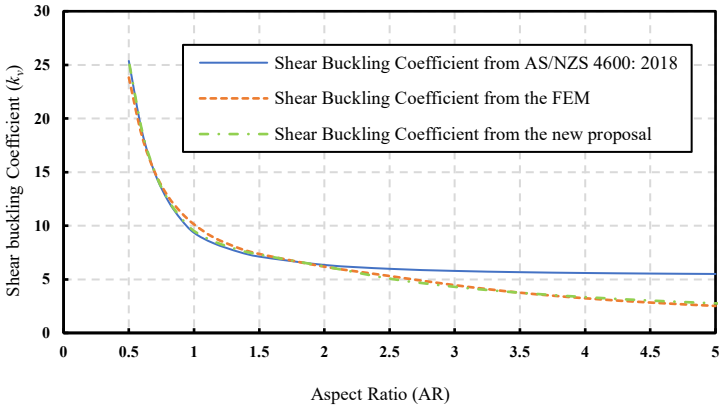

(b) $b_2/b_1 = 0.25$

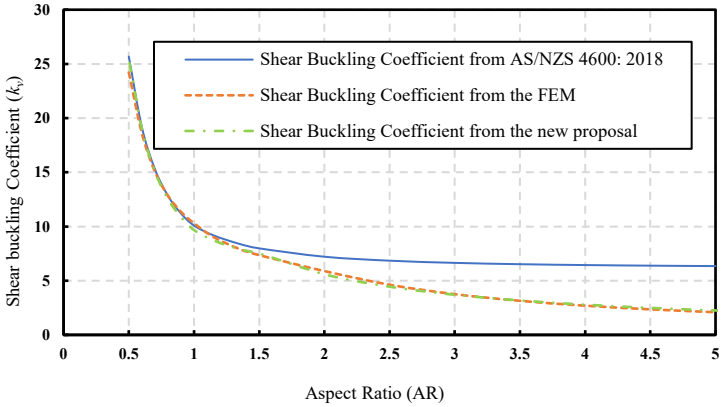

(c) $b_2/b_1 = 0.30$

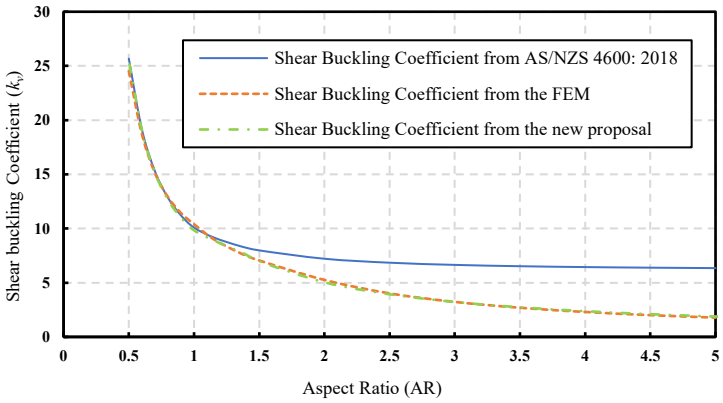

(d) $b_2/b_1 = 0.35$

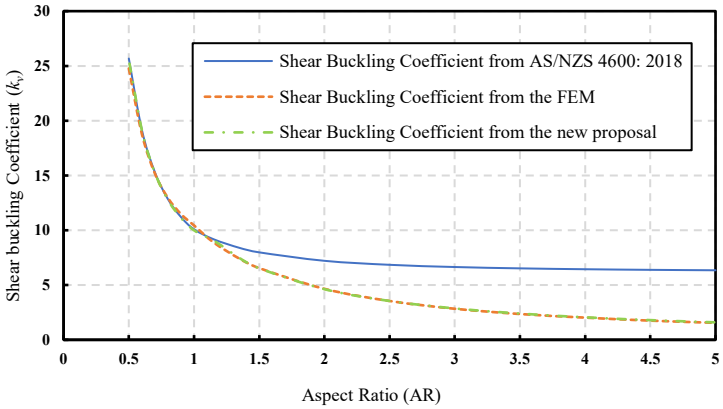

(e) $b_2/b_1 = 0.40$

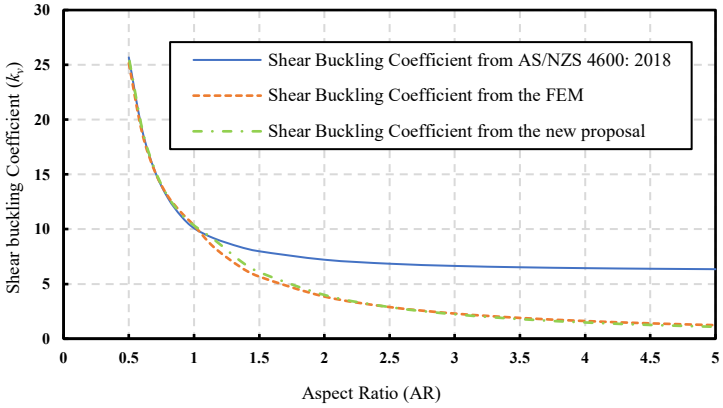

(f) $b_2/b_1 = 0.50$

Figure 5.9: Shear buckling coefficient of un-lipped channel sections with b_2/b_1 from 0.2 to 0.5.

To provide a prediction of the shear buckling coefficient for a range of aspect ratios (AR_0) in predominantly shear, a combination of two segments of approximation curves is considered for both lipped and un-lipped channels. The first part mainly takes advantage of the current design curve for the shear buckling coefficient referred to in Appendix D3 in AS/NZS 4600:2018 [7] with the modified coefficient of fixity. This part curve is mainly used for predicting the shear buckling coefficient in the local shear buckling of very short members. The second segment of the curve is the new approximation for predicting the continuously reduced shear buckling coefficient of relatively long

members at higher AR caused by the lack of lateral restraint from the narrow flange. The two parts of the curve are combined continuously and intersected at the member aspect ratio called a transition point (AR_{tr}), where the transformation of shear buckling modes will occur from local buckling to twisting. Hence, the value of AR_{tr} is the aspect ratio limit for the use of the current design curve and is the start point for the use of the second curve segment for approximation of k_v. The first curve segment can predict well the shear buckling coefficient for the part where the aspect ratio is less than AR_{tr} regardless of the change of b_2/b_1. The second curve segment predict the shear buckling coefficient for the aspect ratio larger than AR_{tr} where the value of k_v can be influenced by b_2/b_1 significantly. In addition, it is known that the narrow flange cannot provide adequate lateral restraint to stiffen the web plate, leading to twisting of the full channel sections. In other words, the narrow flange is not able to provide additional fixity at the juncture of web and flange. The coefficient k_n provided by current standard equal to 0.23 is not suitable for predicting the shear buckling coefficient of the narrow flange since 23% of fixed boundary conditions is suggested to be too high for the narrow flange, always leading to an over-estimated prediction of k_v. The determination of AR_{tr}, k_n and the new approximation proposal for the second part curve are demonstrated in the following procedure.

To determine the elastic shear buckling coefficient k_v of a lipped channel section subjected to predominantly shear, the buckling analysis should comply with the following steps:

5.5.1 Lipped channel section

For the flange width to depth ratio $0.1 \leq b_2/b_1 < 0.3$

- ***Step 1:*** The value of k_n can be determined as follows:

$$k_n = 1.15\frac{b_2}{b_1} - 0.115 \tag{5-6}$$

  Where b_1 is the depth of the web panel and b_2 is the flange width. The dimensions used in the sections are all centreline and not overall.

- ***Step 2:*** AR_{tr} is the factor of a transition point to indicate a specific aspect ratio where the buckling mode of the channel section transforms from local buckling to twisting. The value of AR_{tr} is calculated as follows:

$$AR_{tr} = -42.86\left(\frac{b_2}{b_1}\right)^2 + 32.14\left(\frac{b_2}{b_1}\right) - 0.8 \tag{5-7}$$

- ***Step 3:*** The equations for calculating the shear buckling coefficient depends on the value of AR_{tr} calculated in Step 2.

  (a) For the case of $AR_0 \leq AR_{tr}$, the shear buckling coefficient can be determined by the following procedure:

  For $AR_0 \geq 1.0$

$$k_{ss} = 5.34 + \frac{4}{(AR_0)^2} \tag{5-8}$$

$$k_{sf} = 8.98 + \frac{5.61}{(AR_0)^2} - \frac{1.99}{(AR_0)^3} \tag{5-9}$$

  For $AR_0 < 1.0$

$$k_{ss} = 4 + \frac{5.34}{(AR_0)^2} \tag{5-10}$$

$$k_{sf} = \frac{5.34}{(AR_0)^2} + \frac{2.31}{AR_0} - 3.44 + 8.39(AR_0) \tag{5-11}$$

$$k_v = k_{ss} + kn\left(k_{sf} - k_{ss}\right) \tag{5-12}$$

  where k_{ss} and k_{sf} are the shear buckling coefficients of plates with simple-simple and simple-fixed boundary. AR_0 is the aspect ratio of the channel section.

  (b) For the case of $AR_0 > AR_{tr}$, the shear buckling coefficient can be determined by the following procedure:

$$k_v = \left[C_1 - C_2\left(\frac{1}{AR_0{}^2}\right)^n\right]\left(\frac{1}{AR_0{}^2}\right)^n \tag{5-13}$$

  Factor C_1 is equal to the value of the shear buckling coefficient at the transition point $AR_{tr,}$ which can be calculated by **Eq (5-12).**

  Factor C_2 can be determined by the following equation:

$$C_2 = \frac{C_1 - \dfrac{C_1}{\left(\dfrac{1}{AR_{tr}{}^2}\right)^n}}{\left(\dfrac{1}{AR_{tr}{}^2}\right)^n} \tag{5-14}$$

Factor *n* depends on the flange width to depth ratio and can be calculated as follows:

$$n = -1.6\frac{b_2}{b_1} + 0.605 \tag{5-15}$$

For the flange width to depth ratio $0.0 \leq b_2/b_1 < 0.1$

- ***Step 1:*** The value of AR_{tr} in this range is calculated as follows:

$$AR_{tr} = -128\left(\frac{b_2}{b_1}\right)^2 + 30.56\left(\frac{b_2}{b_1}\right) + 0.21 \tag{5-16}$$

- ***Step 2:*** The equations for calculating the shear buckling coefficient depends on the value of AR_{tr} calculated in Step 1.
  (a) For the case of $AR_0 \leq AR_{tr}$, the shear buckling coefficient can be determined by the following procedure:

$$k_v = C_3 \times k_{ss} \tag{5-17}$$

  Factor C_3 is related to the flange width to depth ratio and is determined as follows:

$$C_3 = 2\left(\frac{b_2}{b_1}\right) + 0.8 \tag{5-18}$$

  k_{ss} can be determined by **Eq. (5-8)** and **Eq. (5-10)** depending on the aspect ratio.
  (b) For the case of $AR_0 > AR_{tr,}$ the shear buckling coefficient can be determined by **Eq (5-13).** Factor C_1 is equal to the value of shear buckling coefficient at the transition point calculated by **Eq (5-17)**. Factor C_2 can be determined by **Eq (5-14)**.
  Factor n can be determined by the following equation:

$$n = 58\left(\frac{b_2}{b_1}\right)^2 - 12.71\frac{b_2}{b_1} + 1.136 \tag{5-19}$$

5.5.2 Un-lipped channel

To determine the elastic shear buckling coefficient k_v of an un-lipped channel section subjected to a predominantly shear, the buckling analysis should comply with the following steps:

For the flange width to depth ratio $0.2 \leq b_2/b_1 \leq 0.5$

- ***Step 1:*** The value of k_n can be determined as follows:

$$k_n = \frac{b_2}{b_1} - 0.2 \tag{5-20}$$

- ***Step 2:*** AR_{tr} for the unlipped channel section in this range of the flange width to depth ratio is the factor of a transition point to indicate a specific aspect ratio where the buckling mode of the channel section transforms from local buckling to bending of the flange. The value of AR_{tr} is calculated as follows:

$$AR_{tr}=16.67\left(\frac{b_2}{b_1}\right)^2 - 15.45\left(\frac{b_2}{b_1}\right)+4.667 \tag{5-21}$$

- ***Step 3:*** The equations for calculating the shear buckling coefficient k_v depends on the value of AR_{tr} calculated in Step 2.
  (a) For the case of $AR_0 \leq AR_{tr}$, the shear buckling coefficient can be determined by the following procedure:
  For $AR_0 \geq 1.0$, the value of k_{ss} and k_{sf} can be determined by **Eq (5-8)** and **Eq (5-9)**.
  For $AR_0 < 1.0$, the value of k_{ss} and k_{sf} can be determined by **Eq (5-10)** and **Eq (5-11)**.
  The shear buckling coefficient k_v under this case can be calculated by **Eq (5-12).**
  (b) For the case of $AR_0 > AR_{tr}$, the shear buckling coefficient k_v can be determined by **Eq (5-13)** Factor C_1 is equal to the value of shear buckling coefficient k_v at the transition point AR_{tr}, which can be calculated by **Eq (5-12).** Factor C_2 can be determined by **Eq (5-14).**

  Factor n depends on the flange width to depth ratio and can be calculated as follows:

$$\mathrm{n} = 1.34(\frac{b_2}{b_1})+0.014 \tag{5-22}$$

For the flange width to depth ratio $0.1 \leq b_2/b_1 \leq 0.2$

- ***Step 1:*** The value of transition points for the sections in this range of b_2/b_1 can be determined as follows:

$$AR_{tr} = -136.16\left(\frac{b_2}{b_1}\right)^2 +51.92\left(\frac{b_2}{b_1}\right)-2.694 \tag{5-23}$$

- ***Step 2:*** The equations for calculating the shear buckling coefficient depends on the value of AR_{tr} calculated in Step 1.
  (a) For the case of $AR_0 \leq AR_{tr}$, the shear buckling coefficient k_v can be determined by the following procedure:

$$k_v = C_4 \times k_{ss} \tag{5-24}$$

Factor C_4 is related to the flange width to depth ratio and is determined as follows:

$$C_4 = \left(\frac{b_2}{b_1}\right) + 0.8 \tag{5-25}$$

(b) For the case of $AR_0 > AR_{tr}$, the shear buckling coefficient k_v can be determined by **Eq. (5-13)**. Factor C_1 is equal to the value of shear buckling coefficient at the transition point calculated by **Eq (5-24)**. Factor C_2 can be determined by **Eq (5-14).**

Factor n can be determined by the following equation:

$$n = -2.42\left(\frac{b_2}{b_1}\right) + 0.766 \tag{5-26}$$

For the flange width to depth ratio $0.0 \leq b_2/b_1 \leq 0.1$

- ***Step 1:*** The value of transition points for the sections in this range of b_2/b_1 can be determined as follows:

$$AR_{tr} = 2.4\left(\frac{b_2}{b_1}\right) + 0.895 \tag{5-27}$$

- ***Step 2:*** The equations for calculating the shear buckling coefficient depends on the value of AR_{tr} calculated in Step 1.

(a) For the case of $AR_0 \leq AR_{tr}$, the shear buckling coefficient k_v can be determined by the following procedure:

$$k_v = C_5 \times k_{ss} \tag{5-28}$$

Factor C_5 depends on the flange width to depth ratio and is determined as follows:

$$C_5 = -28.57\left(\frac{b_2}{b_1}\right)^2 + 8.26\left(\frac{b_2}{b_1}\right) + 0.36 \tag{5-29}$$

(c) For the case of $AR_0 > AR_{tr}$, the shear buckling coefficient k_v can be determined by **Eq (5-13).** Factor C_1 is equal to the value of shear buckling coefficient at the transition point calculated by **Eq (5-28)**. Factor C_2 can be determined by **Eq (5-14)**.

Factor n can be determined by the following equation:

$$n = 113.14\left(\frac{b_2}{b_1}\right)^2 - 26.55\left(\frac{b_2}{b_1}\right) + 2.048 \tag{5-30}$$

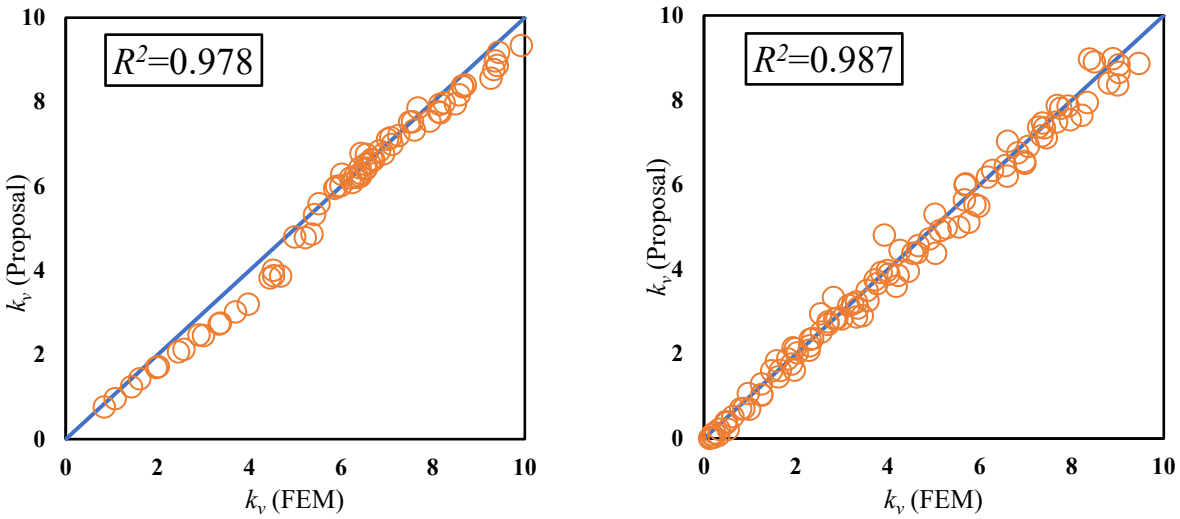

a) Lipped channels b) Un-lipped channels

Figure 5.10: The performance of the approximation curve parts in prediction of elastic buckling coefficient of channels under predominantly shear.

Figure 5.10 compares the elastic shear buckling coefficient k_v generated by the explicit procedure of the new proposal and the target values of the elastic buckling coefficient from the FEM buckling analysis. The comparison involves using 72 and 108 FEM models for lipped and un-lipped channel sections respectively. It is clear that almost all the points of approximation from the new proposal are well fitted to the linear target line of k_v *(Proposal)*=k_v *(FEM)* as shown in **Figure 5.10**. The magnitudes of squared residual R^2 are equal to 0.978 and 0.987 for lipped and unlipped channel sections respectively, which are close to unity. This indicates high agreement between the shear buckling coefficient obtained by the new proposal and the results from the FEM buckling analysis. A little difference between k_v (Proposal) and k_v (FEM) can be found for values in the range from 2.to 6 for lipped channels as shown in **Figure 5.10** (a). This is because the results predicted by the new proposal are a little more conservative than the FEM results for the channels in twisting buckling mode with very narrow flanges ($0.05 \leq b_2/b_1 \leq 0.15$). As a result, the proposed approximation of the shear buckling coefficient for both lipped and un-lipped channel sections under predominantly shear can generate a reliable and accurate prediction compared with the FEM models.

5.6 CHAPTER CONCLUSION

This chapter described the new proposal for determining the shear buckling coefficient of channels with narrow flange. First, the chapter compared the current design rules with the shear buckling analyse resulting from the FEM models. It is proven that using previous proposals by Keerthan and Mahendran [6] is unable to predict well the shear buckling coefficient of channels with flange width to depth ratios smaller than 0.3 for lipped channels. Furthermore, there are no design methods for un-lipped channel sections in the current Australian Standard AS/NZS 4600:2018 [7].

The new proposal is developed by identifying the switch of shear buckling modes between twisting and local buckling to define the fixity coefficient k_n at the juncture of the web to flange. A combination of two segments of approximation curves is considered for both lipped and un-lipped channels. The first part mainly uses the current design rules for predicting the shear buckling coefficient in the local shear buckling of very short members. The second curve segment is the new approximation for predicting the continuously reduced shear buckling coefficient of relatively long members in twisting buckling mode.

The squared residual R^2 is equal to 0.978 and 0.987 for the lipped and unlipped channel sections respectively, which indicates a high agreement between the shear buckling coefficient obtained by the new proposal and the results from the FEM buckling analysis.

CHAPTER 6 : CONCLUSION

6.1 SUMMARY OF RESEARCH AND CONCLUSION

The study in this thesis provides an insightful understanding of the elastic shear buckling behaviour of thin-walled channel sections with narrow flanges. The study involves used different numerical approaches to investigate the relationship between the shear buckling coefficient (k_v) and aspect ratios in the predominantly shear range by varying the flange width to depth ratios b_2/b_1. On the basis of the numerical investigations, a new explicit approach for the determination of the value of k_v for both lipped and un-lipped channel sections with narrow flanges is proposed.

In order to perform a comprehensive investigation of the elastic shear buckling behaviour of channels with narrow flanges, three numerical methods, including the finite element method (FEM), the Semi-analytical finite strip method (SAFSM) and the resemi-analytical finite strip method (reSAFSM) were used to simulate both lipped and un-lipped channels with b_2/b_1 from 0.025 to 0.6 and shear span length from 30 to 9000 mm based on the commercial software ABAQUS and computer programs bfinst7R.cpp and bfinst8R.cpp. The effect of different boundary conditions on the shear buckling coefficient was investigated by comparing the shear buckling results from the SAFSM and reSAFSM. The reliability of the FEM models was validated against the reSAFSM by comparing the shear buckling stress and shear buckling mode shapes. As a result, the three methods highly agree that the twisting buckling mainly governs the shear buckling failure mode in channels with narrow flanges due to the reduced flange rigidity. However, the FEM can provide a more practical investigation since the static equilibrium is maintained by applying a couple of bending moments at two section ends to balance the shear force.

Comparing the current design rules for the shear buckling coefficient of lipped channels with the FEM buckling analysis results shows the use of previous proposals by Keerthan and Mahendran [6] is unable to predict well the shear buckling coefficient of channels with narrow flanges. Especially for b_2/b_1 smaller than 0.3, there is a significant over-estimation resulting from using current design rules. Therefore, a more accurate practical design approach is proposed for the determination of k_v for both lipped and un-lipped channels with narrow flange. The underlying idea of the new proposal

is based on identifying how much fixity the narrow flanges can provide to the web panel by observing the switch of shear buckling modes between twisting and local buckling when changing the aspect ratios and flange width to depth ratios. The new approach for the shear buckling coefficient combines two segments of approximation curves in order to respond to the buckling mode switch. The first part uses the current design curve with the modified coefficient of fixity for predicting k_v in the local shear buckling of very short members. The second segment of the curve is the new approximation for predicting the continuously reduced shear buckling coefficient of relatively long members due to the twisting buckling.

6.2 RECOMMENDATIONS FOR FUTURE STUDIES

Future studies aim to develop a new Direct Strength Method (DSM) design for cold-rolled aluminium channels in shear with narrow flanges. Elastic shear buckling load (V_{cr}) and shear yielding load (V_y) are the two major inputs required in the Direct Strength Method. The study presented in this thesis has provided the elastic shear buckling analyses. Hence, in future research, the experiments for aluminium channels section under predominantly shear will be conducted based on Pham [30] and Pham [31] using the dual actuator test rig apparatus in order to conduct the shear strength analyse. In addition, non-linear numerical simulations will be developed to compare and calibrate against the test results. After calibration and validation, the numerical models will be used to create a full range database. Finally, the results of shear buckling and shear strength analyses will be combined for further parametric study, which will be used to develop the final Direct Strength Method for designing aluminium members in shear with narrow flanges.

REFERENCES

1. Permalite. *https://permalite.com.au/news/gallery/, Caloundra Potable Water Reservoir Re-roof*. 2014.
2. Pham, C.H. and G.J. Hancock, *Shear buckling of thin-walled channel sections.* Journal of Constructional Steel Research, 2009. **65**(3): p. 578-585.
3. Lau, S.C.W. and G.J. Hancock, *Buckling of thin flat-walled structures by a spline finite strip method.* Thin-walled structures, 1986. **4**(4): p. 269-294.
4. Hancock, G.J. and C.H. Pham, *Shear buckling of channel sections with simply supported ends using the semi-analytical finite strip method.* Thin-Walled Structures, 2013. **71**: p. 72-80.
5. Pham, C.H. and G.J. Hancock, *Shear buckling of channels using the semi-analytical and spline finite strip methods.* Journal of Constructional Steel Research, 2013. **90**: p. 42-48.
6. Keerthan, P. and M. Mahendran, *Shear buckling characteristics of cold-formed steel channel beams.* International Journal of Steel Structures, 2013. **13**(3): p. 385-399.
7. *AS/NZS 4600:2018, AS 4600 Cold-formed Steel Structures, in AS/NZS 4600:2018. Standards Australia, 2018: Standards Australia / Standards New Zealand.* 2018.
8. ExSteel. *https://www.exsteel.com/*.
9. ClarkDietrich. *https://www.clarkdietrich.com/*.
10. NEWSDAY, *https://newsday.co.tt/2021/09/02/bureau-of-standards-gives-60-day-moratorium-on-steel-rule/Cold-formed steel framing*. 2021.
11. iSPAN. *https://www.ispansystems.com/*.
12. ExSteel. *https://www.exsteel.com/component-resources/?_sft_products=c-sectionsExSteel Building Components C-Section Load Table*. 2017.
13. ClarkDietrich. *https://www.clarkdietrich.com/products/tradeready-steel-joist#resources TradeDready Steel Joist and Rim Track Section Properties*. 2022.
14. Timoshenko, S. and J. Gere, *Theory of elastic stability*. 2d ed. Engineering societies monographs. 1961, New York,: McGraw-Hill. 541 p.
15. LaBoube, R.A. and W.-w. Yu, *Cold-formed steel beam webs subjected primarily to shear.* 1978, American Iron and Steel Institute, University of Missouri-Rolla, Rolla, USA.
16. Pham, C.H. and G.J. Hancock, *Elastic buckling of cold-formed channel sections in shear.* Thin-walled structures, 2012. **61**: p. 22-26.
17. Basler, K., *Strength of plate girders in shear.* Journal of the Structural Division, 1961. **87**(7): p. 151-180.
18. Porter, D., K. Rockey, and E. HR, *The collapse behaviour of plate girders loaded in shear.* Journal of Structural Engineering (United States), 1975. **53:313-25**.
19. Chern, C. and A. Ostapenko, *The ultimate strength of plate girders under shear.* Fritz engineering laboratory report, 1969. **328.7**.
20. Sharp, M.L. and J.W. Clark, *Thin aluminum shear webs.* Journal of the Structural Division, 1971. **97**(4): p. 1021-1038.
21. Lee, S.C., J. Davidson, and C. Yoo, *Shear buckling coefficients of plate girder web panels.* Computers & structures, 1996. **59**(5): p. 789-795.
22. Keerthan, P. and M. Mahendran, *Elastic shear buckling characteristics of LiteSteel beams.* Journal of Constructional Steel Research, 2010. **66**(11): p. 1309-1319.
23. Anderson, M. and F. Williams. *Buckling of simply supported plate assemblies subject to shear loading*. in *Dawe, et al., editors. Aspects of the analysis if plate structures.* 1985. Oxford: Clarendon Press.

24. Pham, D.K., C.H. Pham, and G.J. Hancock, *Explicit approach for elastic local buckling analysis of thin-walled channels under combined bending and shear.* Thin-Walled Structures, 2022. **173**: p. 108925.
25. Cheung, Y., *Finite strip method analysis of elastic slabs.* ASCE J. Eng. Mech. Div., 1968. **94**(EM6): p. 1365-1378.
26. Cheung, Y.K., *Finite strip method in structural analysis*. 2013: Elsevier.
27. Przemieniecki, J., *Finite element structural analysis of local instability.* AIAA Journal, 1973. **11**(1): p. 33-39.
28. Plank, R. and W. Wittrick, *Buckling under combined loading of thin, flat-walled structures by a complex finite strip method.* International Journal for Numerical Methods in Engineering, 1974. **8**(2): p. 323-339.
29. Hancock, G.J., *Local, distortional, and lateral buckling of I-beams.* Journal of the Structural Division, 1978. **104**(11): p. 1787-1798.
30. Hancock, G.J. and C.H. Pham, *A Signature Curve for Cold-Formed Channel Sections in Pure Shear (No. R919).* Research Report, 2011. **R919**.
31. Hancock, G.J. and C.H. Pham. *Direct strength method of design for shear of cold-formed channels based on a shear signature curve*. in *the 21st International Specialty Conference.* 2012. St Louis, Missouri: Missouri University of Science & Technology.
32. Pham, S., C. Pham, and G. Hancock, *Shear buckling of channel sections with complex web stiffeners.* Research Rep, 2012. **924**.
33. Pham, S.H., C.H. Pham, and G.J. Hancock, *Shear buckling of thin-walled channel sections with complex stiffened webs.* Research Report, 2012. **R924**.
34. Fan, S.C., *Spline finite strip in structural analysis.* HKU Theses Online (HKUTO), 1982.
35. Pham, C.H. and G.J. Hancock. *Shear buckling of thin-walled channel sections with intermediate web stiffener*. in *ICASS '09/IJSSD - Proceedings of Sixth International Conference on Advances in Steel Structures and Progress in Structural Stability and Dynamics*. 2009.
36. Pham, C.H. and G.J. Hancock, *Direct strength design of cold-formed C-sections for shear and combined actions.* Journal of Structural Engineering (United States), 2012. **138**(6): p. 759-768.
37. Pham, C.H., *Shear buckling of plates and thin-walled channel sections with holes.* Journal of Constructional Steel Research, 2017. **128**: p. 800-811.
38. Pham, S.H., *Design of cold-formed steel beams with holes and transverse stiffeners in shear*. 2018, PhD Thesis, School of Civil Engineering, The University of Sydney.
39. Pham, D.K., *Shear behaviour and design of cold-formed channel sections with elongated openings based on direct strength method.* 2019, PhD Thesis, School of Civil Engineering, The University of Sydney.
40. Pham, D.K., C.H. Pham, and G.J. Hancock, *Parametric study for shear design of cold-formed channels with elongated web openings.* Journal of Constructional Steel Research, 2020. **172**: p. 106222.

APPENDICES A

Appendix A1: Shear buckling results of lipped channel sections of b_2 = 5 from different methods based on k_v versus the new proposed equations

b_1 (mm)	b_2 (mm)	a (mm)	t (mm)	d_{lip} (mm)	$k_{v\text{-}FEM}$	$k_{v\text{-}reSAFSM}$	$k_{v\text{-}SAFSM}$	$k_{v\text{-}proposal}$
200	5	100	2	20	21.33745	21.45994	7.509115	21.556
200	5	120	2	20	15.95745	15.91264	5.820831	16.00833
200	5	140	2	20	12.59764	12.60057	4.7371	12.66327
200	5	160	2	20	10.36639	10.44115	3.976265	10.49219
200	5	180	2	20	8.809927	8.938947	3.404864	8.997509
200	5	200	2	20	7.668509	7.568516	2.954299	7.772656
200	5	230	2	20	6.416033	6.681915	2.426838	6.339818
200	5	270	2	20	5.215698	5.658599	1.904701	4.967912
200	5	300	2	20	4.51533	4.965789	1.605412	4.213763
200	5	400	2	20	2.897456	3.293762	0.954971	2.65483
200	5	500	2	20	1.973728	2.377451	0.607498	1.83955
200	5	600	2	20	1.423834	1.824287	0.410775	1.358249
200	5	700	2	20	1.073207	1.458017	0.292954	1.04912
200	5	800	2	20	0.834523	1.196125	0.218353	0.83799
200	5	900	2	20	0.663856	0.991052	0.168675	0.686908
200	5	1000	2	20	0.537585	0.771521	0.134127	0.574771
200	5	1200	2	20	0.368025	0.494434	0.090616	0.421941

Appendix A2: Shear buckling results of lipped channel sections of b_2 = 10 from different methods based on k_v versus the new proposed equations

b_1 (mm)	b_2 (mm)	a (mm)	t (mm)	d_{lip} (mm)	$k_{v\text{-}FEM}$	$k_{v\text{-}reSAFSM}$	$k_{v\text{-}SAFSM}$	$k_{v\text{-}proposal}$
200	10	100	2	20	22.14376	21.92354	8.310915	22.824
200	10	120	2	20	16.97674	16.36199	6.723828	16.95
200	10	140	2	20	13.70186	13.17343	5.726937	13.40816
200	10	160	2	20	11.45719	11.17023	5.050246	11.10938
200	10	180	2	20	9.862001	9.802534	4.564096	9.533333
200	10	200	2	20	8.702189	8.802206	4.197495	8.406
200	10	230	2	20	7.487193	7.70786	3.783276	7.528117
200	10	270	2	20	6.427927	6.696871	3.367744	6.781309
200	10	300	2	20	5.853968	6.150745	3.107553	5.978749
200	10	400	2	20	4.444242	4.791521	2.37496	3.680881
200	10	500	2	20	3.36755	3.774063	1.783976	2.574706
200	10	600	2	20	2.572167	3.049344	1.328875	1.942948
200	10	700	2	20	2.009825	2.522725	0.993019	1.541187
200	10	800	2	20	1.6075	2.128983	0.750877	1.266188
200	10	900	2	20	1.310577	1.825177	0.577527	1.067643
200	10	1000	2	20	1.084216	1.583699	0.452888	0.918392
200	10	1200	2	20	0.765897	1.221225	0.29431	0.710453

Appendix A3: Shear buckling results of lipped channel sections of $b_2 = 15$ from different methods based on k_v versus the new proposed equations

b_1 (mm)	b_2 (mm)	a (mm)	t (mm)	d_{lip} (mm)	$k_{v\text{-}FEM}$	$k_{v\text{-}reSAFSM}$	$k_{v\text{-}SAFSM}$	$k_{v\text{-}proposal}$
200	15	100	2	20	22.58495	22.24844	8.722963	24.092
200	15	120	2	20	17.52442	16.60519	7.239631	17.89167
200	15	140	2	20	14.36143	13.43026	6.324685	14.15306
200	15	160	2	20	12.17554	11.49695	5.699346	11.72656
200	15	180	2	20	10.58547	10.22458	5.24134	10.06296
200	15	200	2	20	9.400344	9.323332	4.891225	8.873
200	15	230	2	20	8.142198	8.355258	4.499494	7.946346
200	15	270	2	20	7.075049	7.442049	4.13104	7.158048
200	15	300	2	20	6.541474	6.898706	3.920183	6.761889
200	15	400	2	20	5.415408	5.677717	3.355656	5.299905
200	15	500	2	20	4.524181	4.8169	2.821044	3.866079
200	15	600	2	20	3.690765	4.095613	2.309294	3.014301
200	15	700	2	20	2.993439	3.502841	1.858272	2.456691
200	15	800	2	20	2.451151	3.023708	1.483442	2.066193
200	15	900	2	20	2.034581	2.636096	1.1832	1.778864
200	15	1000	2	20	1.710122	2.319457	0.947945	1.559315
200	15	1200	2	20	1.243209	1.836461	0.624758	1.247166

Appendix A4: Shear buckling results of lipped channel sections of $b_2 = 20$ from different methods based on k_v versus the new proposed equations

b_1 (mm)	b_2 (mm)	a (mm)	t (mm)	d_{lip} (mm)	$k_{v\text{-}FEM}$	$k_{v\text{-}reSAFSM}$	$k_{v\text{-}SAFSM}$	$k_{v\text{-}proposal}$
200	20	100	2	20	22.92656	22.51684	8.93093	25.36
200	20	120	2	20	17.78305	16.78717	7.517883	18.83333
200	20	140	2	20	14.48866	13.58473	6.691106	14.89796
200	20	160	2	20	12.43915	11.66555	6.149247	12.34375
200	20	180	2	20	11.0781	10.43465	5.75623	10.59259
200	20	200	2	20	9.921748	9.590776	5.449141	9.34
200	20	230	2	20	8.647282	8.718832	5.089372	8.364575
200	20	270	2	20	7.546802	7.864843	4.735025	7.534787
200	20	300	2	20	7.005206	7.270863	4.533572	7.117778
200	20	400	2	20	6.004719	6.202759	4.052456	6.296562
200	20	500	2	20	5.356906	5.55464	3.622526	4.738918
200	20	600	2	20	4.675485	4.951335	3.156762	3.783604
200	20	700	2	20	3.969446	4.377444	2.686945	3.142808
200	20	800	2	20	3.339197	3.863285	2.251082	2.68527
200	20	900	2	20	2.819868	3.420194	1.868521	2.3432
200	20	1000	2	20	2.401085	3.04405	1.544628	2.078281
200	20	1200	2	20	1.784252	2.453279	1.058796	1.695501

Appendix A5: Shear buckling results of lipped channel sections of $b_2 = 40$ from different methods based on k_v versus the new proposed equations

b_1 (mm)	b_2 (mm)	a (mm)	t (mm)	d_{lip} (mm)	$k_{v\text{-}FEM}$	$k_{v\text{-}reSAFSM}$	$k_{v\text{-}SAFSM}$	$k_{v\text{-}proposal}$
200	40	100	2	20	23.69414	23.30979	9.248018	25.51813
200	40	120	2	20	18.13296	17.31341	7.853408	18.99939
200	40	140	2	20	14.70165	13.95812	7.122516	15.09725
200	40	160	2	20	12.58755	11.96747	6.736594	12.59209
200	40	180	2	20	11.21226	10.72502	6.538267	10.90052
200	40	200	2	20	10.26986	9.91456	6.441357	9.7149
200	40	230	2	20	9.319298	9.150915	6.381998	8.772702
200	40	270	2	20	8.484222	8.549272	6.338971	7.961964
200	40	300	2	20	7.924508	8.03356	6.291934	7.550859
200	40	400	2	20	6.918766	7.017628	6.032297	6.776281
200	40	500	2	20	6.533176	6.723446	5.755317	6.413578
200	40	600	2	20	6.357531	6.575186	5.485722	6.215141
200	40	700	2	20	6.236654	6.442129	5.173212	6.094907
200	40	800	2	20	5.989367	6.316211	4.802655	5.902439
200	40	900	2	20	5.603916	6.046038	4.392641	5.326568
200	40	1000	2	20	5.182229	5.67158	3.97	4.863842
200	40	1200	2	20	4.279246	4.858846	3.164617	4.164921

Appendix A6: Shear buckling results of lipped channel sections of $b_2 = 60$ from different methods based on k_v versus the new proposed equations

b_1 (mm)	b_2 (mm)	a (mm)	t (mm)	d_{lip} (mm)	$k_{v\text{-}FEM}$	$k_{v\text{-}reSAFSM}$	$k_{v\text{-}SAFSM}$	$k_{v\text{-}proposal}$
200	60	100	2	20	24.358	23.84393	9.411382	25.67625
200	60	120	2	20	18.45244	17.68241	7.964313	19.16545
200	60	140	2	20	14.91879	14.21649	7.207268	15.29655
200	60	160	2	20	12.7448	12.14961	6.819036	12.84044
200	60	180	2	20	11.33632	10.85562	6.642824	11.20846
200	60	200	2	20	10.37856	10.01289	6.593353	10.0898
200	60	230	2	20	9.427452	9.229859	6.65133	9.180829
200	60	270	2	20	8.639122	8.64382	6.833683	8.389141
200	60	300	2	20	8.236106	8.305694	6.982331	7.983941
200	60	400	2	20	7.248343	7.274282	7.278881	7.212563
200	60	500	2	20	6.830529	6.980739	7.249229	6.847155
200	60	600	2	20	6.663735	6.866709	7.076087	6.645837
200	60	700	2	20	6.53207	6.770851	6.850542	6.523284
200	60	800	2	20	6.404969	6.740482	6.577628	6.443192
200	60	900	2	20	6.187279	6.691734	6.251619	6.387995
200	60	1000	2	20	5.959909	6.67005	5.880689	6.341839
200	60	1200	2	20	5.335054	6.630439	5.074242	5.970015

APPENDICES B

Appendix B1. Shear buckling results of un-lipped channel sections of $b_2 = 5$ from different methods based on k_v versus the new proposed equation.

b_1 (mm)	b_2 (mm)	a (mm)	t (mm)	d_{lip} (mm)	$k_{v\text{-}FEM}$	$k_{v\text{-}reSAFSM}$	$k_{v\text{-}SAFSM}$	$k_{v\text{-}proposal}$
200	5	100	2	0	18.83692	19.08637	6.649435	13.91361
200	5	120	2	0	13.23564	13.36334	4.868668	10.33279
200	5	140	2	0	9.661036	9.860304	3.707984	8.173672
200	5	160	2	0	7.253149	7.59688	2.903514	6.772321
200	5	180	2	0	5.585152	6.059063	2.322847	5.81156
200	5	200	2	0	4.40116	4.894646	1.891092	4.81395
200	5	230	2	0	3.193005	3.524361	1.427291	3.337287
200	5	270	2	0	2.218233	2.391635	1.022242	2.154423
200	5	300	2	0	1.746772	1.849098	0.816626	1.605644
200	5	400	2	0	0.917989	0.920438	0.436956	0.708913
200	5	500	2	0	0.561374	0.543776	0.26853	0.372952
200	5	600	2	0	0.376635	0.3581	0.18115	0.220096
200	5	700	2	0	0.269306	0.253887	0.130392	0.14077
200	5	800	2	0	0.20175	0.189498	0.098389	0.095534
200	5	900	2	0	0.156583	0.14676	0.076911	0.067851
200	5	1000	2	0	0.125012	0.117163	0.061808	0.049953
200	5	1200	2	0	0.084946	0.079994	0.042459	0.029399

Appendix B2. Shear buckling results of un-lipped channel sections of $b_2 = 10$ from different methods based on k_v versus the new proposed equation.

b_1 (mm)	b_2 (mm)	a (mm)	t (mm)	d_{lip} (mm)	$k_{v\text{-}FEM}$	$k_{v\text{-}reSAFSM}$	$k_{v\text{-}SAFSM}$	$k_{v\text{-}proposal}$
200	10	100	2	0	20.42357	21.11557	7.784159	17.79194
200	10	120	2	0	15.18094	15.50031	6.223944	13.213
200	10	140	2	0	11.97046	12.1817	5.243166	10.45204
200	10	160	2	0	9.802167	10.08919	4.560458	8.660066
200	10	180	2	0	8.206617	8.694063	4.042858	7.431498
200	10	200	2	0	6.965236	7.717908	3.623259	6.552711
200	10	230	2	0	5.53845	6.716069	3.106004	5.003339
200	10	270	2	0	4.172562	5.696107	2.550135	3.603772
200	10	300	2	0	3.435871	4.881946	2.205926	2.907643
200	10	400	2	0	1.963355	3.182145	1.38143	1.622619
200	10	500	2	0	1.252808	2.287389	0.893219	1.034037
200	10	600	2	0	0.863253	1.750621	0.602367	0.716118
200	10	700	2	0	0.6244	1.392466	0.42491	0.525104
200	10	800	2	0	0.469219	1.133541	0.312497	0.401435
200	10	900	2	0	0.363584	0.882561	0.238269	0.316804
200	10	1000	2	0	0.28866	0.678687	0.187221	0.256356
200	10	1200	2	0	0.193414	0.428965	0.1241	0.17774

Appendix B3. Shear buckling results of un-lipped channel sections of b_2 = 15 from different methods based on k_v versus the new proposed equation.

b_1 (mm)	b_2 (mm)	a (mm)	t (mm)	d_{lip} (mm)	$k_{v\text{-}FEM}$	$k_{v\text{-}reSAFSM}$	$k_{v\text{-}SAFSM}$	$k_{v\text{-}proposal}$
200	15	100	2	0	21.15388	21.63344	8.134841	20.76461
200	15	120	2	0	15.94305	15.92859	6.614333	15.42062
200	15	140	2	0	12.81034	12.57692	5.698336	12.19836
200	15	160	2	0	10.75196	10.47515	5.098196	10.10699
200	15	180	2	0	9.297042	9.08335	4.674172	8.673149
200	15	200	2	0	8.211182	8.119605	4.351689	7.647534
200	15	230	2	0	6.976082	7.151816	3.97076	6.507353
200	15	270	2	0	5.757515	6.35638	3.5513	5.119341
200	15	300	2	0	5.031681	5.959205	3.265662	4.380706
200	15	400	2	0	3.309198	4.284949	2.418968	2.879691
200	15	500	2	0	2.284036	3.28081	1.753328	2.089467
200	15	600	2	0	1.652647	2.609771	1.267164	1.611312
200	15	700	2	0	1.241809	2.1359	0.925319	1.295069
200	15	800	2	0	0.956453	1.785997	0.688433	1.072552
200	15	900	2	0	0.75186	1.516476	0.523852	0.908669
200	15	1000	2	0	0.60224	1.301304	0.407912	0.783659
200	15	1200	2	0	0.409149	0.977364	0.263454	0.606953

Appendix B4. Shear buckling results of un-lipped channel sections of b_2 = 20 from different methods based on k_v versus the new proposed equation.

b_1 (mm)	b_2 (mm)	a (mm)	t (mm)	d_{lip} (mm)	$k_{v\text{-}FEM}$	$k_{v\text{-}reSAFSM}$	$k_{v\text{-}SAFSM}$	$k_{v\text{-}proposal}$
200	20	100	2	0	21.76438	22.0472	8.375406	22.83161
200	20	120	2	0	16.50842	16.26545	6.859061	16.95565
200	20	140	2	0	13.35153	12.88417	5.962094	13.41263
200	20	160	2	0	11.28742	10.77015	5.392589	11.11308
200	20	180	2	0	9.854437	9.373098	5.00953	9.536511
200	20	200	2	0	8.802893	8.407726	4.737266	8.408802
200	20	230	2	0	7.660937	7.44253	4.445252	7.486345
200	20	270	2	0	6.590913	6.660314	4.155949	6.2072
200	20	300	2	0	5.973973	6.281456	3.963292	5.496273
200	20	400	2	0	4.440963	5.025881	3.306378	3.963254
200	20	500	2	0	3.340099	4.096471	2.641236	3.088684
200	20	600	2	0	2.548231	3.414717	2.057858	2.525164
200	20	700	2	0	1.984254	2.882008	1.587806	2.132572
200	20	800	2	0	1.574922	2.461513	1.225451	1.843759
200	20	900	2	0	1.269326	2.126552	0.952745	1.62259
200	20	1000	2	0	1.03577	1.855113	0.749535	1.447916
200	20	1200	2	0	0.711301	1.441187	0.484269	1.189848

Appendix B5. Shear buckling results of un-lipped channel sections of b_2 = 40 from different methods based on k_v versus the new proposed equation.

b_1 (mm)	b_2 (mm)	a (mm)	t (mm)	d_{lip} (mm)	$k_{v\text{-}FEM}$	$k_{v\text{-}reSAFSM}$	$k_{v\text{-}SAFSM}$	$k_{v\text{-}proposal}$
200	40	100	2	0	24.14382	23.14486	8.972199	25.36
200	40	120	2	0	18.56185	17.1376	7.440572	18.83333
200	40	140	2	0	15.16461	13.67508	6.556827	14.89796
200	40	160	2	0	12.91393	11.53335	6.017181	12.34375
200	40	180	2	0	11.33954	10.12689	5.676954	10.59259
200	40	200	2	0	10.18531	9.157299	5.459998	9.34
200	40	230	2	0	8.994645	8.186659	5.275515	8.364575
200	40	270	2	0	7.964935	7.396601	5.177057	7.534787
200	40	300	2	0	7.443447	7.014229	5.160045	7.117778
200	40	400	2	0	6.268939	6.229442	5.180459	6.34
200	40	500	2	0	5.656321	5.617822	5.068447	5.646365
200	40	600	2	0	5.130206	5.243056	4.749215	4.919373
200	40	700	2	0	4.535368	4.951287	4.294114	4.386231
200	40	800	2	0	3.978176	4.65487	3.791837	3.97654
200	40	900	2	0	3.51267	4.321126	3.299394	3.65062
200	40	1000	2	0	3.13535	3.97401	2.844694	3.384332
200	40	1200	2	0	2.563908	3.331685	2.085104	2.97344

Appendix B6. Shear buckling results of un-lipped channel sections of b_2 = 60 from different methods based on k_v versus the new proposed equation.

b_1 (mm)	b_2 (mm)	a (mm)	t (mm)	d_{lip} (mm)	$k_{v\text{-}FEM}$	$k_{v\text{-}reSAFSM}$	$k_{v\text{-}SAFSM}$	$k_{v\text{-}proposal}$
200	60	100	2	0	24.20487	23.81367	9.301265	25.4975
200	60	120	2	0	18.6159	17.64963	7.759486	18.97773
200	60	140	2	0	15.06681	14.13	6.883278	15.07126
200	60	160	2	0	12.83993	11.9744	6.35868	12.5597
200	60	180	2	0	11.35724	10.57127	6.036668	10.86036
200	60	200	2	0	10.3022	9.610223	5.839489	9.666
200	60	230	2	0	9.022013	8.650994	5.687203	8.719468
200	60	270	2	0	7.915141	7.865192	5.639032	7.906246
200	60	300	2	0	7.357271	7.477645	5.668476	7.49437
200	60	400	2	0	5.88859	6.702841	5.925264	5.592469
200	60	500	2	0	4.627164	6.191958	6.175607	4.444509
200	60	600	2	0	3.757637	5.923846	6.255837	3.700178
200	60	700	2	0	3.144471	5.771627	6.124034	3.178009
200	60	800	2	0	2.695943	5.682305	5.81895	2.79105
200	60	900	2	0	2.356613	5.62014	5.408729	2.492489
200	60	1000	2	0	2.0912	5.519928	4.952894	2.254904
200	60	1200	2	0	1.704426	5.029162	4.044241	1.900051

Appendix B7. Shear buckling results of un-lipped channel sections of b_2 = 80 from different methods based on k_v versus the new proposed equation.

b_1 (mm)	b_2 (mm)	a (mm)	t (mm)	d_{lip} (mm)	$k_{v\text{-}FEM}$	$k_{v\text{-}reSAFSM}$	$k_{v\text{-}SAFSM}$	$k_{v\text{-}proposal}$
200	80	100	2	0	24.76581	24.26059	9.504764	25.635
200	80	120	2	0	18.78983	17.98322	7.953373	19.12213
200	80	140	2	0	15.18212	14.41727	7.081757	15.24456
200	80	160	2	0	12.95119	12.24856	6.568168	12.77565
200	80	180	2	0	11.48154	10.84841	6.259737	11.12813
200	80	200	2	0	10.44061	9.897236	6.076803	9.992
200	80	230	2	0	8.889648	8.955242	5.945553	9.074361
200	80	270	2	0	7.395658	8.185045	5.924628	7.443967
200	80	300	2	0	6.547846	7.800166	5.975247	6.538138
200	80	400	2	0	4.655077	6.958568	6.327036	4.617801
200	80	500	2	0	3.54515	6.500812	6.741656	3.545593
200	80	600	2	0	2.835834	6.268375	7.062672	2.865401
200	80	700	2	0	2.355439	6.134635	7.202261	2.39722
200	80	800	2	0	2.025778	6.058053	7.143814	2.05617
200	80	900	2	0	1.750994	6.01746	6.915959	1.797147
200	80	1000	2	0	1.549548	5.992951	6.572165	1.594028
200	80	1200	2	0	1.25708	5.922198	5.730464	1.296549

Appendix B8. Shear buckling results of un-lipped channel sections of b_2 = 100 from different methods based on k_v versus the new proposed equation.

b_1 (mm)	b_2 (mm)	a (mm)	t (mm)	d_{lip} (mm)	$k_{v\text{-}FEM}$	$k_{v\text{-}reSAFSM}$	$k_{v\text{-}SAFSM}$	$k_{v\text{-}proposal}$
200	100	100	2	0	25.14669	24.58165	9.641491	25.7725
200	100	120	2	0	18.89427	18.22019	8.079285	19.26653
200	100	140	2	0	15.25244	14.61561	7.2076	15.41786
200	100	160	2	0	13.00784	12.43263	6.699058	12.9916
200	100	180	2	0	11.54249	11.03157	6.397667	11.39589
200	100	200	2	0	10.34137	10.08667	6.222119	10.318
200	100	230	2	0	8.38108	9.159283	6.100923	9.117241
200	100	270	2	0	6.594566	8.406673	6.090758	7.138428
200	100	300	2	0	5.673089	8.028323	6.148154	6.093501
200	100	400	2	0	3.85097	7.098181	6.528253	3.988209
200	100	500	2	0	2.890391	6.675535	7.006949	2.889661
200	100	600	2	0	2.298082	6.464226	7.447902	2.227993
200	100	700	2	0	1.90076	6.328583	7.763593	1.791458
200	100	800	2	0	1.61629	6.238025	7.904027	1.484698
200	100	900	2	0	1.403849	6.183041	7.861443	1.258908
200	100	1000	2	0	1.238945	6.149662	7.663794	1.086709
200	100	1200	2	0	1.001204	6.098446	6.983534	0.843253